A Methodology for Modeling of Hydronic Radiant Slab Heating Systems for Predictive Control and Energy Flexibility

Ali Saberi Derakhtenjani

A Thesis

In

The Department of

Building, Civil, and Environmental Engineering

Presented in Partial Fulfillment of the Requirements
For the Degree of
Doctor of Philosophy (Building Engineering) at
Concordia University
Montreal, Québec, Canada

December 2020

CONCORDIA UNIVERSITY

SCHOOL OF GRADUATE STUDIES

This is to certify that the thesis prepared

By: Ali Saberi Derakhtenjani

Entitled: A Methodology for Modeling of Hydronic Radiant Slab Heating
                Systems for Predictive Control and Energy Flexibility

and submitted in partial fulfillment of the requirements for the degree of
                Doctor Of Philosophy (Building Civil and Environmental
                Engineering)

complies with the regulations of the University and meets the accepted standards with respect to originality and quality.

Signed by the final examining committee:

_____Chair Dr.
Hovhannes A. Harutyunyan

_____External Examiner Dr.
Dirk Saelens

_____External to Program Dr.
Ali Dolatabadi

_____Examiner Dr.
Hua Ge

_____Examiner Dr.
Fariborz Haghighat

_____Thesis Supervisor Dr.
Andreas K. Athienitis

Approved by   _____
                     Dr. Michelle Nokken, Graduate Program Director

December 18, 2020   _____
                     Dr. Mourad Debbabi, Dean

                     Gina Cody School of Engineering and Computer Science

ABSTRACT

A methodology for modeling of hydronic radiant slab heating systems for predictive control and energy flexibility

Ali Saberi Derakhtenjani, Ph.D.

Concordia University, 2020

Radiant slab heating systems are receiving considerable attention due to the multiple advantages they offer such as improved thermal comfort in buildings and suitability for other related applications in cold climates, particularly snow melting and de-icing of pavements and infrastructure. Hydronic radiant heating can utilize low temperature renewable energy heat sources. The operation of these systems can be optimized by applying predictive control and further the energy costs can be reduced by optimizing their interaction with smart grids by utilizing the flexibility in their demand profiles. However, compared to conventional air heating systems, radiant systems have several added complexities such as the slow transient heat conduction within the slab. Efficient design and operation of radiant slabs require several critical decisions on design and control variables to maintain comfortable thermal conditions in the space and achieve slab surface temperatures within the recommended range depending on the application.

This thesis presents a methodology for modelling of hydronic radiant slab heating systems with significant thermal mass (a concrete layer with embedded tubes) for predictive control to utilize the energy flexibility of the building and/or infrastructure in interaction with smart grids and dynamic pricing of electricity. The modelling approaches include low-order grey box models as

well as frequency domain techniques. Each approach has its own specific advantages and unique information can be obtained from each one that complement each other when optimizing system operation and designing the control strategies.

Using the developed frequency domain model of the zone, key transfer functions are calculated for a case study. By means of transfer functions, the effect of different levels of thermal mass on the zone thermal response and quantification of the energy flexibility in response to grid signals is studied. The model is used to evaluate different design and operation options on a relative basis. It is shown how transfer function analysis provides insight into the building thermal dynamics without the need for simulations. A new transfer function that relates the radiant floor heat source at the bottom of the slab to the zone air temperature is introduced and its derivation is demonstrated. By means of the transfer function, the delay between the heat input of the radiant slab and zone air temperature is determined. Experiments with a full scale test room in an environmental chamber are used to validate the key design parameters obtained from the frequency domain transfer function regarding the operational strategies for energy flexibility of the thermal zone. Frequency domain techniques may also be utilized to establish the appropriate order for low-order RC models for different applications.

A low-order thermal network RC model for a case study, validated with experimental measurements, is utilized to study several predictive control strategies in response to changes in the grid price signal, including short term, more reactive changes of the order of 10-15 minutes notice. An index is utilized to quantify the energy flexibility with the focus on the peak demand reduction for specific periods of time when the electricity prices are higher than usual. It is shown that the developed predictive control strategies can aid greatly in minimizing the electricity cost of

the building and up to 100% reduction in peak power demand and energy consumption is achieved during the high price periods.

Low-order thermal models are also utilized to study radiant slab heating systems of infrastructure that have much higher thermal mass than the radiant slabs in buildings due to structural reasons. Hydronic heating of roads and pavements surfaces to avoid ice formation has several advantages compared to traditional surface salting and other anti-skid methods which have a lot of limitations. However, the traditional method of designing such systems does not consider the thermal mass of the system and its potential for predictive control, energy flexibility and optimized performance. Finally, predictive control strategies are presented and studied to take advantage of the hydronic slab thermal mass and minimize the energy consumption and peak power demand and are validated in a full scale experiment in an environmental chamber.

ACKNOWLEDGEMENTS

Table of Contents

Nomenclature

Symbols

A_i	Area of surface represented by node i (m^2)
C_i	Thermal capacitance of node i (J/K)
C_a	Thermal capacitance of air (J/K)
$F(i,j)$	View factor between surfaces i and j
$F_{i,j}^*$	Radiant exchange factor between surfaces i and j
j	Node j, or the imaginary unit, $j = \sqrt{-1}$
k	Thermal conductivity of materials (W/m.k)
l_i	Thickness of surface i (m)
n	Harmonics
p	Period of time (seconds), time step
$Psig$	Price signal
Q_{eq}	Equivalent source (W)
$\mathbf{Q}$	Source vector
Q_{aux}	Auxiliary(heating/cooling) source (W)
Q_i	Source entering node i (W)
Q_{sg}	Solar gains (W)
$R_{i,j}$	Thermal resistance between nodes i and j (K/W)
S	Laplace variable

t	Time
$\mathbf{T}$	Temperature vector (ºC)
T_{setpoint}	Air setpoint temperature (ºC)
T_i	Temperature of node i (ºC)
T_o	Outdoor temperature (ºC)
U_{inf}	Infiltration U-value (W/K)
U_{win}	Window U-value (W/m²K)
$\mathbf{u}$	Input vector
$U_{i,j}$	Thermal radiation U-value between surface i and j (W/K)
$\mathbf{Y}$	Admittance matrix
$Y_{\text{self},i}$	Self-admittance for surface i
$Y_{\text{transfer},i}$	Transfer-admittance for node i
$\mathbf{Z}$	Impedance matrix
$Z_{i,j}$	Transfer function between nodes temperature of i and source entering node j

List of Figures

TABLE OF ACRONYMS

Abbreviation	Explanation
ASHRAE	American society of heating refrigeration and air-conditioning engineers
ADR	Active demand response
AHU	Air handling unit
BEFI	Building energy flexibility index
DSM	Demand-side management
FD	Frequency domain
ICT	Information and communication technology
LPFD	Lumped parameter finite difference
MPC	Model predictive control
PZTC	Perimeter zone test cell
RFH	Radiant floor heating
SSEC	Solar simulator environmental chamber

CHAPTER 1: INTRODUCTION

The increasing global energy demand, the foreseen reduction of available fossil fuels and the increasing evidence of global warming during the last decades have generated a high interest in renewable energy sources. However, renewable energy sources, such as wind and solar power, have an intrinsic variability that can seriously affect the stability of the energy system if they account for a high percentage of the total generation. The flexibility of building and other infrastructure energy demand profiles is commonly suggested as part of the solution to alleviate some of the upcoming challenges in the future demand-response energy systems (electrical, district heating and gas grids). Buildings can supply flexibility services to the electric grid in different ways e.g. utilization of thermal mass, adjustability of HVAC system use (e.g. heating/cooling/ventilation), charging of electric vehicles, and shifting of plug-loads. However, there is currently not much quantification and prediction of how much energy flexibility different building systems may be able to offer to the future smart grids. Therefore, there is a need for increasing knowledge and demonstrating the energy flexibility buildings can provide to smart grids. At the same time, there is a need for identifying critical aspects and possible solutions to manage this energy flexibility while maintaining the comfort of the occupants and minimizing the use of non-renewable energy.

Energy flexibility can be defined as "the ability to deviate from the reference electric load profile or baseline power consumption, or the business as usual scenario". Flexibility could be expressed as power kW or energy kWh, the power/energy that can be shifted, increased or decreased in reaction to an external signal (price signal for example) without scarifying the indoor comfort over a certain time span. The penetration of renewable energy sources (RES) is increasing rapidly worldwide, with a 26% increase of installed photovoltaics (PV) capacity to 177 GW and 16%

increase of wind capacity to 370 GW from 2013 to 2014, respectively. This RES integration poses challenges to the grid in terms of stability with the fluctuating supply needing to be balanced with the demand and that's why it is needed to make our buildings more energy flexible to match the supply and demand.

Radiant slab heating systems are receiving considerable attention due to the multiple advantages they offer such as improved thermal comfort in buildings and suitability for other related applications in cold climates, particularly snow melting and de-icing of pavements and infrastructure. Hydronic radiant heating can utilize low temperature renewable energy heat sources and provide significant flexibility to smart grids by storing energy and shifting heating demand. The operation of these systems can be optimized by applying predictive control and further the energy costs can be reduced by optimizing their interaction with smart grids by utilizing the flexibility in their demand profiles. There are two types of radiant floor heating systems: hydronic and electric. There has been recent work on control of electrically heated floor for shifting and/or shaving the building peak energy demand by (Thieblemont et al. 2018) . The focus here on hydronic systems is to enable the use of low-temperature renewable energy sources with heat pumps.
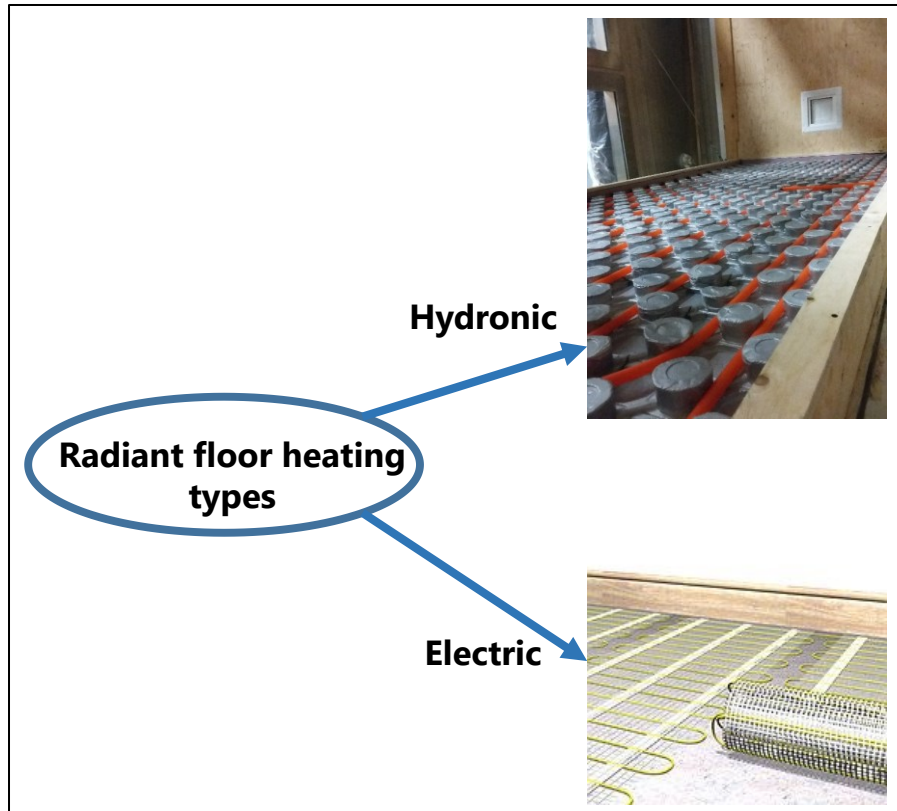
Figure 0-1. Different types of floor heating systems (before application of the final layer – typically concrete for hydronic and ceramic tiles for electric)[1]

This thesis is focused on studying the hydronic radiant slab heating systems embedded deep under a concrete slab with significant amount of thermal mass. Then, the application of such slab heating systems is presented for buildings and pavement de-icing. The inherent slow thermal response of such systems makes them suitable for energy flexibility, power shifting and predictive control. Therefore, major aspects of the approach here are model predictive control and energy flexibility quantification which are applicable to both buildings with radiant floor heating system as well as the de-icing application of radiant slabs.

---

[1] Source: top photo taken at PZTC,
bottom photo: http://www.reuk.co.uk/wordpress/heating/electric-under-floor-heating/
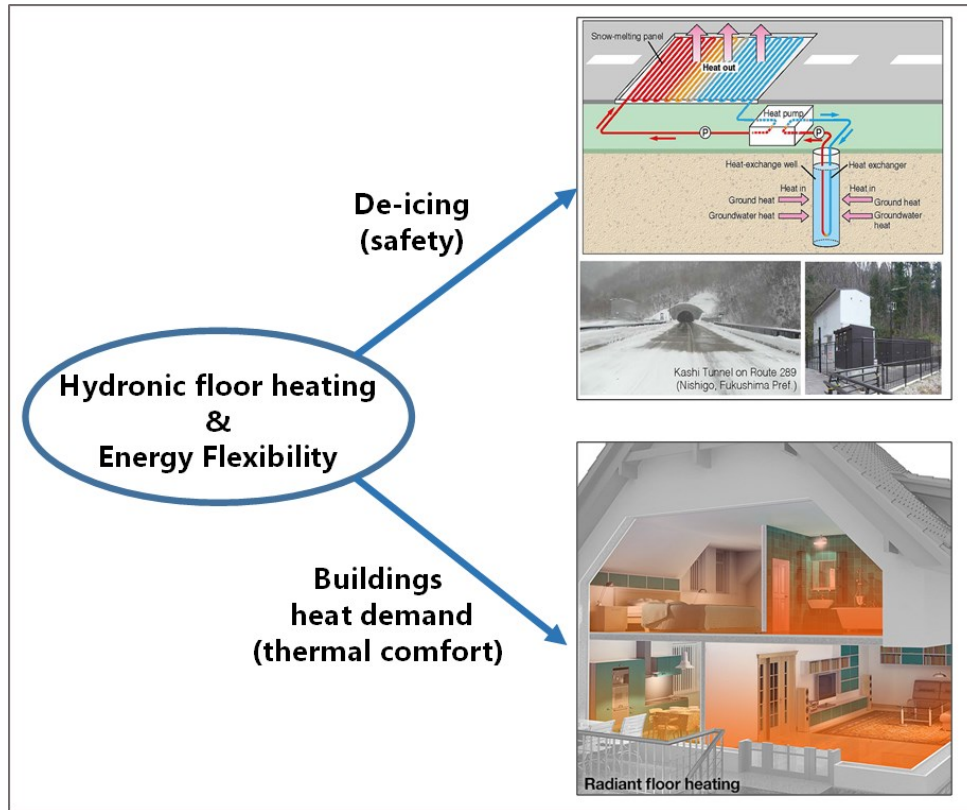
Figure 0-2. Schematic illustrating two examples of hydronic heating application[2]

An important application of hydronic slab heating systems is pavements and de-icing of surfaces in winter. The use of de-icing salts and other antiskid measures typically adopted by road maintenance services have many limitations such as applicable temperatures, location of storage facilities, ease of access to road section and, in the case of salts, infrastructure and environmental damage. An alternative solution that offers several advantages is implementing hydronic heating systems under the desired surfaces. Hydronic de-icing may eliminate the need to add salts to the road surfaces which prolongs the lifetime of infrastructure and pavements and significantly reduce maintenance costs. It is preferred to place the pipes as deep as possible in the concrete in order to reduce the risk of the damage from vehicles. Therefore, the large thermal mass above the pipes

---

provides a great opportunity for predictive control, energy flexibility and demand response strategies and reducing peak power demand of the de-icing system. A part of this research focuses on a methodology to develop low-order thermal models for analyzing the heated slab thermal dynamics for different piping configurations for hydronic de-icing of transportation infrastructure in cold climates. The modelling approach is validated by means of experimental measurements in a controlled environment (Solar Simulator/Environmental Chamber laboratory). The magnitude of time delay to reach the required surface temperature for de-icing, for different slab piping configurations and system capacity is evaluated by means of lumped parameter models.

Knowledge of energy flexibility that buildings can provide is important for the design of future smart energy systems, smart grids and buildings. The knowledge is, however, not only important for utilities such as Hydro-Quebec, but also for companies when developing business cases for products and services supporting the roll out of smart energy networks. Furthermore, it is important for policy makers and government entities involved in the shaping of future energy systems. In this context, the IEA (International Energy Agency) EBC (Energy in Buildings and Communities program) Annex 67: "Energy Flexible Buildings" was started in 2015 (Jensen et al. 2017). As a contributor to the Annex 67, the aim of the research work presented in this thesis is to increase the knowledge and demonstrate the energy flexibility that buildings and infrastructure equipped with hydronic radiant slab heating systems can provide for the energy grids, to identify the critical aspects and possible solutions to manage this energy flexibility.

Currently there is no comprehensive methodology to design hydronic slab de-icing systems while taking into account their predictive control and potential flexibility in interaction with smart grids. The great majority of designers use the existing methodology from the (ASHRAE 2017) Handbook in which the de-icing system design is based on steady-state calculation meaning continuous

operation of system in a way that surface temperature is always kept above the freezing point. This leads to excessive energy consumption. The work described in this thesis, supported by Quebec ministry of transportation (MTQ), is the first step towards the development of thermal models and control strategies to operate a hydronic de-icing system in a predictive way. A major objective here is to size the system in such a way that based on weather predictions and consideration of the slab thermal dynamics and thermal mass, our slab surface temperature can reach above freezing point before the precipitation event starts. This will ensure the safety of the surface for commuters while saving large amounts of energy and peak power compared to the current practice.

1.2 Objectives

The main objectives of this thesis are the following:

- Development of a comprehensive methodology to design hydronic slab de-icing systems while taking into account their predictive control and potential flexibility in interaction with smart grids; this methodology will be based on development of low-order models for thermal zones with hydronic radiant floor heating system that can be used for design and model-based predictive control

- Quantification and evaluation of energy flexibility potential of thermal zones with hydronic radiant floor heating systems by means of the developed low-order models

- Design of model-based predictive control strategies in response to changes in the electricity prices based on energy flexibility potential of thermal zones with hydronic radiant floor heating systems

- Analysis of thermal dynamics of hydronic slab heating systems under cold weather to be utilized for de-icing by means of low-order models

- Development of predictive control strategies for hydronic de-icing systems

1.3 Outline of the thesis

Chapter 1 provides an overview and introduction to the overall topic.

In the second chapter, previous literature regarding building hydronic slab heating system modelling and design, energy flexibility and predictive control as well as modelling of hydronic heating system of pavements for de-icing is discussed.

Chapter 3 presents the modeling approaches including frequency domain techniques and low-order grey box models. The unique advantages of each approach in optimized operation of buildings and infrastructure are presented and it is discussed how these approaches complement each other. A unique new transfer function is presented from which important information for controlling radiant slabs can be obtained.

Chapter 4 presents the results from the modeling approaches applied to the case studies, a full scale experimental verification, as well as the predictive control strategies.

Finally, chapter 5 presents the conclusion and contributions of this thesis as well as the publication list.

CHAPTER 2: LITERATURE REVIEW

This chapter discusses the literature on radiant slab heating, building energy flexibility as well as infrastructure hydronic de-icing systems. In the first section, a brief review of hydronic radiant heating is presented. In the second section, the previous efforts on characterizing buildings energy flexibility and utilizing that through different means are presented and then the current research needs are highlighted. In the last section, the literature review on hydronic de-icing is presented.

2.1 Radiant heating systems

The application of radiant heating systems has several thousand years of history (Bean et al. 2010b; Bean et al. 2010a). The credit is often given to ancient Romans for inventing the radiant systems but research and archeology show Asia to be the earliest known developer of these systems, preceding the Romans by thousands of years. Considering the evolution of the radiant systems from excavated floor ducts of ancient Korea and moving onto the Greek and Roman hypocausts and similar systems used in Middle East and then to subsequent disappearance of European systems post-Roman empire and to the continuing evolution in Asia and radiant floor heating rebirth by the French and British at the end of the 19th century, the history of radiant systems is a parallel study within anthropology, archeology and architecture.

After the introduction of plastic piping, water-based radiant heating and cooling with pipes embedded in room surfaces (floor, wall and ceiling), the application has increased significantly world-wide(Kim and Olesen 2015a). Earlier application of radiant heating systems was mostly for residential buildings. However, due to their large potential in peak load reduction and energy savings as well as their comfort and free use of floor space without any obstructions from installations, the radiant systems are now being widely applied in commercial and industrial

buildings as well as residential buildings. Figure 0-1 shows different types of embedded hydronic radiant systems(Kim and Olesen 2015a) including TABS (thermally activated building systems). The embedded systems are usually insulated from the main building structure (floor, wall and ceiling).
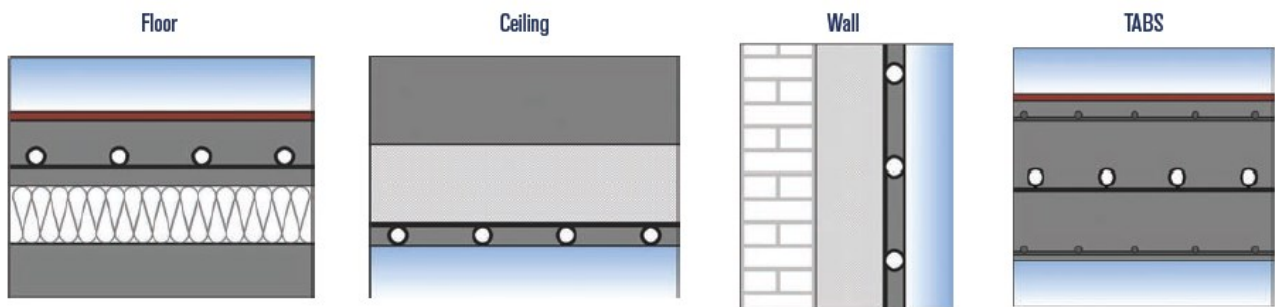
Figure 0-1. Examples of Hydronic Radiant Systems (Kim and Olesen 2015a)

In terms of heating, a floor assembly can be incorporated with a hydronic floor heating system or electrically heated floor (EHF) system (Thieblemont et al. 2016). Hydronic heated floor provides heat by pumping hot water through pipes which are usually laid under the flooring, while the EHF system works with electric cables or mats incorporated into the floor. The main determining factor of their peak shifting potential is thermal mass when just sensible storage is considered.

(Le Dreau and Heiselberg 2016) developed two building models in EnergyPlus to compare the peak shifting flexibility between a baseboard heating system and a hydronic floor heating system. They found that the hydronic floor heating system showed better peak shifting potential while maintaining the indoor air temperature within a comfortable range. A similar comparison between a fan-coil heating system and a hydronic heated floor system has been done by (Lin et al. 2006). It was reported that when the exterior temperature was around 10 °C, turning OFF the heating system resulted in indoor temperature dropping rate of 0.214 °C/h and 1.57 °C/h for floor heating system and fan-coil heating system, respectively. (Jin and Zhang 2011) analyzed the peak shifting

9

capability of a hydronic heated floor with 10mm wood and 30mm concrete on top of the water pipes. Under specific boundary conditions, during the peak period (8 a.m.–5 p.m.), the heating system was turned off and the average generation rate was found to be about 54.6 W/m^2.

EHF heats the building directly by electric cables or panels placed under the floor surface. (Thieblemont et al. 2013) proposed a method to integrate EHFs into TRNSYS and carried out a parametric study to analyze the effect of floor assembly on the EHF performance. Their simulation results showed that the thickness of concrete layer below or above the EHF and thickness of the insulation layer have significant influence over the peak shifting ability of the EHF system. To guarantee an acceptable indoor environment thermal comfort, (Thieblemont et al. 2018) studied the peak shifting potential of an EHF in a multi-room house by using a partial night-control strategy. It was reported that the EHF could shift 84% of building loads to the off-peak period. However, the building model developed in their study was validated using the data collected from the house with baseboards and not with EHF. The same drawback exists in their recent study (Sun et al. 2018b), where a self-learning predictive control strategy for EHF was proposed to reduce the energy demand during peak period.

2.1.1 Occupant Comfort

The key objective in a radiantly heated or cooled space is the occupant comfort. The requirements for general overall thermal comfort should be considered to provide an acceptable thermal environment. The predicted mean vote (PMV) or operative temperature, Top, and local thermal comfort, for example surface temperature, vertical air temperature differences, radiant temperature asymmetry, draft, etc. are to be considered.

For radiant or convective systems, the comfort requirements are the same when expressed by the PMV-PPD index (-0.5<PMV<0.5) or as an operative temperature range corresponding to 20ºC to

24ºC for heating season and 23ºC to 26ºC for cooling season in spaces with sedentary activity(ASHRAE 2010). The operative temperature represents the combined impact of air temperature and mean radiant temperature. In spaces with low air velocities (<0.2 m/s) or with a small difference between mean radiant temperature and air temperature, the operative temperature can be approximated as the average of room air temperature T_{air} and mean radiant temperature T_{mr} (essentially the area-weighted average room surface temperature):

$$T_{op} = \frac{T_{air} + T_{mr}}{2} \tag{2.1}$$

The occupants can have the same comfort level with a lower air temperature in a radiantly heated space and the same comfort level with a higher air temperature in a radiantly cooled space in comparison to convective heating and cooling systems. It is interesting to note that the difference between air and mean radiant temperature is normally smaller in radiantly heated or cooled spaces. This is due to the fact that in winter the windows will have a lower interior surface temperature than the air temperature, which is compensated by a higher surface temperature of the radiant system and vice-versa in summer. With convective systems the colder window temperature in winter will be compensated by a higher air temperature, which will result in an air temperature higher than the mean radiant temperature. Also, higher mean radiant temperature in radiantly heated space means that the air temperature can be kept lower compared to a convectively heated space. This is an advantage so that in winter the relative humidity of the space can be a little higher. Studies show that lower air temperature and lower air humidity have a significant effect on perceived air quality(Babiak et al. 2007). In spaces with sedentary and/or standing occupants, the maximum temperature for heating should not exceed 29ºC (84ºF) and the minimum floor temperature for cooling should not be lower than 19ºC (66ºF). For spaces such as bathrooms,

swimming pools and dressing rooms where occupants are present in bare foot, the optimal floor temperature for comfort also depends on the floor covering material(ASHRAE 2010).

2.1.2 Control of radiant systems

The major goal of the control component of the heating and cooling systems is to maintain the indoor temperatures within the comfort range by retaining the balance between the heat gain/loss of the building and the supplied energy from the auxiliary system under varying internal loads and external climate. Many studies in the literature deal with control of the radiant systems (Olesen 2001; Lim et al. 2006; Rhee et al. 2011).

The control of radiant heating and cooling system can be classified into central control, zone control and individual room control (Kim and Olesen 2015b). The central controller controls the supply liquid temperature for the radiant system, often based on the outside temperature. The room controller then controls the liquid flowrate or temperature for each room according to the room setpoint temperature. It is recommended to control the average liquid temperature (mean value of supply and return water temperature) instead of controlling only the supply temperature. During the heating period, as the internal load increases, the heat output from the radiant system will decrease and the return temperature will rise. Therefore, controlling the average temperature will automatically decrease the supply temperature. This will result in a more efficient and faster control of thermal output to the space and will result in a better energy performance than controlling the supply temperature.

2.2 Energy flexibility and predictive control[3]

The world-wide demand for electricity is increasing drastically and it is expected to get doubled by 2030(Boßmann and Staffell 2015). Electricity is a vital resource in modern societies as the backbone of the economy. Buildings are the largest electricity consumers in the grid. Demand response (DR) control of buildings plays important roles in the interaction between the supply side and demand side. Demand response includes altering the consumers' electricity usage from their normal consumption by incentive based dynamic pricing techniques (Cui et al. 2015; Xue et al. 2015; Huang et al. 2019). Due to recent global efforts on reducing the greenhouse gas emissions, penetration of renewable energy sources (RES) is increasing rapidly worldwide. For example, the total cumulative installed capacity for PV at the end of 2019 reached at least 627 GW with 115 GW of PV installed in 2019 only and the total global installed capacity for wind reached 651 GW with 60.4 GW installed in 2019 (GWEC 2019; IEAPVPS 2020). The trend is expected to continue that several countries are dedicated in increasing the RES share in energy system and already have highly ambitious targets. The Renewable Energy Directive requires the European Union to fulfil at least 20% of its total energy needs with renewables by 2020 , while Germany has a goal to meet at least 80% of gross electricity consumption through renewable energy by 2050. Even some countries have set RES targets as high as 100% of total energy mix, including Denmark who plans to cover 100% of country's energy demand with renewables . How to integrate the intermittent and stochastic production capacity with a notable RES share into existing power system becomes

---

[3]based on journal papers #1 and #3:
- Saberi Derakhtenjani, Ali, Athienitis, Andreas K. (2020)." A Frequency Domain Transfer Function Methodology for Thermal Characterization and Design for Energy Flexibility of Zones with Radiant Systems". Journal of Renewable Energy, 163:1033-1045

- Saberi Derakhtenjani, Ali, Athienitis, Andreas K. (2020)." Predictive Control Strategies for Energy Flexibility in Response to Dynamic Electricity Prices for Zones with Radiant Systems". Submitted to journal of Energies, under review

a large challenge. Simultaneously, these kinds of RES are not only in centralized plants, but also evolve in a distributed manner, as well as distributed storage systems (such as thermal storage systems, battery storage, etc.). This evolution, in combination with advanced ICT sector and its applications, leads to smart energy system in which highly distributed supply-demand profiles are involved. Under these circumstances, more flexibility both from the supply side and demand side is needed to keep the supply and demand matching at each period of time.
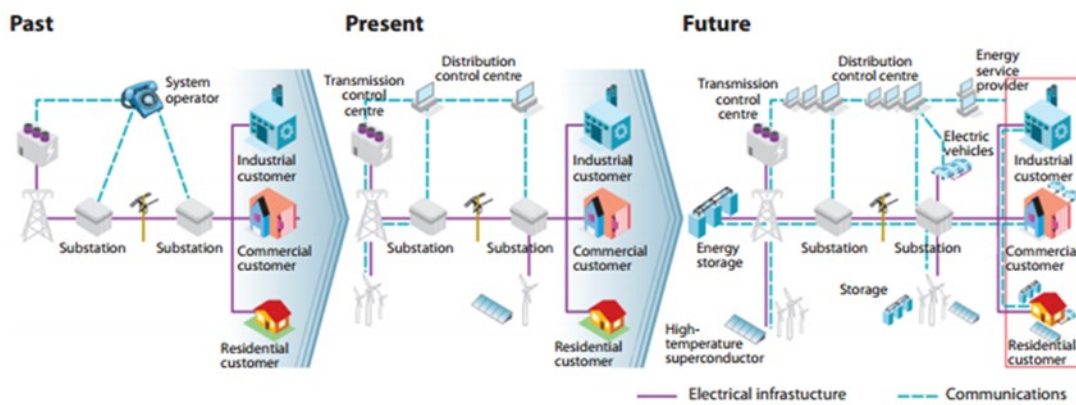
Figure 0-2. The smartening of the electricity system is an evolutionary process, not a one-time event

Supply side flexibility in general refers to large power plants (including conventional power plants, combined heat and power plants, combined gas turbine cycles plants) or large scale storage systems to make up for the mismatching between electricity generation and consumption by ramping up or down in required time and duration (Cochran et al. ; Aduda et al. 2016). More flexibility can be accomplished through simply strengthening the power grid, such as improving the capacity of the grid, adding energy storage systems(Converse 2012), and controlling the grid by smart strategies with the help of ICT (Fang et al. 2012).

On the other hand, the demand side – in form of building's thermal storage mass and its intelligent integration of electricity chain infrastructures – is regarded as the potential supplier of flexibility

in recent studies. The flexibility can be obtained by carefully crafting the load curve, such as reducing the peak power demand (peak-clipping), shifting demand in time (load-shifting) or temporarily increasing the load when the incentives are high or electricity prices are low (valley-filling), through demand side management (DSM). DSM is defined from a utility perspective as "the planning and implementation of those electric utility activities designed to influence customer uses of electricity in ways that will produce desired changes in the utility's load shape" by (Gellings 1985) which can be divided into two categories as energy efficiency (EE) and demand response (DR)(Palensky and Dietrich 2011). Flexibility is much more closely related to DR (De Coninck and Helsen 2016). Hence, when talking about the potential of the flexibility of buildings, most state-of-the-art literature focus on demonstrating how it can reduce the energy cost, shift peak power, increase the use of local renewable electricity production, or achieve the stability of the power grids with optimal control strategies. For example, (Salpakari and Lund 2016) conclude that cost-optimal control for buildings with PV – employing a heat pump, thermal and electrical storage and shiftable loads as flexibility sources – achieved 13 to 25% savings in the annual electricity cost and obtained 8 to 88% decrease in electricity fed into the grid. (Georges et al. 2014) indicates that smart-grid model predictive control strategies responding to a time-varying electricity price can reduce the procurement costs by 2 to 18% while keeping the thermal comfort.

The idea of regarding buildings as potential suppliers of flexibility services to power system is fairly recent. There have been many attempts to define the energy flexibility from the building point of view, but the definitions are mainly case-dependent as they are used to address defined aspects in specific cases.

Flexibility is defined as "the ability to change to suit new conditions or situations" according to the dictionary. When the definition is applied to a given system, it refers to "the ability to deviate

from the plan" as mentioned by (Peterson et al. 2013). Flexibility is a unique, innate, state and time dependent quality. Similarly, (Six et al. 2011) simply defines the flexibility of heat pump as "the number of hours the operation can be delayed or the system is forced to operate". In the LINEAR project (large-scale implementation of smart grid technologies in distribution grids), flexibility is a key concept which is defined as "the maximum time a certain power draw can be delayed or additionally called upon at a certain moment during the day"(Cardinaels and Borremans 2014). The definitions express flexibility in units of time within a single system, such as a thermal storage system (tank) or a heat pump, and it is closely related to the characteristics of the system.

If the flexibility is applied to energy in a building related context, it could be defined as "the ability to deviate from the reference electric load profile (or baseline power consumption, or the business as usual scenario)" (Oldewurtel et al. 2013; De Coninck and Helsen 2016) or "the efficient load of devices in response to real time pricing and reduce peak consumption" (Hong et al. 2015). Flexibility could be expressed as power kW or energy kWh – the power/energy that can be shifted, increased or decreased – in reaction to an external signal (price signal or activation) without scarifying the indoor comfort over a certain time span. Hence, the pivotal issues in defining this kind of flexibility compose of objectives (activations), constraints, the time period (minute, hour, month or year) and corresponding optimal control strategies. In general, the potential flexibility is mostly used to minimize energy cost or procurement cost of purchasing electricity and heat from the power grids, increase RES share in distributed networks, or develop the ability of real-time matching of consumption and generation to keep the stability of grid. Then, a broad set of measures affecting the patterns and magnitudes of the end-use energy consumption are used to accomplish the objectives, which is categorized to reducing (peaking shaving, conservation), or increasing (valley filling, load growth), or rescheduling energy demand (load shifting) (Lund et al. 2015). All

those optimal strategies should be acquired under several constraints: the indoor air comfort levels, the acceptance of users and the available capacity of RES and storage systems within a specific time span. Therefore, another more detailed definition of flexibility is "the ability of demand side installations to respond to power systems requirements for ramping up or down using on-site storage capabilities, increasing or decreasing electricity consumption patterns whilst maintaining acceptable indoor comfort bandwidth during a specific time period (Aduda et al. 2016)".

2.2.1 Thermal energy storage in building structures

Much more like a hot water tank, the building can also be treated as a thermal storage system in which the thermal energy is stored within the structure, i.e. floor, walls ceilings and furnishings. As emphasized by Braun, both energy costs and peak electrical use can be significantly reduced through optimal strategies while considering the use for intrinsic thermal storage within the building structure (Braun 1990). Some simulated-based and experimental results also show that model predictive control (MPC) strategies which take into account both the structural storage capacity of the building, i.e. the thermal mass embedded in the building structure, and the non-structural storage capacity, i.e. the storage capacity embedded in the thermal systems, may result in energy cost saving of 26% to 40%, while maintaining or even improving thermal comfort (Morales et al. 2013a). And these savings mostly come from the maximum use of solar and internal gains for passive heating, offsetting mechanical cooling with "free" cooling at night (such as night ventilation), or different prices of peak and off-peak period.

(Reynders et al. 2018) defines and quantifies a number of performance indicators to evaluate the potential flexibility of building structural thermal storage and concludes that the storage efficiency is strongly related to some building design parameters, i.e. the insulation quality of building, climatic boundary conditions, comfort requirements, occupant behavior, etc. In fact, the flexibility

17

resulting from building thermal mass is sometimes inclusive in the discussion about flexibility caused by controllable loads, in particular, the optimal control of HVAC systems. When shifting the part of load from the peak period to off-peak period or maximizing the energy use when the real-time electricity price is low or vice versa, the control of HVAC system would change, as well as the indoor temperature. The majority of thermal energy will be stored in the intrinsic structure and furnishings when the temperature increases. Then the temperature will decrease because of structure's thermal loss and the HVAC system is required to turn on to satisfy the occupants' requirements of comfort.

2.2.2   Building energy loads and their flexibility

Typically, the loads can be classified into two categories – shiftable loads and non-shiftable loads – according to their capability for being shifted or not. They also can be categorized into three classes based on the requirements and priorities to be changed /shifted or not: shiftable loads, controllable loads, and non-shiftable loads.

Shiftable loads are those that can be rescheduled in accordance with the real-time electricity price, to periods when the energy is cheaper, or when it is off-peak demand hours so that peak demand is reduced as well as the electricity bills for the customers (Hong et al. 2015). Examples of shiftable loads include dishwashers and washing machines whose total consumptions can be consumed at any time but have to be consumed completely for achieving their function once beginning. The flexibility can be obtained through recrafting the use-curve of the machines.

Controllable loads are those that can be adjusted by optimal control strategies like lighting and HVAC units whose consumed energy can be modified by dimming, thermostatic control and by varying the fan speed. Depending on the load, this flexibility can be used to reduce consumption

in peak periods and decrease procurement cost. However, the comfort of users should be the prerequisite constraint while adjusting the appliances.

Non-shiftable loads are those that cannot be stopped and require an uninterrupted power supply while operating regardless of the energy cost and energy volume of the whole energy system. For example, the alarm systems in the buildings and fridges in homes.

The following load types seem to be the most promising ones and studied widely by researchers while integrating with DSM strategies.

- Within the shiftable loads, the devices which can be applied to load shifting or interruption without influencing too much the occupants' comfort and behaviour pattern, are discussed more often. In particular, they can be integrated in large scale to offer flexibility to energy market.

- Regarding the controllable loads, those loads are related to the thermal inertia i.e. air conditioning systems, space heating and water heating and they provide good potential for load curtailment and load shifting.

- As an emerging device, electric vehicle is considered a lot while discussing flexibility from demand loads. It can sometimes be a mobile storage system which can significantly increase the flexibility potential.

Reynders et al. (Reynders 2015) has put forward 4 indicators – available storage capacity (C_{ADR}), storage efficiency (η_{ADR}), power shifting capability (Q_δ), and state of charge (SOC) – for energy flexibility and applies them to quantify the potential of structural thermal energy storage (STES) both under simplified (steady state) boundary conditions(Reynders et al. 2015) and dynamic boundary conditions(Reynders et al. 2016).

The definitions and quantification approaches for these indicators are on the basis of simulations of demand response technologies and a comparison of resulting heating/cooling power to a reference with the building in normal operation. As schematically illustrated in Figure 0-3, the set-point temperature for heating is slightly increased and used to activate the thermal mass so that a part of the heating energy can be stored within the building. Whereas the reference control is assuming that a minimum temperature allowed by users' thermal comfort would be maintained in order to minimize the energy consumption.
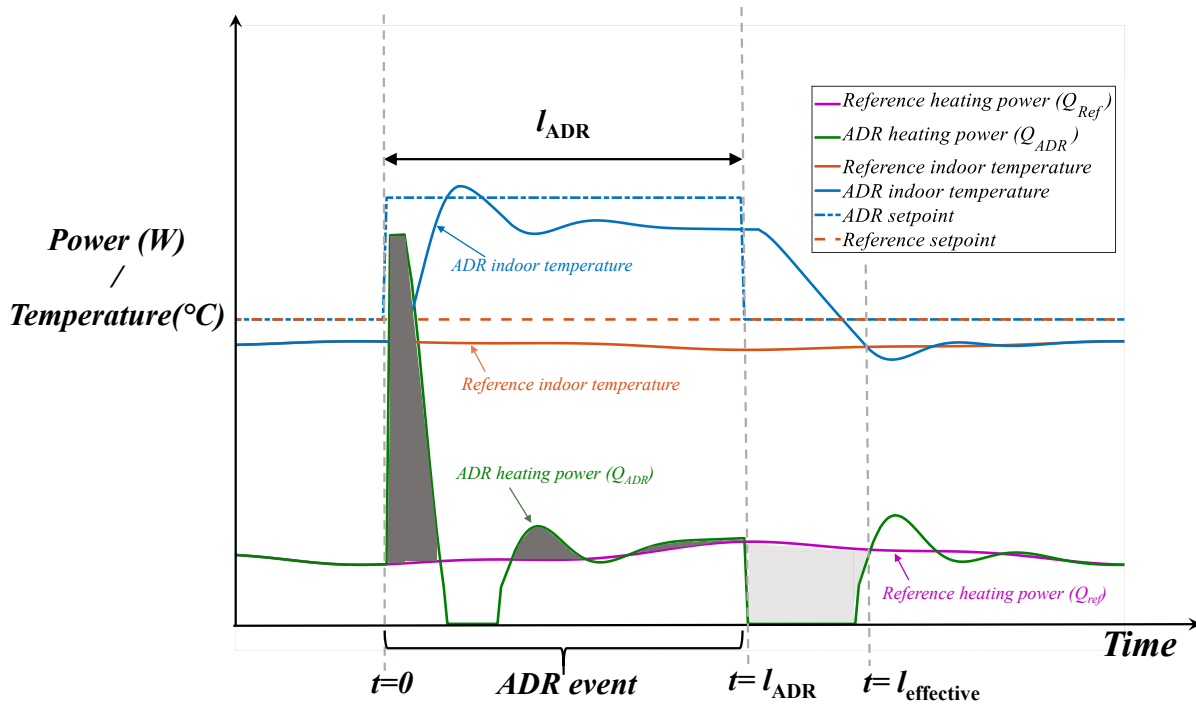
Figure 0-3. Scheme of the simulation experiment used to quantify the available storage capacity and the storage efficiency(Reynders et al. 2018) modified by (Saberi Derakhtenjani and Athienitis 2020).

The following indicators are described here as presented by Reynders et al. 2018.

The available structural energy storage capacity (C_{ADR}) is defined as the amount of heat that can be added to the structural mass of a building of an active demand response (ADR) without jeopardizing indoor thermal comfort in a specific time-frame, which can be quantified as:

$$C_{ADR} = \int_0^{l_{ADR}} \left(Q_{ADR} - Q_{Ref} \right) dt \tag{2.2}$$

The storage efficiency (η_{ADR}) represents the fraction of the heat that is stored during the active demand-response (ADR) event that can be used subsequently to reduce the heating power needed to maintain thermal comfort. Otherwise, the thermal loss resulting from transmission, ventilation, and infiltration would be increased because of the increased indoor temperature. The equation of η_{ADR} is:

$$\eta_{ADR} = \frac{\displaystyle\int_{l_{ADR}}^{l_{effective}} (Q_{ADR} - Q_{Ref}) dt}{\displaystyle\int_0^{l_{ADR}} (Q_{ADR} - Q_{Ref}) dt} \tag{2.3}$$

The power shifting capacity is the relation between the change in heating power (Q_δ) and the duration (t_δ) that this shift can maintained before the normal operation of the system, i.e. thermal comfort, is jeopardized. The power shift (Q_δ) means the difference between the consumed heating during the ADR event and the reference heating power during normal operation within the duration that the thermal comfort boundaries, either T_{max} or T_{min}, are reached.

$$Q_\delta = Q_{ADR} - Q_{Ref} \tag{2.4}$$

Typically, the power shift at the time point is closely related to the current storage state of the building. The more energy has been stored within the building thermal mass, the longer duration

to reduce the heating power can be obtained. Hence, the state of charge (SOC) is used to explain the fraction of stored energy medium at time t compared to the total storage capacity:

$$SOC = \frac{E_{th}(t) - E_{th,min}(t)}{E_{th,max}(t) - E_{th,min}(t)}$$ (2.5)

$E_{th,max}$ and $E_{th,min}$ represent the maximum and minimum energy content which are obtained when the building is consistently heated to the maximum comfort temperature and minimum comfort temperature, respectively.

The performance indicators are exploited to assess the impact of main building design parameters, e.g. geometric properties of the building, thermal properties of components and type and specifications of the heat emission and ventilation system, on the suitability and flexibility of structural thermal energy storage for ADR.

2.2.3 Research needs

As observed from the previous sections, characterizing buildings energy flexibility is quite challenging since it involves various aspects and it is strongly dependent on the boundary conditions and evaluation methods(Reynders et al. 2018). Hence, energy flexibility quantification in buildings is one of the topics of greatest interest in current scientific research (Reynders et al. 2018; Arteconi et al. 2019; Brunner et al. 2020; Hu and Xiao 2020; Saberi Derakhtenjani and Athienitis 2020). There have been a number of studies on different flexibility services that buildings can provide such as reducing peak loads and shifting peak demand through utilization of thermal mass(Le Dreau and Heiselberg 2016; Reynders et al. 2016; Foteinaki et al. 2018; Weiß et al. 2019), storage in batteries(Niu et al. 2019), charging of electric vehicles(Zhou and Cao 2019), and adjustability of the HVAC system use(Zhou and Zheng 2020). However, the current building energy flexibility literature is very limited on studies of predictive control strategies that considers

the electricity price prediction of the following days(Junker et al. 2018) and specifically, there is a lack of such studies for buildings equipped with radiant slab heating systems as well as pavement hydronic de-icing applications. Also, no previous study was found on the short-notice changes in price signal and the strategies to deal with such situations in buildings. This is an important scenario that occurs when power grid faces unexpected load balances and buildings as the largest electricity consumers play a significant role in those situations. Therefore, utilities are looking for solutions to deal with such situations and buildings energy flexibility research is highly supported by Hydro-Quebec.

The next section presents literature review on hydronic de-icing systems.

2.3 Hydronic heating performance under cold climate for de-icing[4]

Roadways are the lifeline for business and industry and are vital to the health of a country's economy. Ice and snow accumulation, especially on bridges, tunnels and overpasses, can cause serious safety as well as economic concerns to a community. Ice and snow cover on the pavement greatly reduces the friction coefficient of pavements, which often result in motor vehicle accidents and endanger the drivers and passengers. As an example, almost 30% of car accidents in Canada occur due to snowy or icy roads(Liu et al. 2019). According to recent statistics, the occurrence of traffic accidents in winter is 4-5 times more than in other seasons, which may result in annual economic loss of tens of millions of dollars(Lai et al. 2015). Therefore, much research has focused on ensuring pavement skid resistance on roadways, in tunnel portals and over bridges (Ialam et al. 2006; Hu 2013; Ren 2013; Cao et al. 2014). De-icing salts and other antiskid measures adopted by

---

highway maintenance divisions have many limitations including applicable temperatures, location of storage facilities, ease of access to road section, etc.(Balbay and Esen 2013; Champagne and Drouin 2017). Additionally, surface salting, the prevalent technology used, can cause chronic structural degradation problems to concrete infrastructure, contaminate water and soil and prevent plant growth (Li et al. 2013; Cristóvão et al. 2016), while it cannot even melt snow at ambient temperatures below -3.9ºC (Liu et al. 2007a). An environmentally clean and sustainable alternative solution that offers several advantages is using hydronic heating systems under the surface to avoid the need to add salts, thus enabling the roads to last longer and reduce maintenance costs (AdlZarrabi et al. 2016). In 2017, hydronic de-icing heating system covered a global total of 1.5 million m^2 of roads (Xu et al. 2017).

Hydronic heating systems circulate a hot fluid, usually glycol mixture, through pipes embedded in the slab to prevent formation of ice on the surface of the slab or to melt the snow and ice already present. When the hydronic heating system is powerful enough, it can completely melt away the snow present on the surface, thus eliminating the need for snow removal by chemical or mechanical means. An experimental bridge deck with embedded hydronic tubes built at Oklahoma State University showed that this system could successfully maintain the surface snow-free even during severe weather conditions (Liu et al. 2003; Liu et al. 2007b). If mechanical means are used to remove the bulk of snow accumulation, such as with the use of snow ploughs, the hydronic heating system can be used to melt away the remaining snow or thin ice cover and prevent further ice formation; it is then referred to as a de-icing system and is the focus of the present research. Freeze protection of the heat carrier fluid is essential in subfreezing weather so a variety of fluids, including brine, oils, and glycol-water mixtures, are suitable as heat carrier fluids. A number of

heat sources can be used for such systems, including solar energy, boilers, electrical heaters, as well as river water, ground water, or ground source heat pumps.
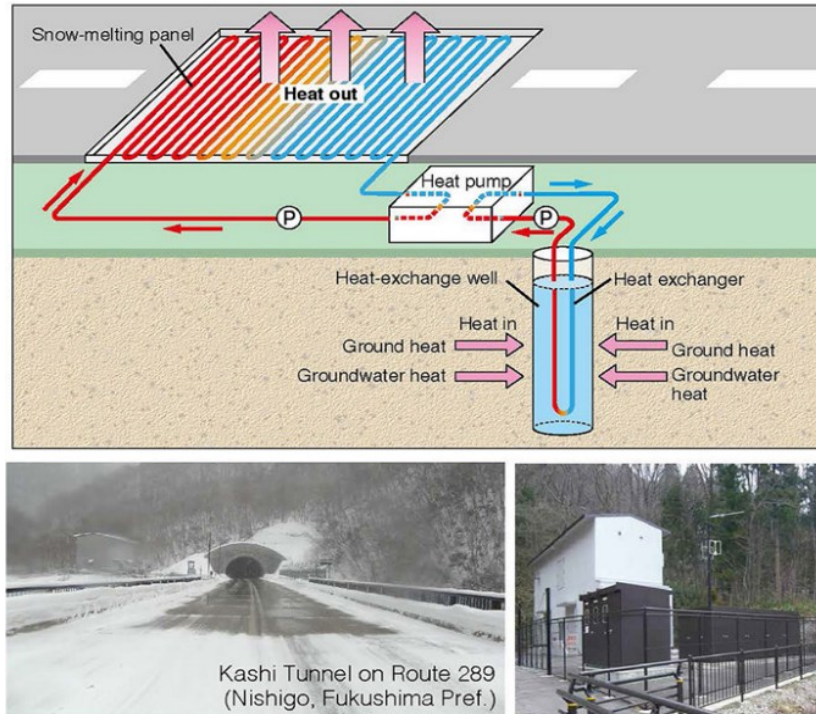
Figure 0-4. Ground-source heat pump road heating concept and application (Kashi Tunnel, Fukushima, Japan), source: http://www.road.or.jp/docs/gdansk/no07/index.html

Geothermal energy can be a good alternative energy resource to support such a hydronic heating system since it is a renewable heat source, economic and environmentally friendly. In the 1990s, several pilot plants for geothermal heat pump systems were realized in Japan and central Switzerland (Eugster 2007). A vertical single U-shaped borehole geothermal system was investigated by Balbay and Esen showed that a bridge slab can be de-iced effectively(Balbay and Esen 2010). As shown in Figure 0-5, solar energy can also be collected during the summer and stored in seasonal thermal energy storages and then the stored heat is released for de-icing during cold periods which increases the energy efficiency of the de-icing system (Chen et al. 2011).
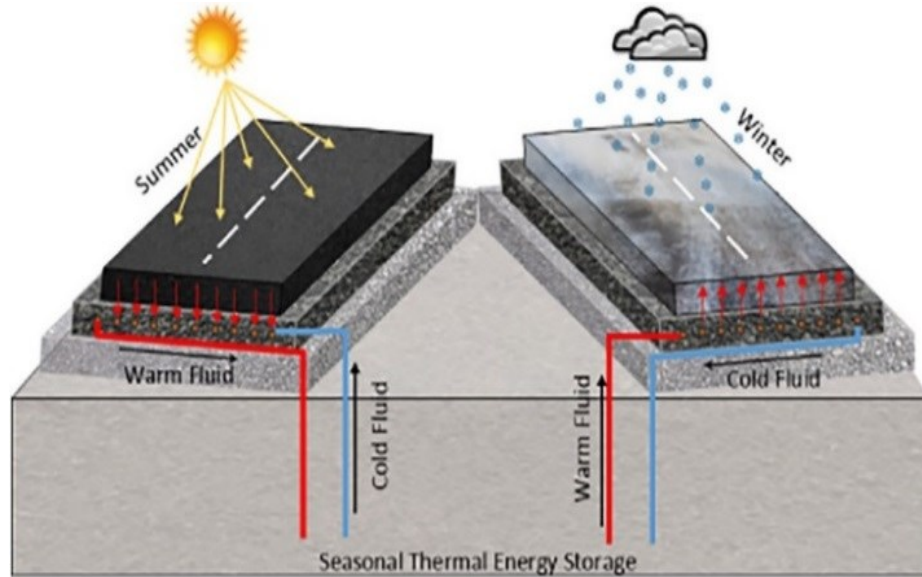
Figure 0-5. Utilization of solar energy for thermal storage(Mirzanamadi et al. 2018)

2.3.1 Research needs

Designers of hydronic snow-melting and de-icing systems often use the ASHRAE guidelines (ASHRAE 2011) to determine the required surface heat flux using a steady-state heat balance at the slab surface. The surface heat flux is calculated assuming that the system is constantly in operation and the slab temperature is kept at above freezing point at all times, which leads to significant energy consumption in cold regions. Also, this approach is limited by the fact that real systems are almost never operated continuously through the winter, nor do weather conditions remain constant. The large thermal mass of the infrastructure requires that transient performance be considered. Therefore, choosing to operate the system predictively, activating it only during/after snowfalls or during periods of ice formation (e.g. black ice) or running it at a lower temperature and boosting the system power in the case of precipitation events, will significantly reduce the energy consumption. A model-based control methodology that acts based on the weather forecast and a physical model of the system can thus save a huge amount of energy while ensuring road safety is maintained. There is a need for such a methodology to be applied in the design of the hydronic de-icing systems. This research presents a methodology to analyze hydronic

26

de-icing systems thermal dynamics based on validated low-order thermal models which can be applied for predictive control.

Model predictive control (MPC) is an advanced method of process control that relies on dynamic models of the process. This method has been used in process industries such as chemical plants and oil refineries since the 1980s and is especially useful to control slow-responding processes. Since transportation infrastructure (roads, tunnels, bridges, etc.) usually have high thermal capacity, they respond slowly to a heat source applied to them. This slow-responding feature makes the application of model predictive control promising. This is currently being studied and applied to buildings and their heating systems, including floor heating (Candanedo et al. 2011; Candanedo and Athienitis 2011; Kim and Braun 2012). However, there have been very few studies on application of model predictive control to hydronic de-icing system of urban infrastructure and designing the de-icing system accordingly(Jenks 2001; Liu and Spitler 2004; Xie and Whiteley 2007).

2.3.2   Discussion on real weather data accuracy

Forecasted weather data for the following 12 to 24 hours ahead is typically needed for model predictive control strategies. Because control decisions are proactive, they rely heavily on forecasted weather conditions. From a real-time operating standpoint, the most challenging aspect of implementing an MPC controller into infrastructure systems is creating and maintaining the network connections to provide the quality weather data and forecasts required (Xie and Whiteley 2007). Actually, one of the reasons that MPC has fallen short of expectations is the lack of tools for incorporating weather forecast data in automation systems in a straightforward manner. With a few exceptions, such as the efforts carried out by MeteoSwiss (Stauch et al. 2010), there is a scarcity of tools designed for this purpose.

Meteorological services around the world make use of numerical weather prediction (NWP) models. NWPs are simulations of the atmosphere carried out by discretising a large 3D domain into hundreds of thousands of control volumes (Bauer et al. 2015). Continuity, momentum and energy balance equations are solved for each of these domains at discrete time steps. The boundary conditions are obtained from satellite imagery and measurements from terrestrial stations. The solution of these systems of millions of equations is among the most computationally demanding tasks carried out nowadays. National weather services perform these simulations by using Gridded Binary (GRIB) files, a compact binary format that facilitates the handling of large meteorological datasets. The Canadian Meteorological Centre runs NWP models periodically (Candanedo et al. 2018b). The raw results (in GRIB format) are made freely available to the public. The GRIB file results are then used by commercial weather forecast companies to perform some post-processing to add additional information and make the results accessible to the public. These weather services tend to focus on populated areas, and target specific variables, such as temperature, humidity, precipitation or wind speed. While these forecasts usually indicate cloud cover conditions (e.g., sunny, overcast, etc.), quantitative solar irradiance variables are not available. In order to provide services that are not readily available in most of the weather tools available, a weather forecast tool is developed by CanmetENERGY-Varennes under the commercial name of CanMETEO and was publicly released, free of charge, in August 2017 (CanMETEO 2017). According to measurements from CanMETEO for ambient temperature forecasts, the 6-hr ahead predictions are within the range of +/-3ºC and deviations can be larger for the 48-hr ahead forecast. Therefore, in terms of load consideration for de-icing system, while implementing MPC, the uncertainty in real weather conditions should be taken into account in order to avoid the unexpected risk. Therefore, it is necessary to get frequent updates from weather stations and weather forecast tools to modify

the load and control algorithm accordingly. Also, ambient weather uncertainty needs to be implemented in the controller especially for long prediction horizons (12 hours, 24 hours, etc).

2.4 Summary

This chapter presented a literature review of modelling and control of radiant slab heating systems and typical applications. Then, recent research papers on energy flexibility of buildings were reviewed. The challenges to quantify the building energy flexibility were discussed. It was observed that the current building energy flexibility literature is limited on studies of predictive control strategies that considers the electricity price prediction of the following days, particularly for buildings with radiant slab heating systems as well as pavement hydronic de-icing applications. Previous research on the hydronic de-icing slab was reviewed and it was concluded that the current design of such systems are based on a steady-state calculation of the heat flow at the slab surface while the large thermal mass of such systems requires the transient performance to be considered for optimal performance. The next chapter presents the modelling methodology utilized in this research.

CHAPTER 3: METHODOLOGY

In this chapter different modeling approaches that are used for the studies are presented as part of an overall modelling methodology that can be applied to hydronic slab heating with application to both energy flexibility with the grid and de-icing, utilizing in both cases predictive control. The approaches include frequency domain techniques and low-order lumped parameter finite difference models. Frequency domain techniques are especially beneficial for thermal characterization and relative design analysis and obtaining important information for designing control strategies while they can be also efficiently applied to establish the required order for the low-order lumped parameter models (Saberi Derakhtenjani et al. 2015). A new transfer function is introduced which gives important information for designing controls for radiant slabs. As mentioned earlier the focus of this thesis is on the zones with radiant slab heating system that have significant level of thermal mass and pipes are deep in the slab (typically at the bottom and in some cases in the middle or lower). Therefore, the lumped parameter thermal network approach can be applied (Bi<0.1) and the heat transfer can be approximated as one-dimensional as validated from experiments too in this thesis.

3.1 Background: thermal modeling approaches[5]

Appropriate modeling is the fundamental tool to study a system. It provides the capability to simulate design conditions for a building and to study its thermal response. Building models allow making the right decisions on the design and control strategies to optimize building energy

performance, while maintaining occupant comfort. Simulation and analysis of thermal dynamics and energy fluxes in a building by means of a model aids at choosing appropriate building materials and energy systems considering the local climatic features and building functions. Therefore, there have been significant efforts in the building engineering field on developing models using experimental and theoretical simulation tools.

The following three types of approximations re commonly introduced in mathematical models to facilitate representation of the building thermal behavior (Athienitis and O'Brien 2015):

1.   *Linearization of heat transfer*. Convective and radiative heat transfer are inherently nonlinear processes and the respective heat transfer coefficients are usually linearized so that the system energy balance equations can be solved by direct linear algebra techniques and represented by a linear thermal network. Linearization generally introduces less error for long-wave radiant exchanges between surface than convection between room surface and room air. In some cases heat flow reversal can occur such as between a cold floor and warm air when the convective heat transfer coefficient can be of the order of 1 W/m^{2}K versus 3 W/m^{2}K for a heated floor and cold air.

2.   *Spatial and temporal discretization*. Transient heat conduction is described by a parabolic, diffusion type partial differential equation. Thus, when using finite difference methods, a conducting medium with thermal capacity such as concrete or brick must be discretized into a number of regions, commonly known as control volumes, which may be modelled by lumped network elements (thermal resistances and capacitances). Also, time domain discretization is required in which an appropriate time step is employed. For frequency domain analysis none of these approximations are required. However, the number of harmonics employed must be kept

32

within reasonable limits. It should be noted that when thermal storage undergoes phase change a linear approximation may not be possible and specialized modeling is required.

3.   *Approximations for reduction in model complexity/establishing appropriate model resolution*. These approximations are employed in order to reduce the number of simultaneous equations to be solved and the required data input or to enable the derivation of closed form analytical solution. They are by far the most important approximations. Examples include combining radiative and convective heat transfer coefficients (so-called film coefficients commonly employed in building energy analysis), assuming that many surfaces are at the same temperature, or considering certain heat exchanges as negligible. Such approximations need to be carefully selected and applied by taking into consideration the expected temperature variations (spatial and temporal) in a zone. For example, a zone with large windows and floor heating may exhibit large spatial temperature variations, in which case the use of combined film coefficients would result in high errors in room operative temperature and floor heating rate calculations.

3.2 Frequency domain techniques

There are currently several approaches for creating building energy models which can be categorized into two general methods: time domain modeling and frequency domain modeling. Each one has its own advantages and can complement each other when utilized properly. A model is created for a specific objective and therefore, the suitable modeling approach should be chosen based on the objective of the study.

Frequency domain techniques have been shown to be a useful tool for the design analysis on a relative basis (Athienitis and Santamouris 2002). By means of the frequency domain modelling techniques important building transfer functions can be obtained and studied and for this usually

no simulation is required. Also, it has been shown to be a practical tool for building simulation and deriving simplified grey-box building models (Saberi Derakhtenjani et al. 2015). Frequency domain techniques are especially useful for periodic analysis of phenomena inside a building. The weather-related inputs affecting energy consumption inside a building such as solar gains, exterior temperature and heating/cooling sources are cyclic phenomena and can be modelled by means of frequency domain techniques assuming periodic conditions in the calculations. There have been a number of studies on the application of frequency domain techniques to analyze building thermal dynamics and control applications including modelling and design of building-integrated thermal energy storage (BITES) (Chen et al. 2013a; Chen et al. 2013b). In the frequency domain approach, a thermal network for a zone is considered which represents the heat transfer between room surfaces, indoor and outdoor temperatures. Floor and all the other elements with significant thermal mass are modeled using the two-port Norton-equivalent representation. This representation gives an exact solution assuming 1-D heat conduction inside the wall (Athienitis et al. 1990).

A general form of a slab is shown in Figure 0-1 with two surfaces (exterior and interior) named surface 1 and 2. The derivation of the exact one-dimensional transient solution for this slab is presented.
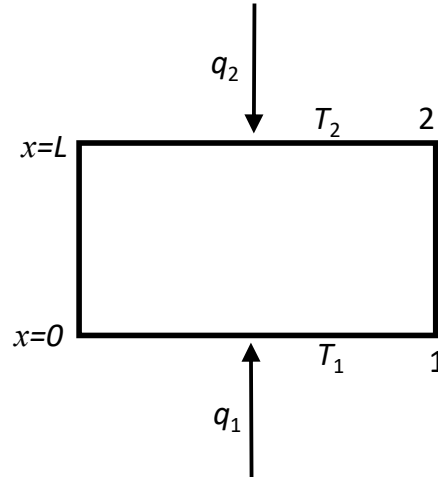
Figure 0-1. Schematic of a slab and interior & exterior surfaces temperatures and heat flows

For the sake of more details for radiant floors and de-icing slabs, the above slab can be shown as:
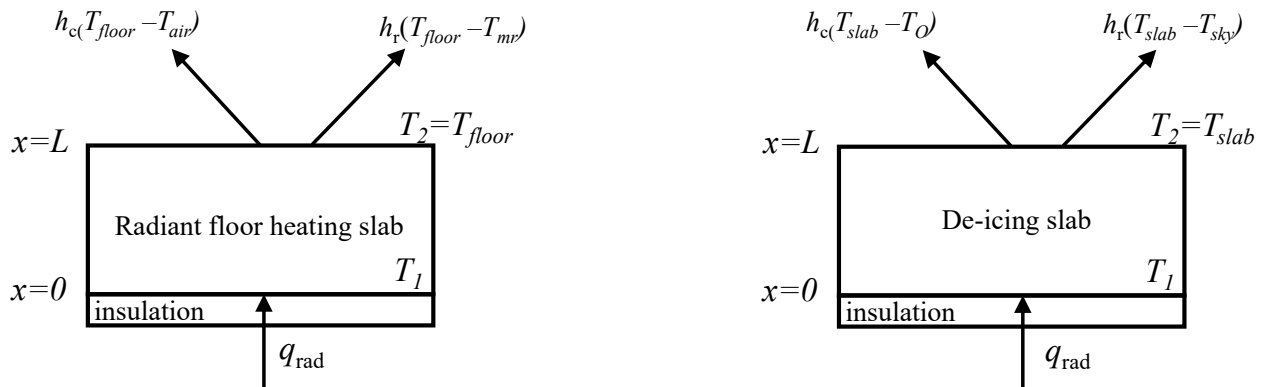
Figure 0-2. Schematic of a radiant floor heating and de-icing slab

The general form of heat diffusion equation can be written as (Lienhard 2003):

$$\frac{\partial^2 T(x,t)}{\partial x^2} + \frac{\partial^2 T(y,t)}{\partial y^2} + \frac{\partial^2 T(z,t)}{\partial z^2} + \frac{\dot{q}}{k} = \rho C_p \frac{\partial T(x,y,z,t)}{\partial t} \qquad (3.1)$$

Because the heat equation is second order in spatial coordinates, two boundary conditions must be expressed for each coordinate to describe the system. For the case of radiant floor, at the pipe level (bottom of the slab), two boundary conditions are usually of interest: 1. specified temperature source under the slab, 2. semi-infinite slab. Also, at the floor surface (T_{floor}) the energy balance equation gives the surface boundary condition which can be expressed as:

$$-k\frac{\partial T}{\partial x} = h_c(T_{floor} - T_{air}) + h_r(T_{floor} - T_{mr})$$

where h_c and h_r are convective and radiative heat transfer coefficients, respectively, T_{air} is the room air temperature (or outdoor air temperature, T_O, for de-icing applications) and T_{mr} would be a mean radiant temperature of the surfaces in a room or the sky temperature (T_{sky}) for de-icing applications. In some cases when T_{mr} is close to T_{air}, a combined film coefficient is used and the two terms above are combine into $h_o(T_{floor}-T_{air})$. In the analysis below this is the assumption.

Considering 1D heat transfer for the case when pipes are deep in the concrete, equation (3.1) can be written as:

$$\alpha\frac{\partial^2 T(x,t)}{\partial x^2} = \frac{\partial T(x,t)}{\partial t} \tag{3.2}$$

where α is thermal diffusivity ($k/\rho C_p$).Applying Laplace transform to the equation above assuming zero initial condition, transforms the partial differential equation to an ordinary differential equation (Kimura 1977):

$$\alpha\frac{\partial^2 T(x,s)}{\partial x^2} = sT(x,s) \tag{3.3}$$

for which the solution is obtained as:

$$T(x,s) = C_1 e^{\gamma x} + C_2 e^{-\gamma x} = M \cosh(\gamma x) + N \sinh(\gamma x) \qquad (3.4)$$

Where $\gamma = (s/\alpha)^{0.5}$. Then, for the heat flux:

$$q = -k\frac{dT}{dx} \Rightarrow q(x,s) = -Mk\gamma \sinh(\gamma x) - Nk\gamma \cosh(\gamma x) \qquad (3.5)$$

Applying last two equations to each surface gives:

$$\begin{cases} T_1 = T(x=0,s) = M \\ q_1 = q(x=0,s) = -Nk\gamma \\ T_2 = T(x=l,s) = M \cosh(\gamma l) + N \sinh(\gamma l) \\ q_2 = q(x=l,s) = Mk\gamma \sinh(\gamma l) + Nk\gamma \cosh(\gamma l) \end{cases}$$

or in matrix form it can be written as:

$$\begin{bmatrix} T_2 \\ q_2 \end{bmatrix} = \underbrace{\begin{bmatrix} \cosh(\gamma l) & -\sinh(\gamma l)/k\gamma \\ k\gamma \sinh(\gamma l) & -\cosh(\gamma l) \end{bmatrix}}_{TR} \begin{bmatrix} T_1 \\ q_1 \end{bmatrix} \qquad (3.6)$$

In equation (3.6), the matrix TR is the transmission matrix for the slab. Equation (3.6) is the exact theoretical solution for the one-dimensional heat transfer that relates the temperatures and heat fluxes on the two surfaces of the slab to each other.

Now equation (3.6) can be rearranged as:

$$\begin{bmatrix} q_1 \\ q_2 \end{bmatrix} = \begin{bmatrix} k\gamma/\tanh(\gamma l) & -k\gamma/\sinh(\gamma l) \\ -k\gamma/\sinh(\gamma l) & k\gamma/\tanh(\gamma l) \end{bmatrix} \begin{bmatrix} T_1 \\ T_2 \end{bmatrix} \qquad (3.7)$$

and the respective admittance transfer functions are obtained as (Athienitis 1994):

$$\text{(self-admittance)} \quad Y_{1,1} = \frac{q_1}{T_1} = \frac{k\gamma}{\tanh(\gamma l)} \quad (T_2 = 0) \qquad (3.8)$$

$$\text{(Transfer-admittance)} \quad Y_{1,2} = \frac{q_1}{T_2} = \frac{-k\gamma}{\sinh(\gamma l)} \quad (T_1 = 0) \tag{3.9}$$

If the transmission matrix in equation (3.6) is rewritten as:

$$\text{TR} = \begin{bmatrix} A & B \\ C & D \end{bmatrix}$$

then it can be shown that:

$$Y_{1,1} = D/B \ , \ Y_{1,2} = (BC - AD)/B \tag{3.10}$$

In the case when there is negligible thermal mass (an insulation layer) the TR matrix for the layer will be equal to:

$$\begin{bmatrix} 1 & 1/u \\ 0 & 1 \end{bmatrix}$$

where u is the insulation conductance. Therefore, in the case where there is an insulation layer on the exterior bottom surface of the slab, the transmission matrix will be equal to the product of the two transmission matrices:

$$\begin{bmatrix} \cosh(\gamma l) & \sinh(\gamma l)/k\gamma \\ k\gamma \sinh(\gamma l) & \cosh(\gamma l) \end{bmatrix} \begin{bmatrix} 1 & 1/u \\ 0 & 1 \end{bmatrix} \tag{3.11}$$

Then, the admittance transfer functions will be obtained as:

$$Y_{1,1} = \frac{u + k\gamma \tanh(\gamma l)}{\dfrac{u}{k\gamma} \tanh(\gamma l) + 1} \ , \ \text{Self admittance } (Y_s)$$

$$Y_{1,2} = \frac{-1}{\dfrac{\cosh(\gamma l)}{u} + \dfrac{\sinh(\gamma l)}{k\gamma}} \ , \text{Transfer admittance } (Y_t)$$

Then using the above transfer functions, the Norton-equivalent thermal network for a multilayered wall can be found as shown below (Athienitis and O'Brien 2015). The exact solution described above can also be used to calibrate low-order grey-box models. The details can be found at Appendix 1.
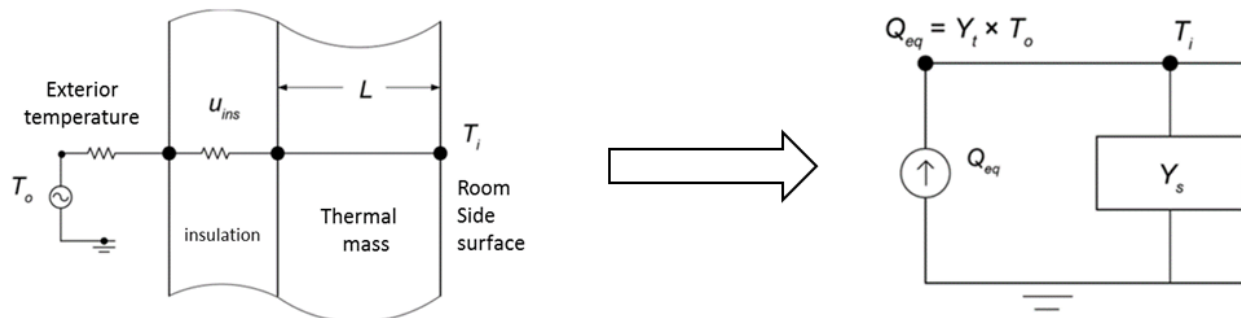
Figure 0-3. Norton-equivalent thermal network of a multi-layered wall

If there is no thermal mass (zero thermal capacity) then we obtain the simple equality $Y_s=-Y_t=Au_0$. A similar result is obtained for windows in eliminating all nodes exterior to the inner glazing. An important result is obtained for an infinitely thick wall or a wall with no heat loss at the back (adiabatic surface, or high amount of insulation $u_0=0$); in this case Y_s is given by:

$$Y_s = Ak\gamma \tanh(\gamma x) \tag{3.12}$$

Walls with thick massive layers have admittance which is close to that given by the above equation. When the penetration depth, given by:

$$d = \sqrt{2k / c_p \rho \omega} = \sqrt{2\alpha / \omega} \tag{3.13}$$

is significantly less than the wall thickness then, the wall behaves like a semi-infinite solid. The magnitude. Phase angle (and time lag/lead) of a transfer function such as Y_s and Y_t is computed by means of complex variables.

The level of detail in the thermal network depends on how radiation and convection heat transfer are modeled in the room interior zone. Combined radiative-convective heat transfer coefficients are often assumed which can be represented by a star network as shown in Figure 0-4.a. This network is used when there are small differences between the surfaces and room air temperature and when the heating source is mainly convective. However, in zones with high level of solar gains or in rooms with radiant heating systems, using combined heat transfer coefficients can produce significant error in the results (Athienitis and O'Brien 2015). In those cases, convective and radiative heat transfer needs to be modeled separately (Figure 0-4.b).

The convective and radiative coefficients are calculated as:

$$\text{Convective } U_{i1} = A_i h_{c,i} \text{ , Radiative } U_{ij} = A_i F_{ij}^*(4\sigma T_m^3)$$

where A_i=area of surface i, $h_{c,i}$=convective heat transfer coefficients of surface i,

F_{ij}^*=radiant heat exchange factor between surfaces i and j and,

$F_{ij}^* = m(i,j)\varepsilon_i\varepsilon_j/\rho_i$, where $m=M^{-1}$, the elements of matrix M are given by: $M(i,j)=I(i,j)-\rho_i F(i,j)$, with $I(i,j)=1$ if i=j, otherwise, $I(i,j)=0$ (I is the identity matrix).

T_m= estimated mean temperature.

It should be noted that convective and radiative heat transfer are inherently nonlinear process and the respective heat transfer coefficients are usually linearized so that the system energy balance equations can be solved by direct linear algebra techniques and possibly represented by a linear thermal network. Linearization generally introduces less error for long-wave radiant exchanges between surfaces than convection between room surfaces and room air (Athienitis and O'Brien 2015). In some cases heat flow reversal can occur such as between a cold floor and warm air when convective heat transfer coefficient can be of order of $1W/m^2K$ versus $3W/m^2K$ for a heated floor and cold air (Athienitis and O'Brien 2015).
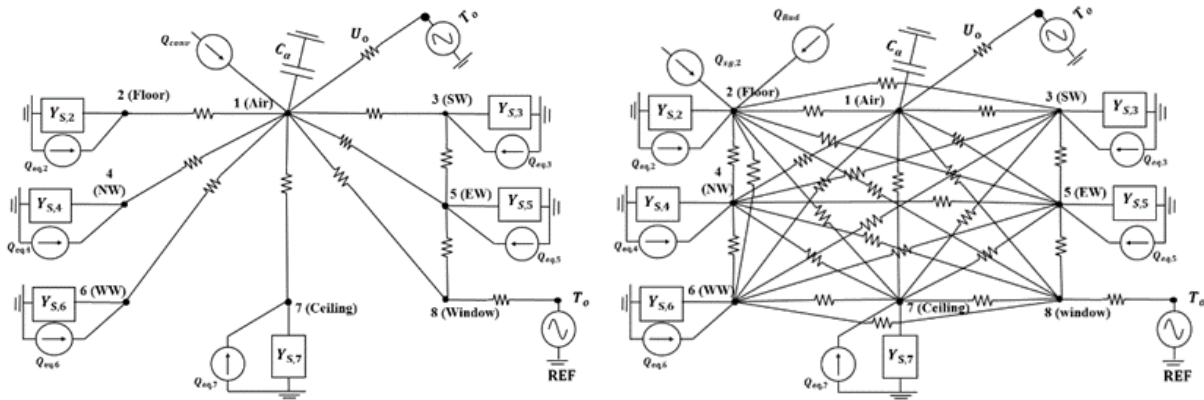
Figure 0-4. Thermal network for frequency domain considering a) combined heat transfer coefficients (left), b) separate modelling of convective and radiative exchanges (right).

In the thermal networks shown in Figure 0-4, all the walls and elements with thermal mass are modelled using the two-port Norton-equivalent subnetwork which consists of the wall self-admittance, Y_s, and an equivalent source, $Q_{eq}=Y_t \times T_{ext}$, which represents the effect of an external temperature on the surface temperature. This representation eliminates all the middles nodes of the wall and gives an exact solution for one-dimensional heat conduction inside the wall without spatial discretization.

41

For the detailed frequency domain model for which the thermal network is shown in Figure 0-4.b., node (1) represents the air inside the zone. Then, energy balance at node (1) gives:

$$C_a \frac{dT_1}{dt} + U_o(T_1 - T_o) + \sum_{J1} U_{1,J1}(T_1 - T_{J1}) = Q_{aux} \tag{3.14}$$

In which $U_{1,J1}$ are the convective conductances between the air node and other surfaces (J1=2, 3,…,8), C_a is the thermal capacitance of the room air, T is temperature and Q_{aux} is the auxiliary source at the air node (which can be equal to zero). Using Laplace transform, equation (3.14) will be:

$$sC_a T_1(s) + U_o T_1(s) + \sum_{J1} U_{1,J1}(T_1(s) - T_{J1}(s)) = \underbrace{Q_{aux}(s) + \underbrace{U_o T_o(s)}_{Q_{eq}}}_{Q_1} \tag{3.15}$$

where s is the Laplace variable. Now, considering the floor (node (2)), the energy balance equation yields:

$$Y_{s,2}(T_2(s) - \underbrace{T_{ref}(s)}_{= 0\,°C}) + \sum_{J2} U_{2,J2}(T_2(s) - T_{J2}(s)) = \underbrace{\underbrace{Q_{sg,2}}_{\text{solar gain}} + Q_{eq,2} + \underbrace{Q_{rad,2}}_{\substack{\text{radiant} \\ \text{source}}}}_{Q_2} \tag{3.16}$$

where J2=1,3,4,…,8 and $U_{2,J2}$ are the radiative conductances between floor and other surfaces. The energy balance for all the nodes can be written in the form below:

$$\begin{bmatrix} sC_a+\sum_j U_{1,j}+U_{inf} & -U_{1,2} & -U_{1,3} & -U_{1,4} & -U_{1,5} & -U_{1,6} & -U_{1,7} & -U_{1,8} \\ -U_{1,2} & Y_{s,2}+\sum_j U_{2,j} & -U_{2,3} & -U_{2,4} & -U_{2,5} & -U_{2,6} & -U_{2,7} & -U_{2,8} \\ -U_{1,3} & -U_{2,3} & Y_{s,3}+\sum_j U_{3,j} & -U_{3,4} & -U_{3,5} & -U_{3,6} & -U_{3,7} & -U_{3,8} \\ -U_{1,4} & -U_{2,4} & -U_{3,4} & Y_{s,4}+\sum_j U_{4,j} & -U_{4,5} & -U_{4,6} & -U_{4,7} & -U_{4,8} \\ -U_{1,5} & -U_{2,5} & -U_{3,5} & -U_{4,5} & Y_{s,5}+\sum_j U_{5,j} & -U_{5,6} & -U_{5,7} & -U_{5,8} \\ -U_{1,6} & -U_{2,6} & -U_{3,6} & -U_{4,6} & -U_{5,6} & Y_{s,6}+\sum_j U_{6,j} & -U_{6,7} & -U_{6,8} \\ -U_{1,7} & -U_{2,7} & -U_{3,7} & -U_{4,7} & -U_{5,7} & -U_{6,7} & Y_{s,7}+\sum_j U_{7,j} & -U_{7,8} \\ -U_{1,8} & -U_{2,8} & -U_{3,8} & -U_{4,8} & -U_{5,8} & -U_{6,8} & -U_{7,8} & \sum_j U_{8,j} \end{bmatrix}_{\mathbf{Y}} \begin{bmatrix} T_1 \\ T_2 \\ T_3 \\ T_4 \\ T_5 \\ T_6 \\ T_7 \\ T_8 \end{bmatrix}_{\mathbf{T}} = \begin{bmatrix} Q_1 \\ Q_2 \\ Q_3 \\ Q_4 \\ Q_5 \\ Q_6 \\ Q_7 \\ Q_8 \end{bmatrix}_{\mathbf{Q}}$$

or :

$$\mathbf{Y}_{8\times8}\,\mathbf{T}_{8\times1} = \mathbf{Q}_{8\times1} \tag{3.17}$$

where, Y is the admittance matrix, T is the temperature vector and Q is the source vector. Elements of equation (3.17) are in terms of the Laplace variable s and can be calculated at different frequencies ($s = j\omega_n$, $j=\sqrt{(-1)}$, $\omega_n=2\pi n/p$, $p = 24$ h, $n =$ harmonic number). An important parameter is the impedance matrix $\mathbf{Z}=\mathbf{Y}^{-1}$ which contains building transfer functions at different frequencies:

$$Z_{i,j} = \frac{T_i}{Q_j} \qquad \rightarrow \qquad Z_{1,1} = \frac{T_1}{Q_1}\,, \quad Z_{1,2} = \frac{T_1}{Q_2}\,, \ \ldots$$

The impedance transfer function represents change in temperature of node i resulting from the effect of the source Q_j at node j. Thus, considering equation(3.17), temperature of node i for each frequency will be calculated as:

$$T_i = \sum_{j=1}^{8} Z_{i,j}Q_j \tag{3.18}$$

Studying important building transfer function provides much insight into building thermal dynamics and design alternatives can be evaluated on a relative basis without detailed simulations.

3.2.1 Derivation of the New Transfer Function $Z_{1,aux}$[6]

Previous section presented the existing frequency domain modeling technique from the previous author research work and other works in literature. This section presents a new transfer function that is derived from the frequency domain model of a zone with hydronic floor heating system. This is a useful transfer function that determines the effect of the radiant floor heating on the zone air temperature and it cannot be automatically calculated from the impedance matrix. Therefore, derivation of this transfer function for the case when the floor-heating pipes are at the bottom of the slab is presented below.

As mentioned in the previous section, $Z_{1,2}$ is the transfer function between the zone air temperature and the source at node 2 (floor surface), $Z_{1,2} = T_1/Q_2$. The source Q_2 represents the summation of all the heating sources that are present at node 2 including solar radiation and the effect of the radiant floor heating when transferred to the surface of the floor (Q_{rad}). Therefore, it can be written as:

$$Q_2 = Q_{sg,2} + Q_{rad} \qquad (3.19)$$

where $Q_{sg,2}$ represents the floor solar gain and Q_{rad} is the equivalent (transferred) heat source due to floor heating (Q_{aux}) at the surface. Figure 0-5 shows the schematic of the floor with the heat sources.

---

[6] based on journal paper #1: Saberi Derakhtenjani, Ali, Athienitis, Andreas K. (2020)." A Frequency Domain Transfer Function Methodology for Thermal Characterization and Design for Energy Flexibility of Zones with Radiant Systems". Journal of Renewable Energy, 163:1033-1045
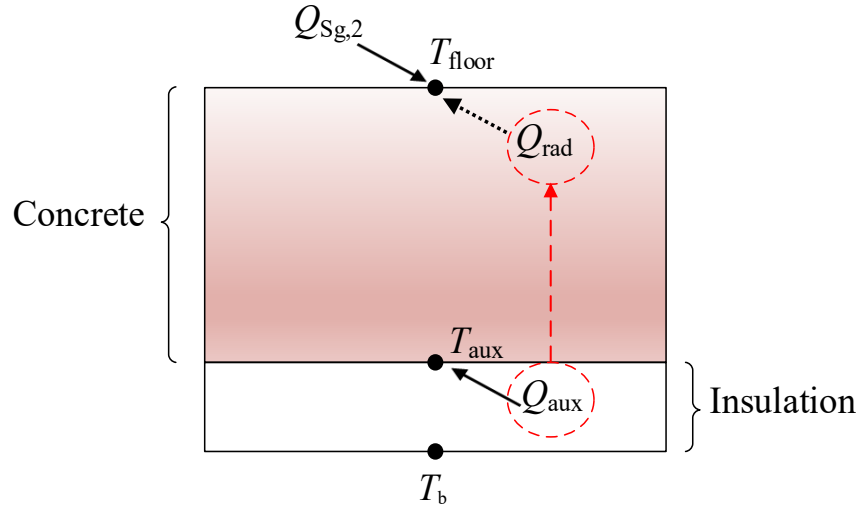
Figure 0-5. Schematic of floor heating

In the frequency domain modelling methodology explained earlier, by using the Norton-equivalent representation all the intermediate nodes were eliminated and the effect of the external temperature, which can be the basement temperature for example, was represented by the equivalent source $Q_{eq} = -Y_t \times T_b$ (please see the appendix for more details). Here, since the pipes are located at the bottom and the auxiliary heating source is at the bottom of the floor slab, using the energy balance equation, the temperature of node T_{aux} can be represented as an equivalent temperature (similar to sol-air temperature):

$$T_{aux} = T_b + Q_{aux} \frac{R_{ins}}{A_2}, \quad A_2 = \text{floor area} \qquad (3.20)$$

Therefore, by means of equation(3.20), T_{aux} can be considered as the external and equivalent temperature and by using the transfer admittance of the floor, the equivalent source representing the effect of the basement temperature and the auxiliary load on the floor surface temperature is defined as:

$$Q_{rad} = Q_{eq} = -Y_t(T_{aux}) = -Y_t(T_b + Q_{aux}\frac{R_{ins}}{A_2}) \qquad (3.21)$$

and it is known from the definition that:

$$Z_{1,2} = \frac{T_1}{Q_{sg,2} + Q_{rad}} = \frac{T_1}{Q_{sg,2} - Y_{t,2}(T_b + Q_{aux}\frac{R_{ins}}{A_2})} \qquad (3.22)$$

$$T_1 = Z_{1,2}(Q_{sg,2}) + Z_{1,2}(-Y_{t,2}T_b) + Z_{1,2}(-Y_{t,2}Q_{aux}\frac{R_{ins}}{A_2}) \qquad (3.23)$$

Now, in the above equation let us put all the sources to zero except Q_{aux}. Then:

$$Z_{1,aux} = \frac{T_1}{Q_{aux}} = Z_{1,2}\left[\frac{-Y_{t,2}R_{ins}}{A_2}\right] \qquad (3.24)$$

Equation (3.24) is used to calculate transfer function $Z_{1,aux}$ at different frequencies with which the effect of radiant floor heating source on the room air temperature can be studied. A similar approach can be used for the zone operative temperature. In the following sections application of this transfer function for the case study is presented.

3.2.2   Limitations of frequency domain techniques

Generally, the main advantage of frequency domain techniques is comparing different designs on a relative basis. However, since this is a linear approach, it is not a suitable method to model **non-linearity** and **variables that change over time**. That is the reason that time domain models are used for building thermal simulations to deal with non-linearities and variables that change with time. Time domain techniques are the most commonly used approaches in building energy simulation tools, in which the calculations are made from one time step to the next. As an example, in time domain approach, equation (3.14) is discretized in time and is written as:

$$C_a \frac{\Delta T_1}{\Delta t} + U_o(T_1 - T_o) + \sum_{J1} U_{1,J1}(T_1 - T_{J1}) = Q_{aux} \tag{3.25}$$

Where ΔT_1 is the difference of temperature T_1 between two time steps: $\Delta T_1 = T_1^{p+1} - T_1^p$, with p being the time step. Also, other nodes with thermal mass are modeled using the lumped capacitances. Models with fewer parameters facilitate setting-up initial conditions which is a key consideration in controls. In the next section the development of low-order models for the case study is discussed.

Radiant floor heating systems (RFH) have been receiving considerable attention recently due to the multiple advantages they offer such as improved thermal comfort and lower energy consumption. Recent research has been done on operation and control of different types of radiant floors including electrical floor heating systems (Thieblemont et al. 2018) as well as hydronic. The use of radiant heating leads to improvement in the efficiency of low-temperature heat sources: condensing oil or gas boilers, heat pumps and solar collectors assuring lower fuel or electric energy consumption (Werner Juszczuk 2018). Moreover, radiant systems operate quietly and save space. However, compared to conventional systems, radiant systems has several added complexities such as the delayed transient heat conduction within the system itself, combined surface convection and radiation from/to the system, and a drastically different resulting thermal environment, which make them difficult to model and integrate in a comprehensive simulation. Various modeling techniques can be used to study RFHs (Rey et al. 2018). However, there is still a need for rapid development of low-order thermal models which facilitate the design and application of control strategies for hydronic floor heating systems.

3.3 Low-order thermal model for hydronic system[7]

The low-order Lumped Parameter Finite Difference (LPFD) Models, developed and used for this study, have been shown to be suitable for MPC applications (Candanedo et al. 2013; Cole et al. 2014). The order of the model is chosen depending on the objectives of the study and the frequency domain techniques can be utilized in determining the appropriate order of LPFD models (Saberi Derakhtenjani et al. 2015). In frequency domain, the magnitude and phase angles of the important transfer functions of the LPFD model can be compared with the ones from the exact solution. Then, the LPFD model parameters calibration is done accordingly to match the magnitude and phase angle of the transfer functions.

In the LPFD approach, the volume under consideration is discretized into a number of sub-layers. Each of those discretized control volumes is represented by a node and considered to be isothermal. Each of the nodes, has a lumped thermal capacitance connected to it and thermal conductances connecting it to adjacent nodes. This type of models are also called resistance-capacitance (RC) thermal network models. This approach is valid when the so-called Biot number is less than 0.1 (*Bi*<0.1). Values of the Biot number smaller than 0.1 imply that the heat conduction inside the body is much faster than the heat convection away from its surface, and temperature gradients are negligible inside of it and typically indicates less than 5% error will be present when assuming a lumped-capacitance model of transient heat transfer (Incropera et al. 2006).

Figure 0-6 shows thermal the network representation for the second-order and fourth-order lumped capacitance model of a concrete slab with insulation under the bottom of the slab. Considering the

---

[7] based on journal paper #2

time interval p and time step Δt, the general form of the explicit finite-difference model for the nodes with a lumped thermal capacitance can be stated as (Athienitis 1994):

$$T_{i,p+1} = T_{i,p} + \frac{\Delta t}{C_i}\left(Q_i + \sum_j \frac{T_{j,p} - T_{i,p}}{R_{i,j}} \right) \tag{3.26}$$
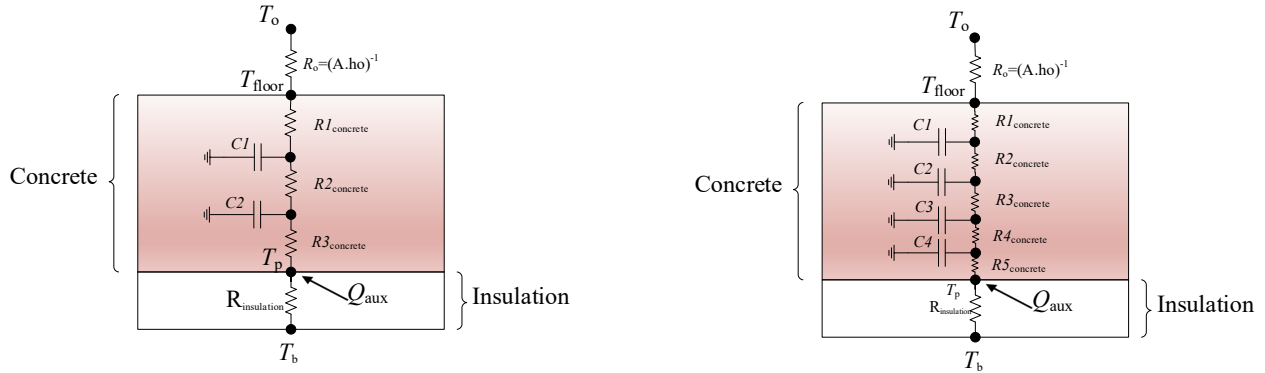
Figure 0-6. Second-order (left) and fourth-order (right) thermal network models

where $T_{i,p}$ represents the temperature of node "i" at time step "p", $T_{j,p}$ represents temperature of node "j" at time step "p", C_i is the thermal capacitance of node "i", $R_{i,j}$ is the thermal resistance between nodes i and j and Q_i is the heat source at node i. In the above thermal networks (Figure 0-6), Q_{aux} is the heat from the hydronic system of the radiant slab. Q_{aux} is controlled by the slab surface temperature setpoint or in some cases with by the zone air temperature setpoint, for example through proportional control as: $Q_{aux}=Kp(T_{sp}-T_{floor})$. Kp is the proportional control constant and T_{sp} and T_{floor} are the setpoint and slab surface temperature respectively.

An important part of a model for zones with radiant floor heating system is the radiative and convective heat transfer which are inherently nonlinear processes. However, the respective heat transfer coefficients are usually linearized so that the system energy balance equations can be

solved with linear algebra techniques and represented with a linear thermal network. In the case of radiant floor heating, this linearization generally introduces less error for the for long-wave radiation heat transfer (h_r) than the convection heat exchange between the radiant floor surface and room air (h_{cf})(Athienitis and O'Brien 2015). For example, in the case of radiant floor heating where usually the floor is hotter than air and the heat flow is upward, h_{cf} is in the order of 3 W/m^{2}K while it is in the order of 1 W/m^{2}K for heat flow downwards (from warm air to a cold floor).

For heat flow upwards h_{cf} can be calculated as(ASHRAE 2017):

$$h_{cf}(t) = 1.52(T_{floor}(t) - T_{air}(t))^{1/3} \qquad (3.27)$$

where, T_{floor} is the floor surface temperature and T_{air} is the zone air temperature. Therefore, usually a certain amount of calibration for the convection heat exchange between the radiant floor and room air is required for a model especially when considering the low order models.

3.4 Hydronic floor and environmental chamber[8]

The second-order thermal network model (Figure 0-6) is validated against data from experiments performed in a test facility: the Solar Simulator-Environmental Chamber (SSEC laboratory at Concordia University), shown in Figure 0-7, in which temperature can be controlled between -40ºC and +50ºC with any desired profile.

---

[8] based on journal paper #2: Saberi Derakhtenjani, Ali, Athienitis, Andreas K. (2020)." A numerical and experimental study of hydronic de-icing and its predictive control". Submitted to ASHRAE journal of Science and Technology for the Built Environment, under review
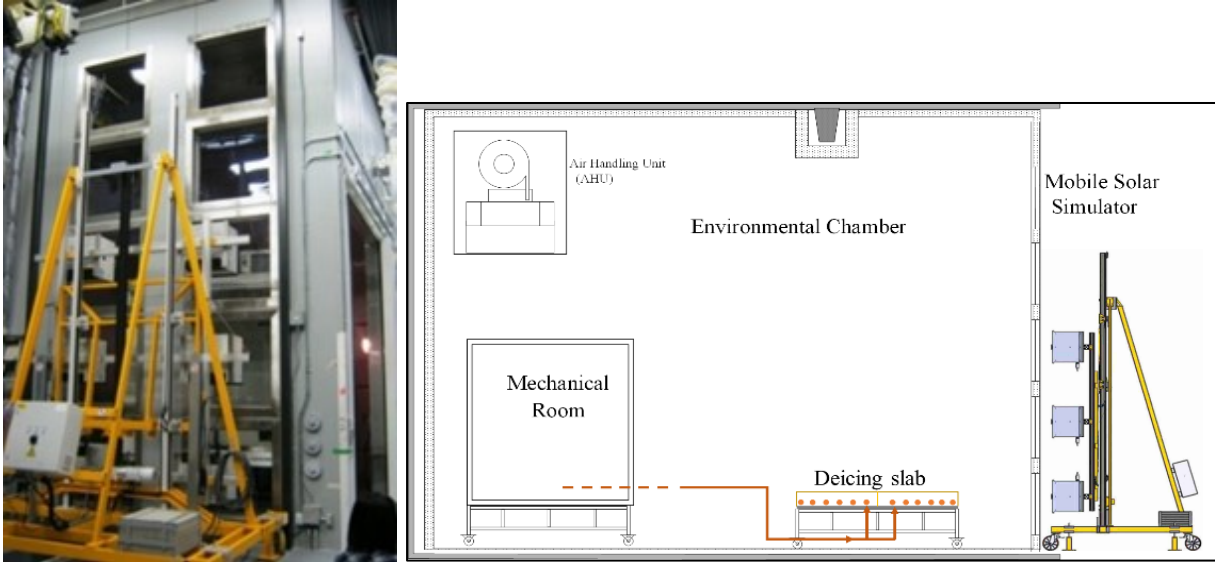
Figure 0-7. Solar simulator/ environmental chamber facility with schematic

A radiant floor system was installed inside the Solar Simulator/Environmental Chamber (SSEC) facility so that it could be tested under typical winter conditions. Figure 0-8 shows the piping configuration of the radiant floor before the concrete was poured (left) and a final photo of the radiant floor slab (right). Figure 0-9 shows a schematic cross-section of the radiant floor, indicating more details of the piping layout.
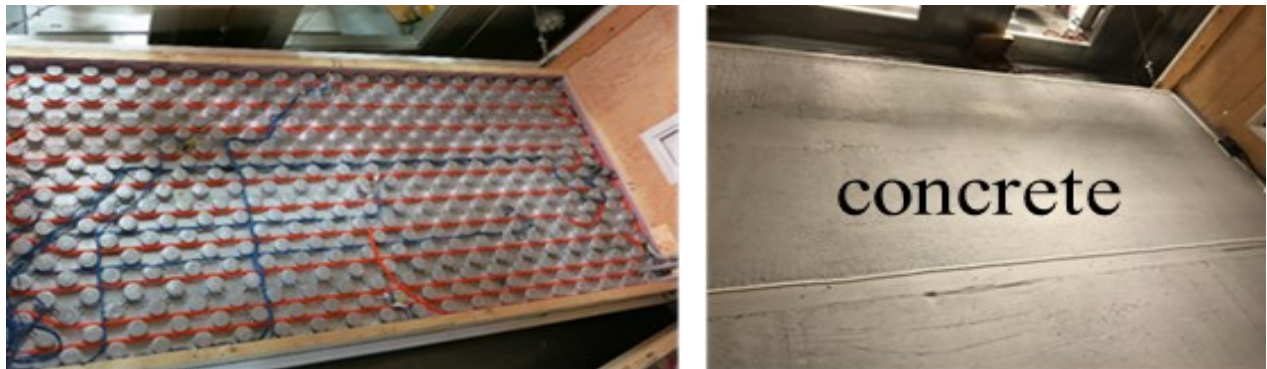
Figure 0-8. Radiant floor before (left) and after (right) pouring the concrete
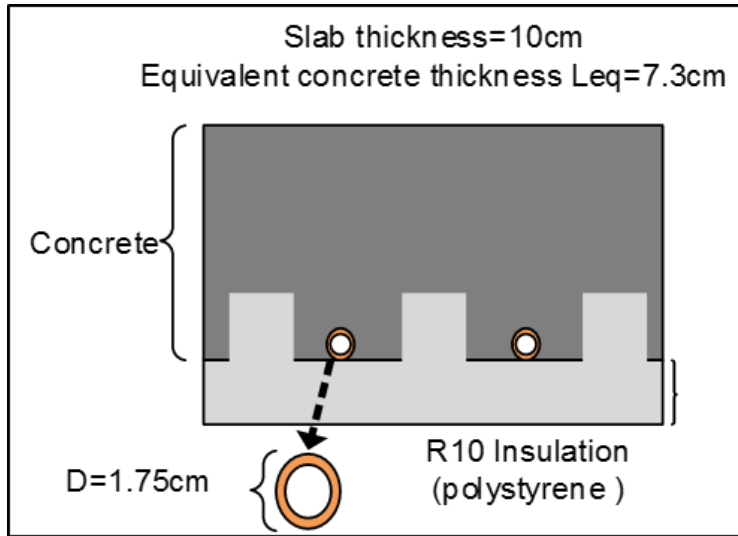
Figure 0-9. Radiant floor schematic

The pipes of the radiant floor system are made of conventional cross-linked polyethylene (PEX) and have an internal diameter of ½" (12.7 mm), with a wall thickness of 1/16" (1.59 mm). The pipes are installed in a "foam matrix" of insulating material that also facilitates keeping them in place. The pipes have an approximate separation of 15cm. A mechanical room in the environmental chamber provides controlled flow rate of fluid (propylene-glycol and water mixture) for the radiant floor.

The working fluid for the hydronic system is a propylene-glycol and water mixture (50%). A test was performed with this system at cold temperatures representative of winter conditions in the region. The test was used to analyze the thermal performance of the hydronic system in cold temperatures and also to calibrate and validate the lumped capacitance model of the slab. During the test, the environmental chamber temperature was set to -4 ºC and after reaching steady-state, the hydronic floor radiant system was started with a supply temperature of 37 ºC and a flowrate of about 0.5 gpm as shown in Figure 0-10.
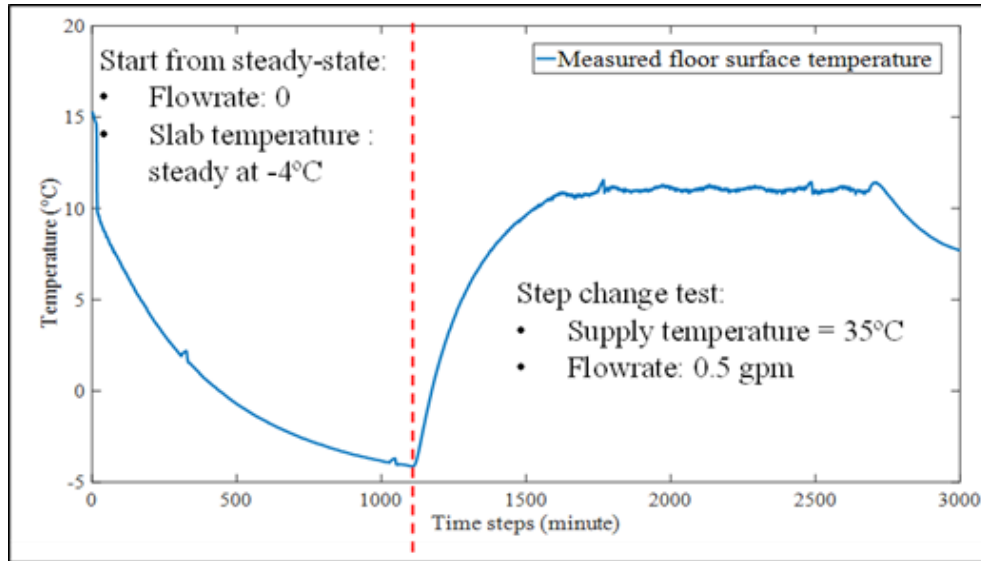
Figure 0-10. Measured floor surface temperature

Results from tests show that the surface temperature of the floor is relatively uniform, with temperature variation of ±0.5°C, once it has reached steady-state after the hydronic system has been active for about eight hours (Figure 0-11).Therefore, at that point the major part of the heat transfer can be considered to be one dimensional (1D).

The floor surface temperature was measured by taping a type T thermocouple sensor (accuracy: ± 0.5º) to the center of the floor. An ultrasonic flowmeter (accuracy: ±2% for 100:1 turndown ratio) was used to measure the flowrate.
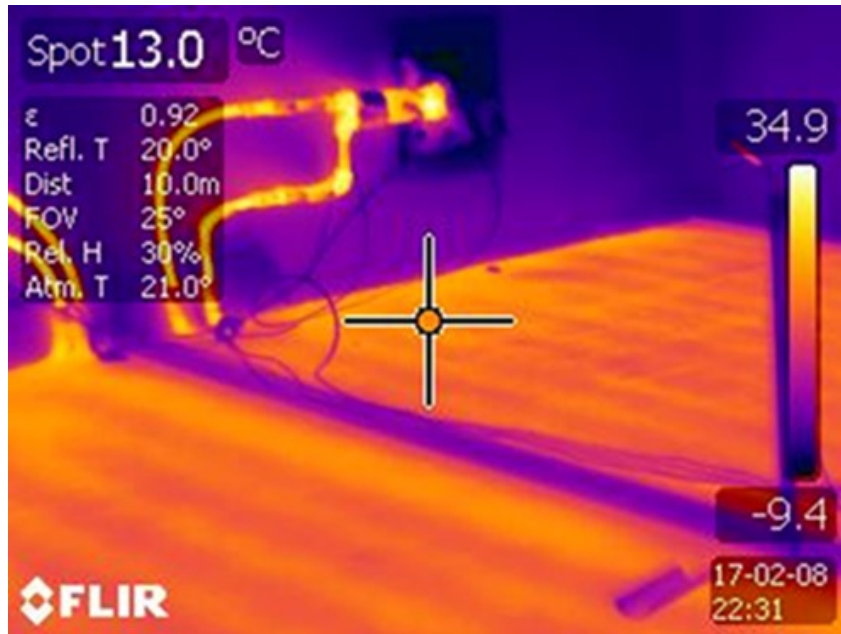
Figure 0-11. Thermographic photo of floor surface temperature at steady-state

3.4.1 Sensitivity analysis to heat transfer coefficients

One of the main assumptions considered in the low-order RC models is using the combined radiative/convective surface heat transfer coefficient (h_o). In some cases, if more information is available and more details are required then separate modeling of the convective (h_c) and radiative (h_r) coefficients can be considered (for example, the radiation heat transfer between the surface and sky in the case of a de-icing slab). The surface film coefficient (h_o) changes over time which is an important consideration in calibration of low-order models against experimental measurements. Figure 0-12 shows a sensitivity analysis and the result of considering different values for surface film coefficient for the second-order RC model.
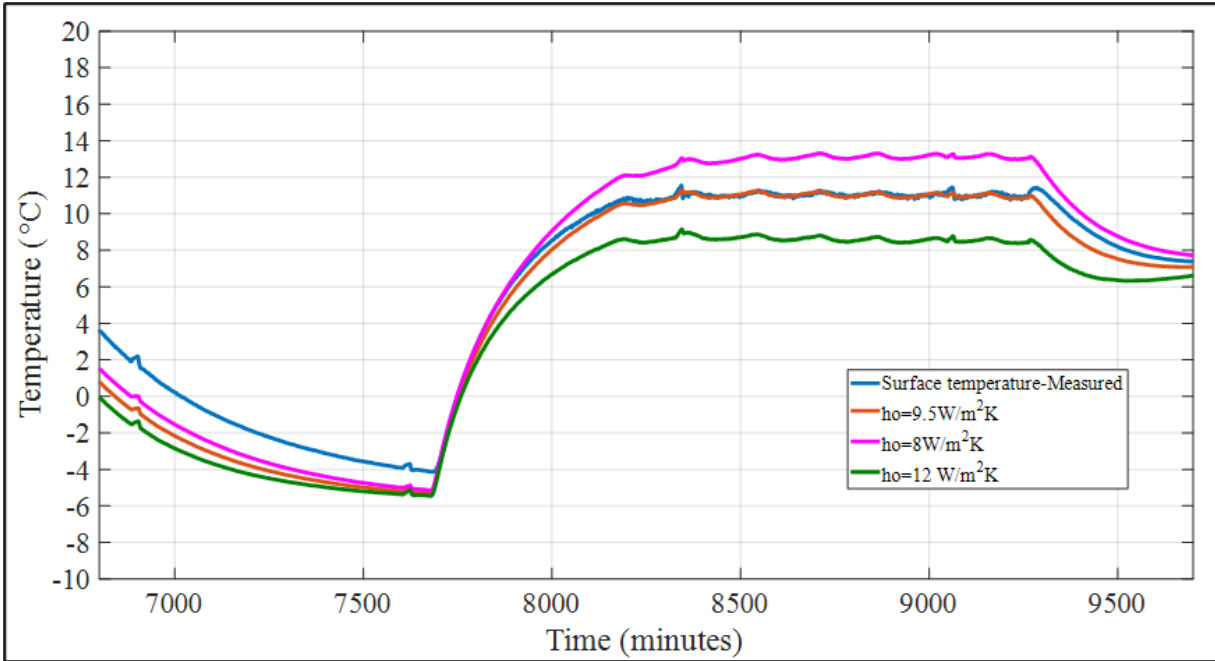
Figure 0-12. Comparing models results with considering different values for surface film coefficient

As observed from Figure 0-12, considering only one value for h_o for the total duration of the experiment does not give acceptable results and different values should be used for different parts of the experiment. As shown in Figure 0-13, while having the chamber cooled down and before running the hot liquid in the hydronic floor piping, since all the surfaces were at the same temperature, there was not much radiation heat transfer happening and the majority of the heat transfer was due to convection thus giving the total floor film coefficient of about 5 W/m^2K. Then, when the hot liquid starts to run in the hydronic piping, the radiation heat transfer becomes more significant and the total surface film coefficient of 9.5W/m^2K is applicable.

Figure 0-13 shows the floor surface temperature calculated with the calibrated second-order finite difference model compared with the experimental measurements. It can be observed that the

calibrated second order finite difference model, for which the thermal network is shown in Figure 0-6, matches well with measurements.
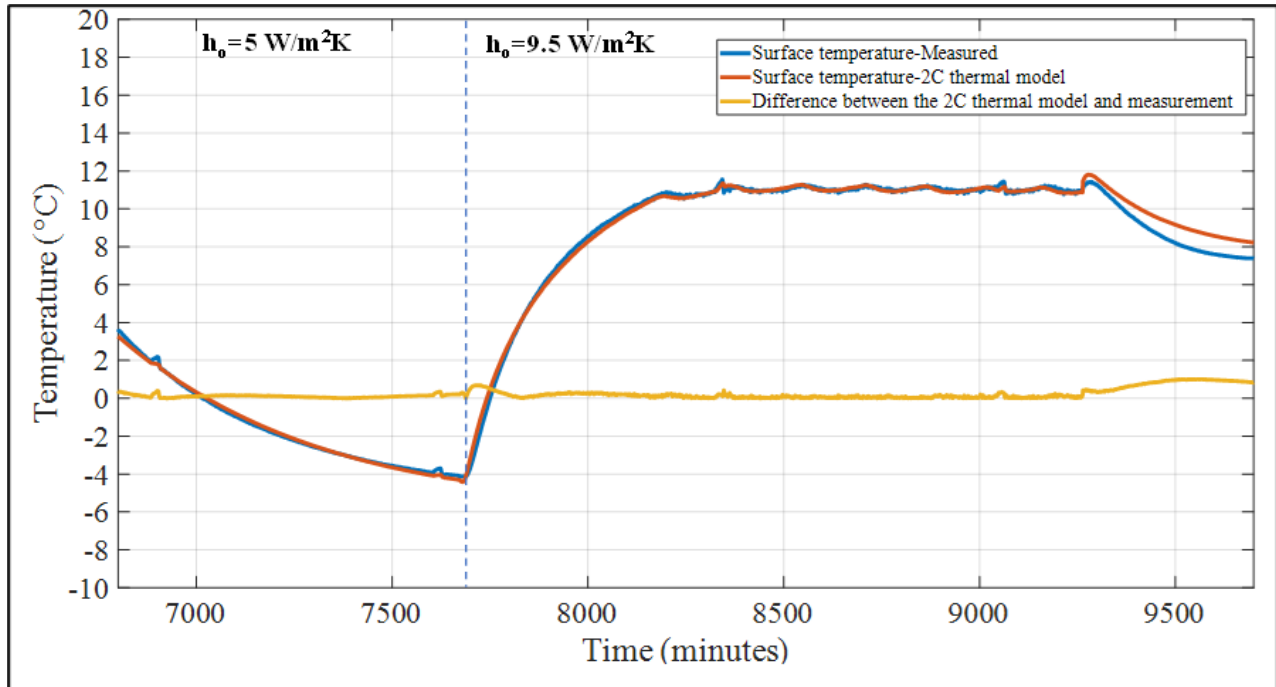
Figure 0-13. Comparison of the thermal model simulation results with experimental results

A sensitivity analysis was conducted to verify if significantly more accuracy can be obtained by considering smaller control volumes using a 4th order model (4 capacitances). As shown in Figure 0-14, there is no significant improvement in terms of accuracy between the second-order the fourth-order models and the second-order model gives enough resolution in terms of discretization for this thickness of concrete.
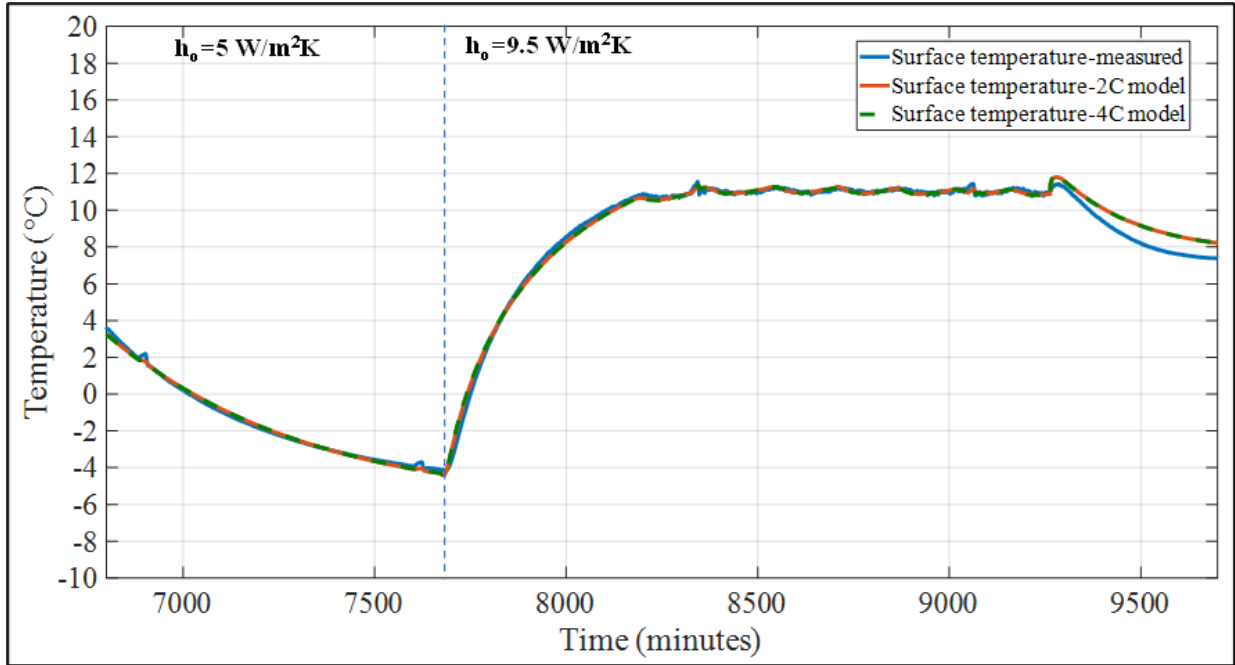
Figure 0-14.Comparison of second-order and fourth-order models with experiment

3.4.2 Comparison with a detailed 3D model

Figure 0-15 compares the experimental data with the results of the COMSOL model, and the results of the RC network with three different heat transfer coefficients (Candanedo et al. 2018a). It is observed that the well-calibrated 1D low-order RC model performs very well compared to the 3D COMSOL model. More details on this study can be found on Appendix 2.
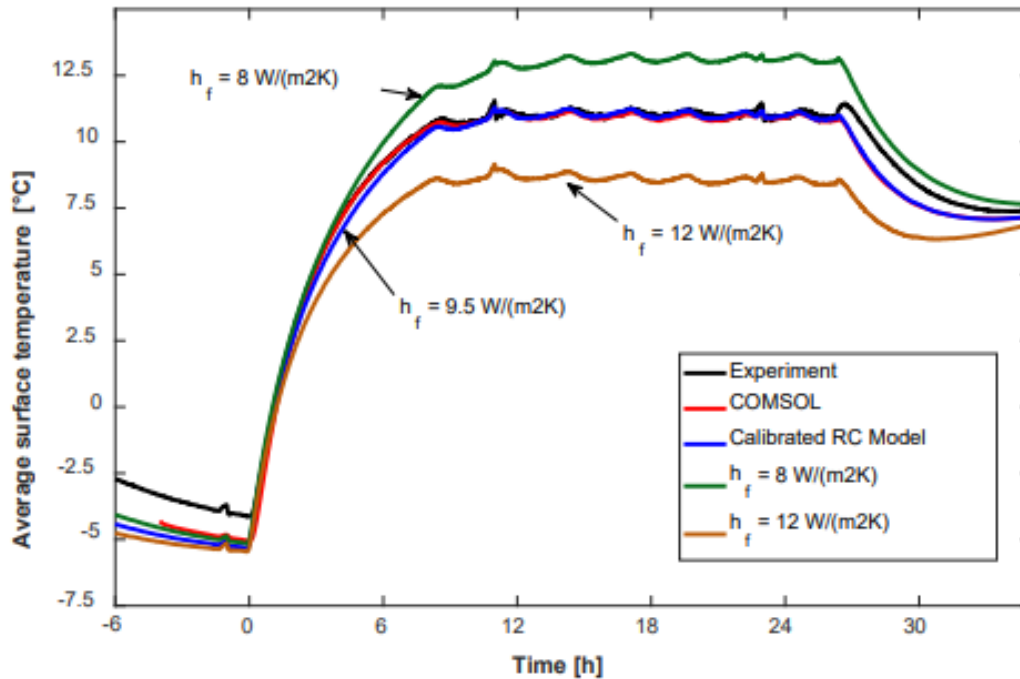
Figure 0-15. Comparison of 3D COMSOL model, experiment and the 2nd order RC model

This study shows that a simple 2nd order finite difference model can be quite adequate for the purpose of calculating a particular variable of interest (in this case, the temperature of the floor surface). The information obtained by performing parametric runs with a detailed model can aid with the rapid derivation of low-order models. This being said, a low-order model will almost always need the calibration, especially considering the complexity of heat transfer at the surface of the floor. A low-order RC model is also useful since it provides significant insight in the physics of the problem (time constants, delays, rule-based control, etc.). This RC model could be readily incorporated into advanced control algorithms, either in its finite difference formulation or a state-space equivalent.

Therefore, as observed from the comparison with experiment, the low-order 1D RC model is suitable for predicting the dynamic thermal response of radiant slab heating and de-icing slab

systems. Thus, the same type of 1D RC models which are validated and shown to be suitable for the purpose of this study are developed and utilized for infrastructure de-icing system.

3.5 Summary

This chapter presented the modeling methodologies utilized in this thesis. In the first section, utilization of thermal models for different applications was presented and major assumptions were discussed. In the next section frequency domain techniques were presented and the advantages as well as limitations of this approach were discussed. A new transfer function that is practical for radiant floor heating systems was presented and its derivation was demonstrated and in the following sections its application to a case study was presented. This transfer function is a major contribution of this thesis for frequency domain modeling of the zones with radiant floor heating systems.

In the next section 1D low-order grey box modeling (time domain) for zones with radiant heating systems was presented and it was demonstrated that a well-calibrated 1D model can be accurate enough for studying high mass radiant systems. By means of experimental measurements, the 1D model was compared to a 3D model and it was demonstrated that with appropriate calibration the 1D model can perform as good as the super-detailed 3D model. It was observed that the main parameter to calibrate is the heat transfer coefficient between the floor surface and the air in the zone. Therefore, considering numerous advantages of low-order models, these types of models can be efficiently and rapidly used for control studies in the zone with high mass radiant floor heating systems.

In the next chapter, results of application of the modeling approaches to case studies are demonstrated.

CHAPTER 4: NUMERICAL AND EXPERIMENTAL RESULTS

This section presents results for application of the methodology to the case studies. The first section presents the model development for hydronic de-icing slabs. Then predictive control strategies for different piping configuration and important scenarios are presented. The next section present results for an experimental case study - a perimeter zone test cell, which is a typical individual office-size zone located inside an environmental chamber (SSEC lab) with a controlled simulated outdoor environment. The energy flexibility quantification of the case study through experimental measurements is presented. Then predictive control results with consideration of dynamic electricity pricing are presented.

4.1 Analysis of thermal dynamics of hydronic de-icing system designs by means of control-oriented thermal models[9]

A hydronic road de-icing system provides an opportunity to take advantage of the slab's thermal mass for short-term thermal storage which is useful for keeping the slab surface at a certain temperature while lowering the energy consumption. Various piping depths can be of interest depending on the requirements of the infrastructure. For example, if pipes are installed close to the surface, they can capture the solar radiation and the hydronic system's reaction time will be shorter compared to deeper positioned pipes. However, there will be more stress on the pipes from the cars and trucks and higher risk of pipe damages and the concrete cracking due to the passing traffic. On the other hand, increased pipe depth provides the opportunity to store excess heat to be released in periods of high demand to shift and/or reduce the peak load.

---

[9] based on journal paper #2: Saberi Derakhtenjani, Ali, Athienitis, Andreas K. (2020)." A numerical and experimental study of hydronic de-icing and its predictive control". Submitted to ASHRAE journal of Science and Technology for the Built Environment, under review

4.1.1 Assumptions and limitation of the study presented in this thesis

The study that is presented in the following sections for the de-icing slab, are under the cloudy day assumption. Therefore, no solar radiation is considered in this study. Also, it was assumed that the sky temperature is close to ambient temperature. Hence, a combined convective/radiative film coefficient was used between the slab surface and the ambient air temperature. Also, it should be noted that the aim of the research presented here is preheating the slab to get to above the freezing point before the precipitation event to avoid the ice formation. Under these conditions no ice or snow melting would be needed and any significant snow accumulation would be removed by snowplows.

The case study is a major transportation infrastructure located in Montreal, Quebec-the Louis-Hippolyte Lafontaine (LHL) Tunnel. This tunnel connects the Montreal borough of Mercier-Hochelaga-Maisonneuve with the south-shore of the river at Longueil, Quebec and carries 120,000 vehicles a day[10].

Figure 0-1. LHL tunnel in different seasons[10]

In this study, the thickness of the concrete slab is imposed by the structural requirements of typical major freeways with significant traffic. An overall slab thickness of 35 cm was considered. The

---

effect of different piping depths on the de-icing system's thermal performance was evaluated by means of the 1D finite difference model presented in the previous sections. Two different depths were considered for the pipes: 17.5 cm (middle) and 35 cm (bottom) as shown in Figure 0-2. The bottom of the slab was assumed to be insulated with a layer of R10 (RSI 1.76 m²W/K) insulation.
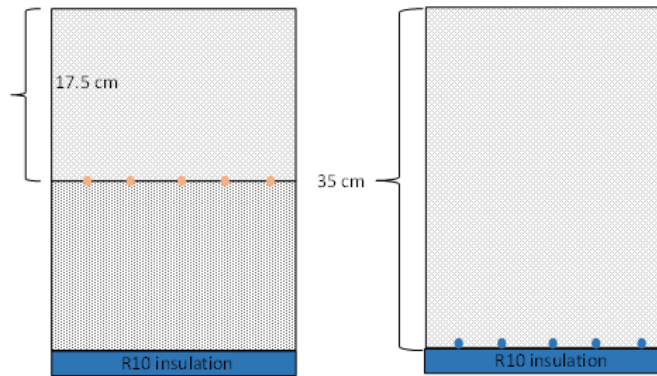
Figure 0-2. Different piping depth for the road concrete slab

A constant ground temperature of 7 ºC was assumed as a boundary condition for the model based on the assumption that prolonged heating would also keep the ground under it relatively warm. Simulations with lower bottom boundary condition (down to 2º C) showed that it had no significant impact on the results. Thermal properties of concrete are shown in Table 0-1.

Table 0-1. Thermal properties of concrete

Properties	
Thermal conductivity	1.7 W/m-K
Specific heat	800 J/kg-K
Density	2010 kg/m³

In the previous section it was shown that a second order (two-capacitance) RC model was able to model the dynamics of a 7.3cm thick concrete slab with a very good accuracy. In that model one thermal capacitance (control volume) was considered for every 3.65cm thickness of the concrete slab. For the new case of the 35cm thick concrete slab, a 10 capacitance (10C) model would be

expected to provide similar accuracy. Figure 0-3 shows the comparison of the concrete slab thermal response (surface temperature) considering different models for the slab with the design that considers the hydronic pipes in the middle (at 17.5cm depth) and an outdoor temperature of -10°C. A constant heating load of 615 W/m^2 is assumed to be delivered by the system.
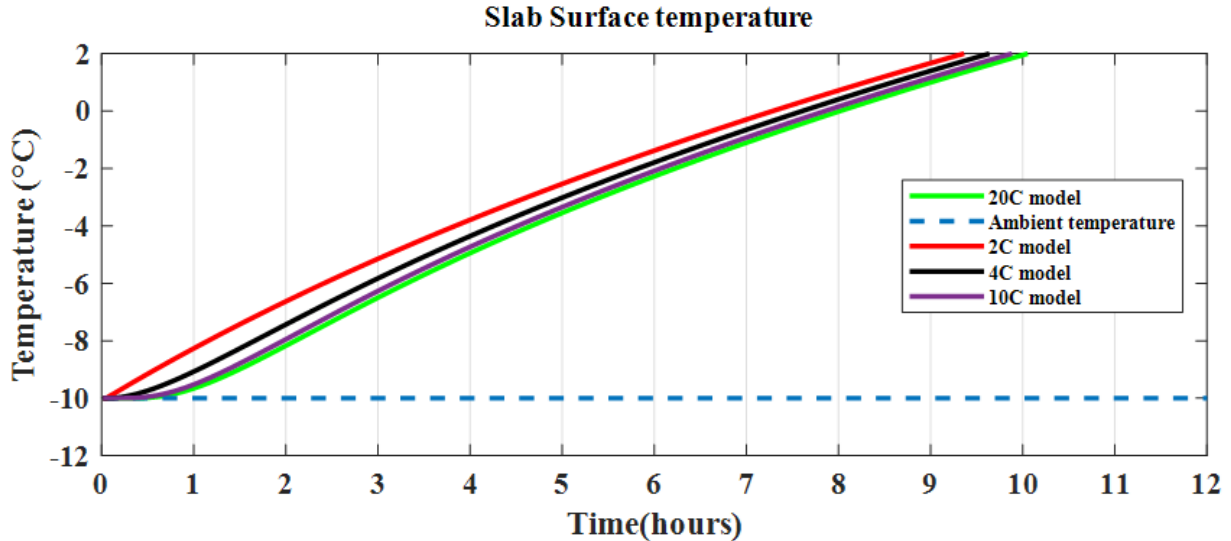
Figure 0-3. Sensitivity analysis of impact of model order on surface temperature prediction for the 35cm concrete slab

As observed in Figure 0-3, there is a significant difference between the 2C model and 10C model and there is a very little difference between the 10C and 20C models. However, for better accuracy in the following hydronic piping configuration studies, the 20C model is used.

The magnitude of the delay in the thermal response of the different piping configurations when exposed to different ambient temperature (-5°C, -10°C and -20°C) and when there is no preheating of the slab is studied. To start, it is assumed that the slab is at the same temperature as the ambient temperature. Then, it is examined how long it takes for the slab to reach a surface temperature of +2°C considering different parameters. Considering a constant outdoor wind speed of 20 kph, a slab heat transfer coefficient of 20 W/m^{2}K was calculated from (Duffie and Beckman 2013) and

used for all the test cases. It was observed that the overall heat transfer coefficient of the slab changes less than 0.5 W/m²K for the temperature range of -5ºC to -20ºC. The model was used to determine the amount of time it takes for the slab surface temperature to reach +2ºC considering different combinations of system capacity, initial slab temperature and piping depth. Due to practical reasons of the infrastructure, the maximum system capacity is preferred to be in the range of 600-630 W/m². Here, two different system capacities were considered: 615 W/m² and 400 W/m².

Table 0-2 summarizes the results for different test cases and parameters. It can be observed as the pipe depth is increased, the time to reach slab temperature of +2 ºC is increased respectively. Also, Figure 0-4 and Figure 0-5 show the evolution of the surface temperature for different piping depths under different ambient temperature conditions.

Table 0-2. Time to reach +2ºC for different combinations

Pipe depth	Initial temperature	Time to reach to +2ºC in hours	
		615 W/m²	400 W/m²
17.5cm	-5ºC	5.2	8.8
	-10ºC	10	18.8
	-20ºC	26	>48
35cm	-5ºC	9.5	13.2
	-10ºC	14.8	24.5
	-20ºC	33.7	>48

Figure 0-4. Surface temperature plots for 17.5 cm pipe depth

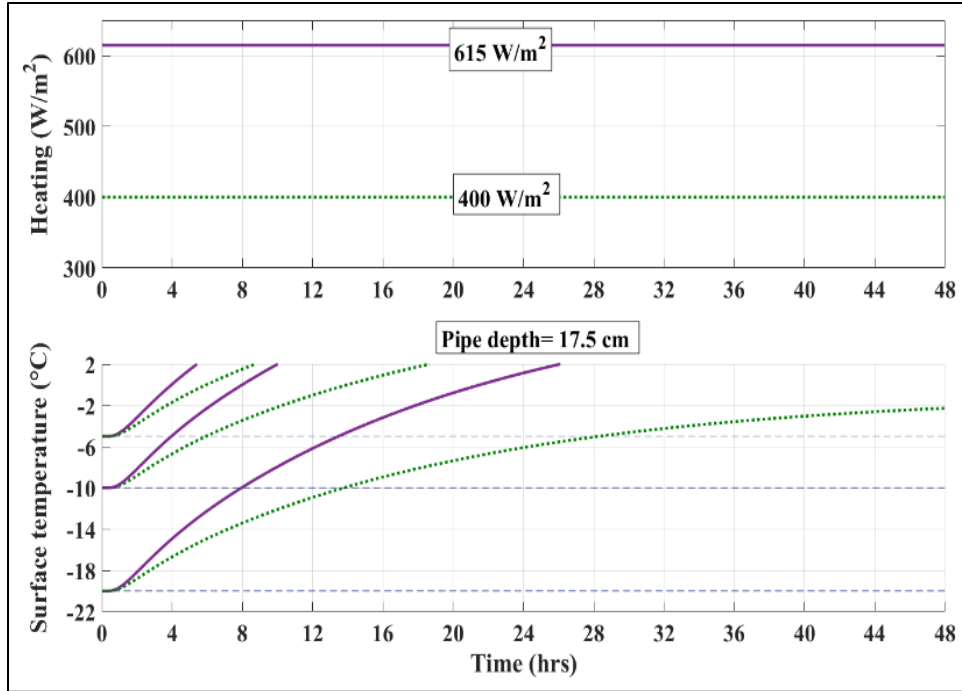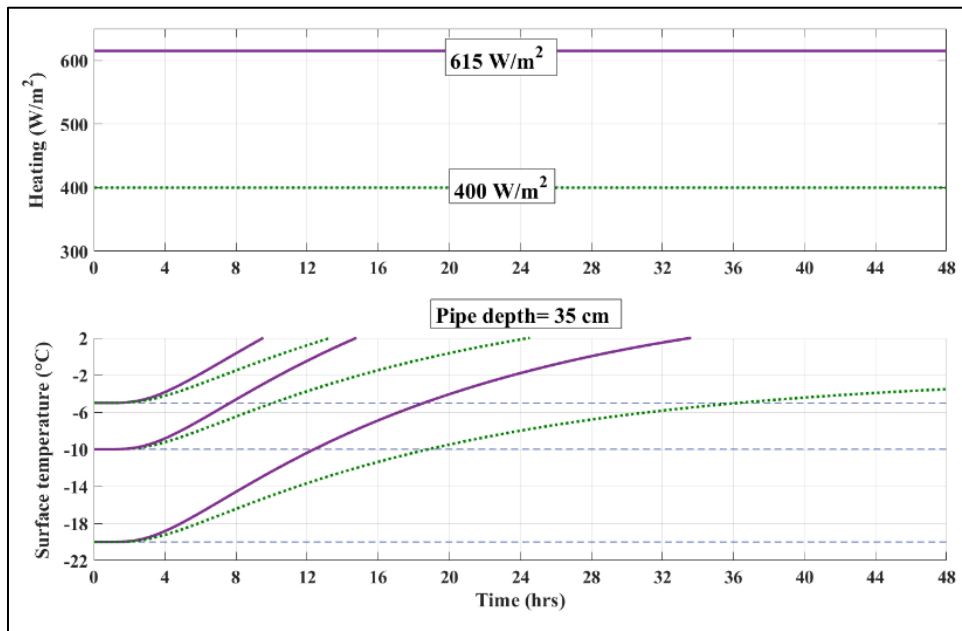Figure 0-5. Surface temperature plots for 35 cm pipe depth

As observed from Table 0-2 for 17.5 cm pipe depth at a cold ambient temperature of -20 °C, it takes more than 24 hours to reach +2 °C even with the higher system capacity. With 400 W/m²

heating power, it is almost impossible to get above 0ºC. It is apparent that the timing is much longer for the 35 cm pipe depth. For the purpose of predictive control, it is advisable to consider a prediction horizon up to 24 hours due to increased uncertainty in weather prediction. Even due to increased uncertainty in weather prediction it is advisable to consider a prediction horizon of 12 hours or shorter. This analysis shows that system capacity, piping depth and mode of operation are all factors of influence over system performance and therefore, the operational mode of the de-icing system should be selected before making decision on the piping configuration and system sizing.

4.1.2 Analysis of the slab thermal dynamics under different weather profiles, idling strategies and piping configurations

As it was observed in the previous section, heating up the concrete slab from ambient conditions above freezing point temperature (+2ºC) will often require excessive amounts of time and also puts a significant amount of thermal stress on the slab. Therefore, it is studied how keeping the slab surface at a specific minimum temperature (higher than ambient temperature) by idling certain amount of heat will help in getting the required performance from the slab under different conditions and weather profiles. Initially, it is assumed that the outdoor temperature varies in a sinusoidal form between -5ºC and -15ºC during the day. Also, it is assumed that the slab surface is initially at a temperature of -4ºC. Then, considering the aforementioned conditions, it is studied how the system sizing of 615 W/m² performs under different situations.

Two different wind speeds were considered (10 kph and 20 kph) which give the total heat transfer coefficients of 20 W/m²K and 14 W/m²K. The following formula was used to calculate h_c due to wind (Duffie and Beckman 2013):

$$h_c = 8.6(\frac{V^{0.6}}{L^{0.4}}) \tag{4.1}$$

where V is the wind speed and L is the characteristic length.

A wind speed of 20 kph is appropriate for bridges and tunnel entrances where de-icing is most crucially needed. However, research using wind tunnels has indicated that installation of sunscreen structures above tunnel entrances can significantly reduce wind speed at the road surface. Also, integration of semi-transparent photovoltaics into those sunscreen structures has recently been demonstrated to provide many benefits to energy performance and safety in tunnels (Sun et al. 2018a).

Figure 0-6 shows thermal response of the slab when a heating capacity of 615 W/m^2 is used with different piping configurations. As it is observed, considering the ambient conditions and system size, it takes about 13 hours to get to +2°C for a 35 cm pipe depth. Therefore, in a similar weather conditions, the system needs to supply the 615 W/m^2 at least 13 hours in advance to ensure no ice formation occurs at the road surface. Or, if a safety margin is to be considered, activating the system 15 hours in advance would be recommended. In a more moderate weather condition (ie. wind speed of 10 kph), a faster response of about 11.8 hours is expected. As it was expected, faster thermal response is observed when the heat is supplied in the 17.5cm depth. Therefore, if it is possible to place the pipes in the middle of the slab, a faster thermal response will be achieved and shorter prediction horizon will be required. Considering the heated area of 8890 m^2 for the case study, Table 0-3 summarizes the results.
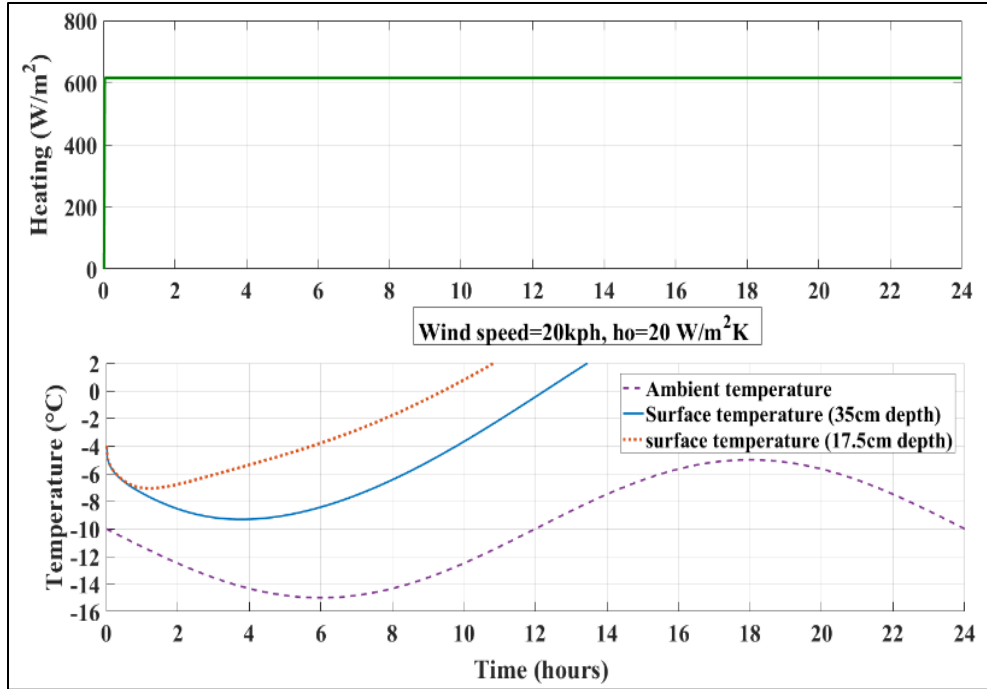
Figure 0-6. Comparison of different slabs surface temperatures for wind speed of 20kph
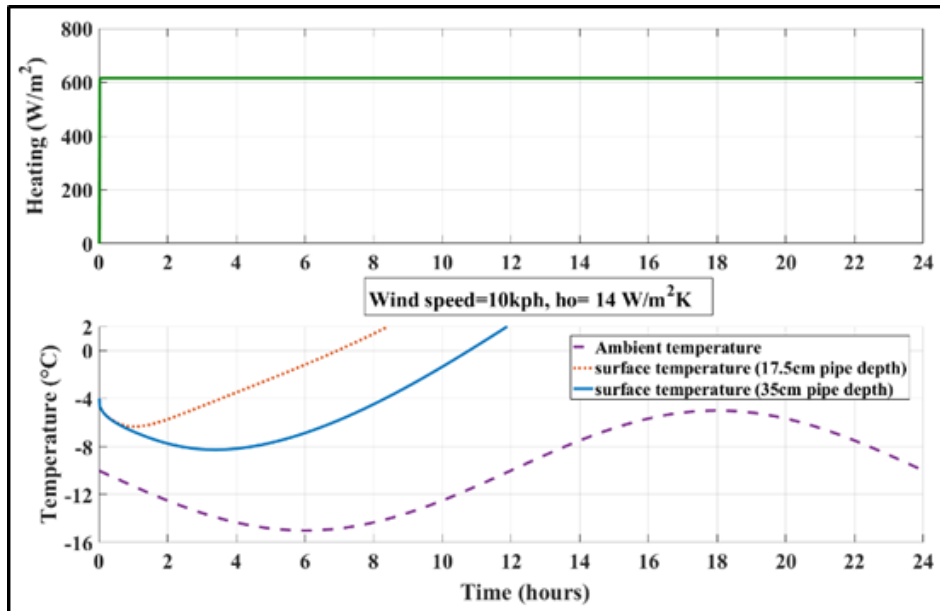
Figure 0-7. Comparison of different slabs surface temperatures for wind speed of 10kph

Table 0-3. Time and energy required to reach +2ºC

Pipe depth	Time and energy required to reach to +2ºC	
	h=20 W/m²K	h=14 W/m2K
35 cm	13.5 hours	11.8 hours
	73.8 mWh energy	64.5 mWh energy
17.5 cm	9.2 hours	6.5 hours
	50.3 mWh energy	35.53 mWh energy

4.1.3   Effect of no insulation under the slab

Here the case of uninsulated slab is studied considering different piping positions. Figure 0-8 and

Figure 0-9 show the results for 35cm and 17.5 cm piping depth respectively.
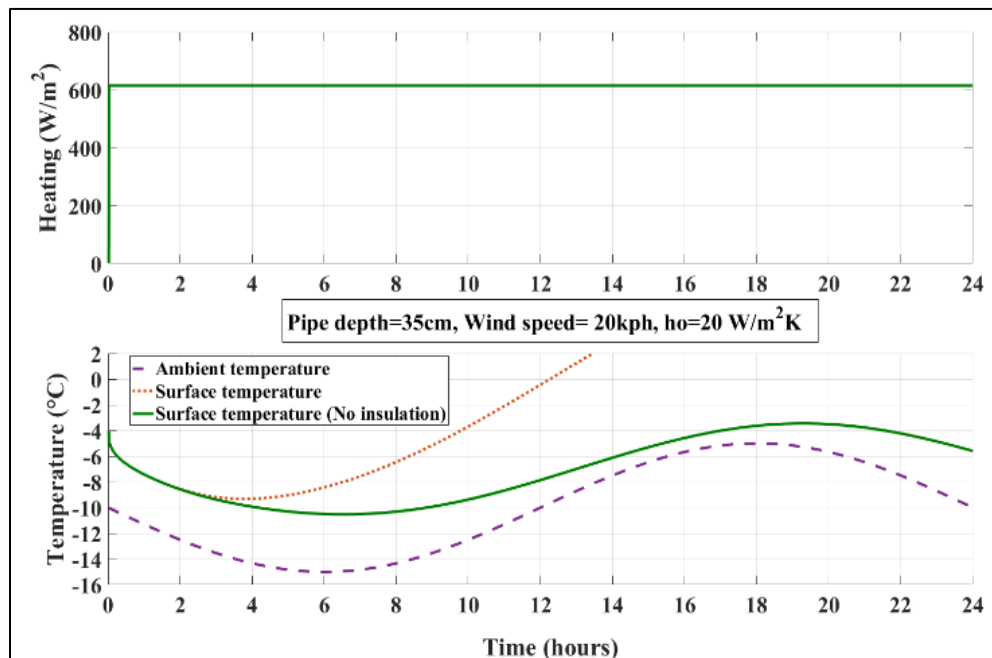
Figure 0-8. Comparison of surface temperature with and without insulation for 35cm pipe depth
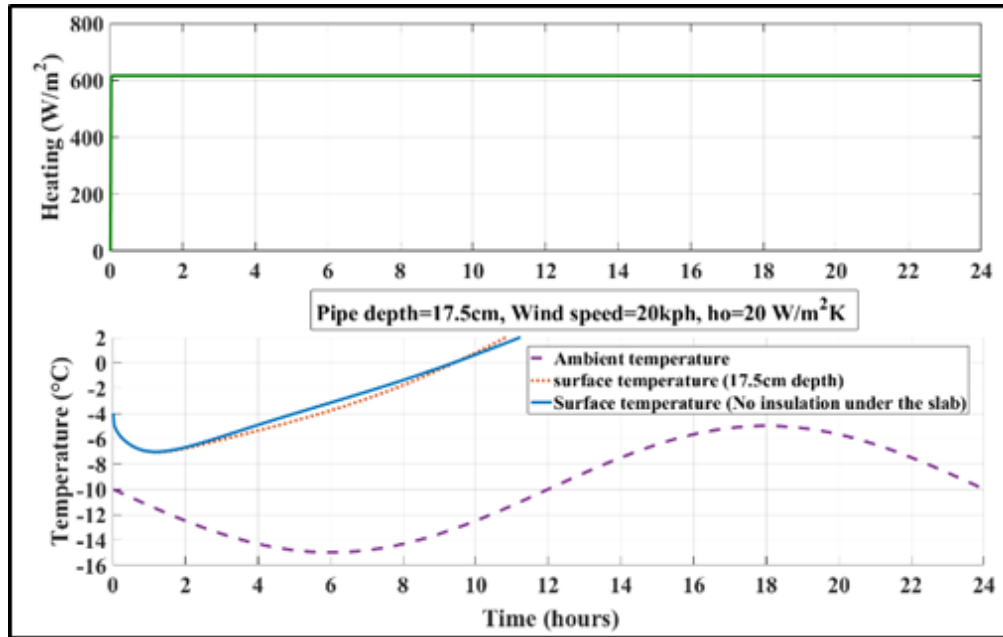
Figure 0-9. Comparison of surface temperature with and without insulation for 17.5cm pipe depth

As can be observed from the above figures, having no insulation for 35cm pipe depth design will affect the surface temperature significantly since there will be a substantial loss of energy to the ground. However, in the case of 17.5 cm pipe depth removing the insulation has a very small effect on the surface temperature since in that case there is already a thick layer of concrete under the pipes that already has a certain thermal resistance which ensures that the greatest part of the heat flow is towards the slab surface. Therefore, removing the insulation can be considered as an option for the design that considers the pipes in the middle of the slab for the outdoor temperature range of -10ºC to -15ºC. However, when pipes are placed at the bottom of the slab, having no insulation is not recommended.

4.1.4 Important scenarios

There are certain possible scenarios which are important and the system performance needs to be studied under these situations:

Scenario1) **moderate to cold ambient temperature**. Road surface is kept at -4°C by idling certain amount of heat in the pipes. The outdoor temperature is getting very cold (-20°C) later in the evening and the precipitation is in the forecast around the same time (at hour of 18). Therefore, the slab surface temperature needs to be at +2°C during all this period when there is precipitation.

Figure 0-10 shows the results for the 35cm pipe depths. It can be observed that by applying 615 W/m² heating, the slab surface temperature reaches +2°C in about 9.5 hours. However, when the ambient temperature reaches -20°C, the heating capacity is not capable of holding the surface temperature above +2°C and the temperature falls even slightly under 0°C. This shows that the system is undersized for this situation. Increasing the system size by 100W/m² (applying 715W/m²), it is observed that the surface temperature can be kept above +2°C at all the time hence ensuring there is no risk for ice formation on the road surface. It should be noted that in both scenarios 1 and 2 there is no preheating of the slab so the slab surface temperature is initially -4°C.
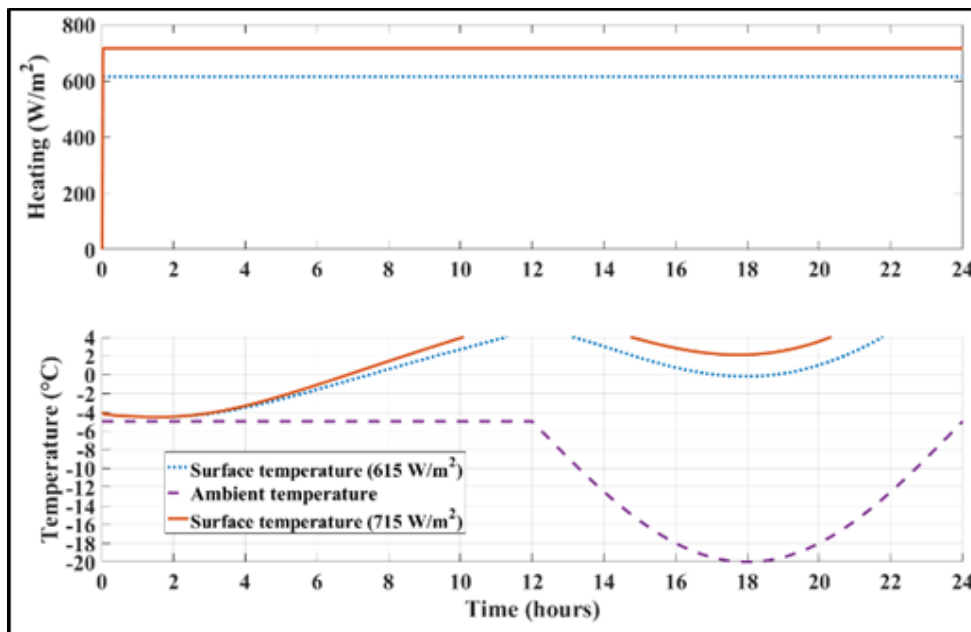
Figure 0-10. Slab (35cm pipe depth) thermal response under a specific ambient temperature profile

Scenario 2) **cold ambient temperature**. Floor surface is kept at -4°C by idling certain amount of heat in the pipes. The ambient temperature is at -20°C and remains relatively constant during the day. It is seen in the forecast that in 12 hours ahead there will be a high chance of precipitation. The slab surface temperature needs to be around +2°C before the precipitation event starts in order to avoid the risk of icing.

The results for the slab with 35cm pipe depth are shown in Figure 0-11. It is observed that by applying 615 W/m^2 heating in this case it takes more than 17 hours (97.42 mWh energy) for the slab surface temperature to reach +2°C. However, if the heating system capacity is increased by 200W/m^2 (applying 815W/m^2) then the +2°C surface temperature is achieved in less than 11 hours (76.8 MWh energy) and this sizing meets the 12 hours requirement. Also, further simulations show that applying 1015 W/m^2, decreases the response time to 8.5 hours (76.7 MWh energy). Therefore, if faster response is required, a larger heating capacity needs to be applied. Also, it can be observed that less energy will be consumed for larger system sizing of 815 W/m^2 and 1015 W/m^2 compared to 615 W/m^2.
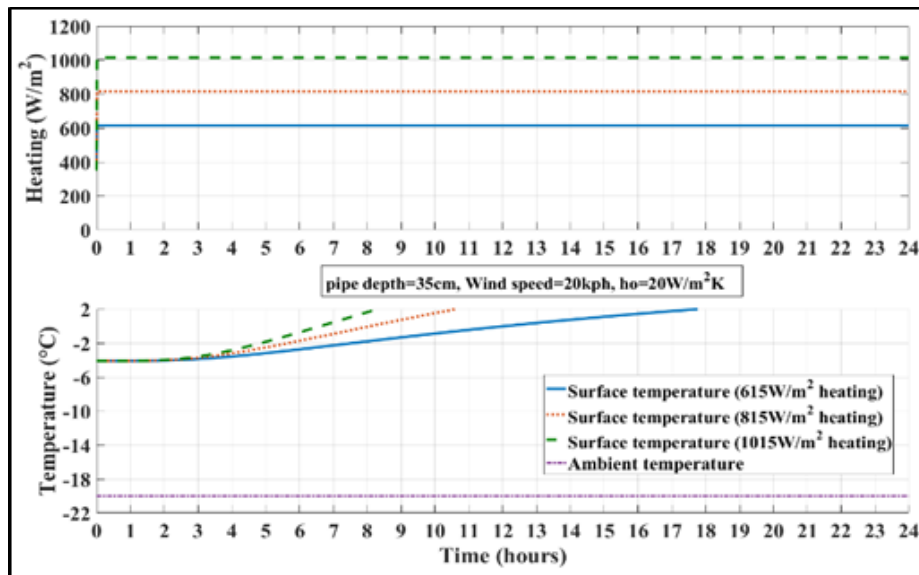
Figure 0-11. Slab thermal response under constant ambient temperature at -20°C

It can be observed from the above results that if it is desired to use a 35cm thick slab and reach the slab temperature of +2°C under cold weather conditions, it is more practical to keep the surface temperature around 0°C instead of -4°C or lower temperatures. This action will lower the risk to minimum since the surface temperature can get to above 0°C in couple of hours. Figure 0-12 shows the results for this case. By keeping the slab temperature at 0°C, with 615 W/m^2 heating the +2°C can be reached in less than 10 hours. In terms of required energy to reach +2°C with idling at 0°C the required energy is 53 mWh (5965.5 kWh/m2) compared to 97.32 mWh (10947 kWh/m2) when idling at -4°C. It should be noted that for this scenario the slab was preheated a number of days before the actual event day assuming that previous days had the same type of weather as the de-icing event day.
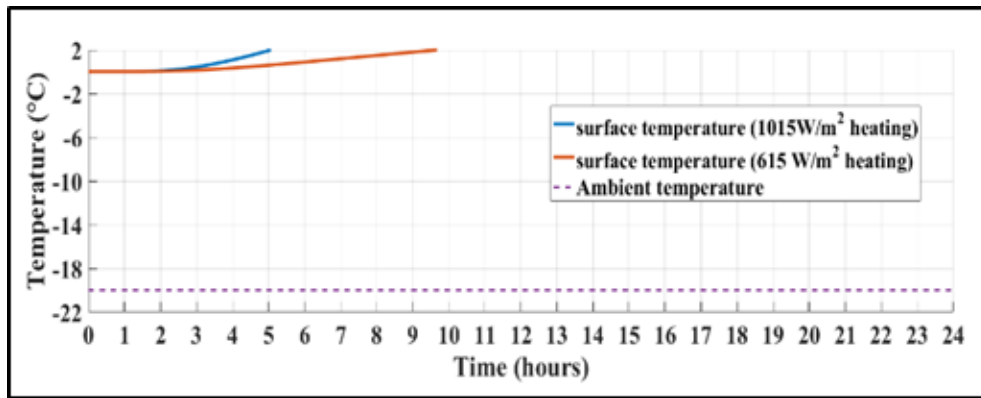
Figure 0-12. Slab thermal response from 0°C idling temperature

Scenario 3) **extremely cold weather.** Usually during the periods of very cold weather, ambient temperature of around -30°C, there is a very little chance of precipitation and the precipitation occurs at lowest around outdoor temperatures of -15°C to -20°C (Davis et al. 1999). Therefore, it is studied to see how the slab behaves under this type of weather condition. It is assumed that there is a period in which we have a day of ambient temperature at -30°C with the rising to -20°C in 24 hours in a sinusoidal form (a typical situation that happens during winter). It is assumed that when the outdoor temperature reaches -20°C there is a chance of precipitation and hence black ice

formation in the forecast. Therefore, our road surface needs to be at +2°C before the icing event starts in order to avoid the risk. It is studied how fast the 17.5 cm piping depth design can react in this situation considering idling a certain amount of heating power to keep slab at temperatures of -4°C, -8°C and -15°C. Figure 0-13 shows the results. Each surface temperature is shown with the same color and number as the heating power. Also, the total heating power considering the heated area of 8890 m² is shown on each heating profile.
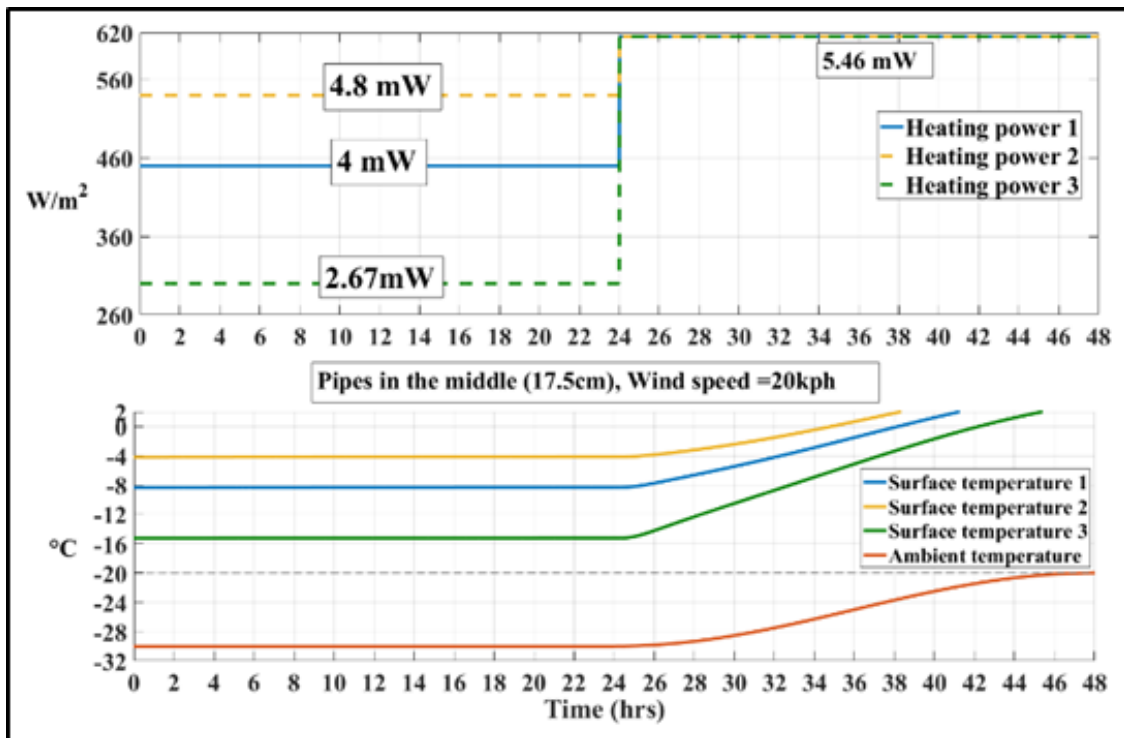
Figure 0-13 . Load and surface temperature profiles for 17.5cm pipe depth

As can be observed from Figure 0-13, the time and energy required to reach +2°C for different idling temperatures of -4°C, -8°C and -15°C is 14 hours and 191 mWh, 18 hours and 194 mWh, 21 hours and 178 mWh respectively. Therefore, even with keeping slab surface at lower temperatures than -4°C it will be still possible to reach the +2°C in less than 24 hours and save a significant amount of energy, up to 18 mWh in this case, as well. However, it should be considered that as the prediction horizon increases the uncertainty in weather prediction increases as well.

Now the performance of the system without considering the insulation at the bottom is shown in Figure 0-14. It is observed that at such ambient conditions, the system is not capable of reaching the desired +2ºC surface temperature without having insulation at the bottom. Therefore, if the system is to be designed without insulation for such extreme weather conditions, a larger or an extra power capacity should be considered.
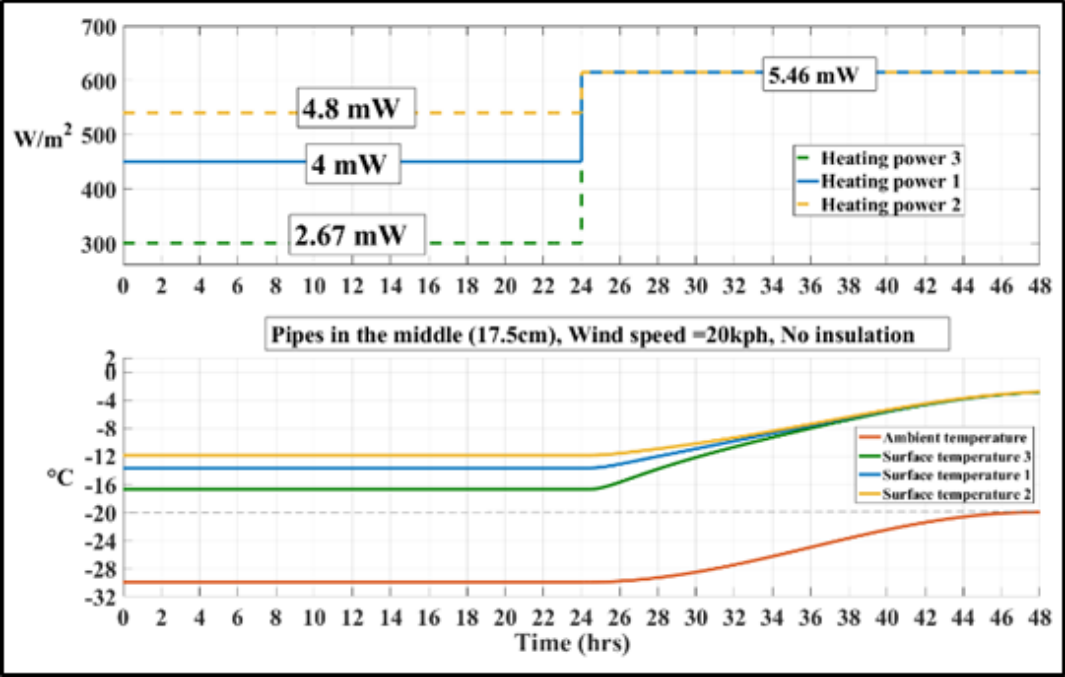
Figure 0-14. Load and surface temperature profiles for 17.5cm pipe depth with no insulation

For the case of the slab with pipes at the bottom (35cm), as it is observed in Figure 0-15, it is not practical to keep the slab at below -4ºC considering the delay in the thermal response. Also, it is required to apply close to 95% of the maximum power to keep the slab at -4ºC at ambient temperature of -30ºC and then with boost to maximum power of 5.46 mW, the slab surface can reach from -4ºC to +2ºC in about 16 hours. Therefore, in this case if it is desired to reach to +2ºC in 12 hours, which is the reasonable prediction horizon, it is required to increase the boosting power to 6.67 mW (750 W/m^2) as shown in Figure 0-16. Therefore, with this design it is always recommended to have a higher boosting capacity for extreme weather conditions.
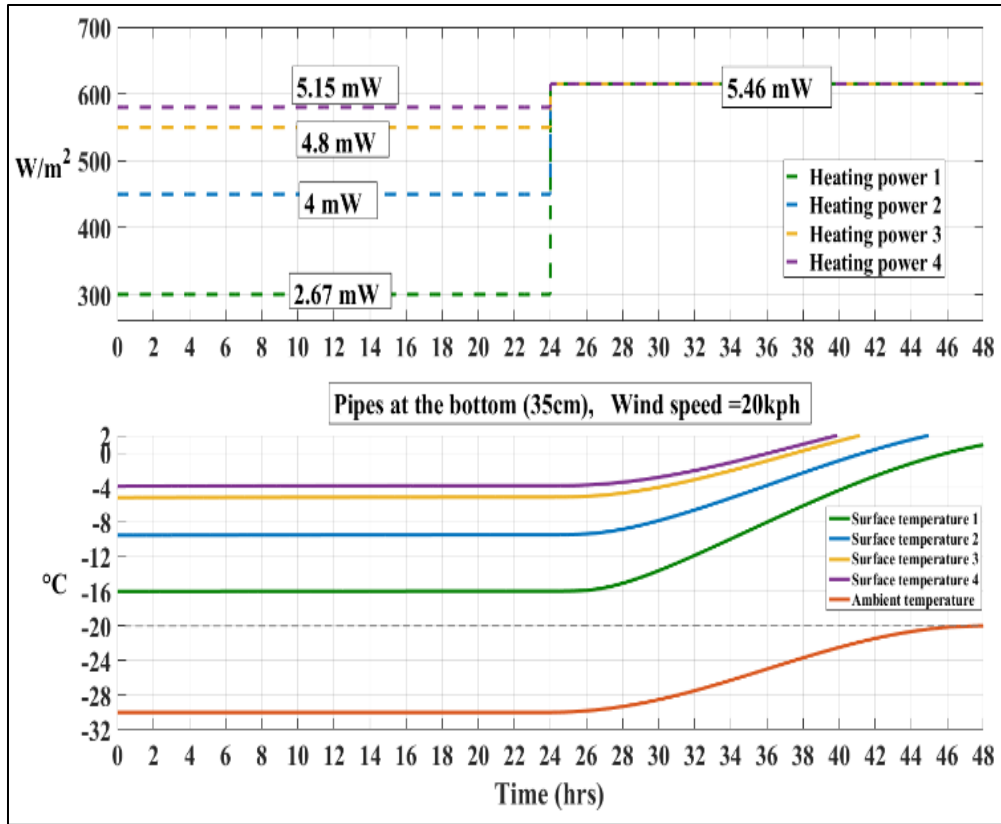
Figure 0-15. Load and surface temperature profiles for 35cm pipe depth
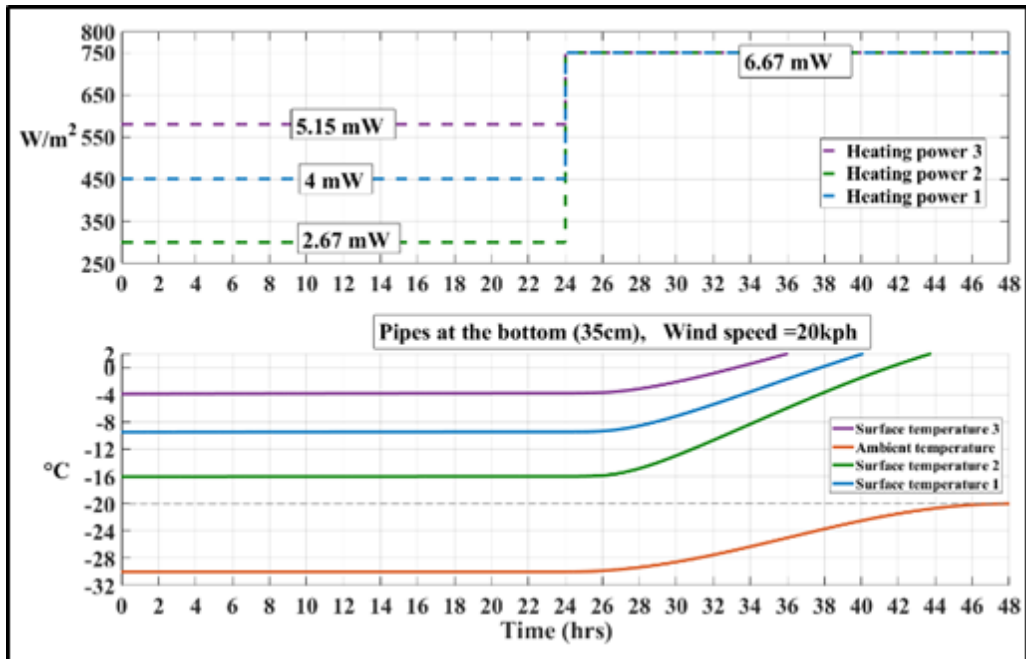
Figure 0-16. Load and surface temperature profiles for 35cm pipe depth

The next section discusses experimental results on evaluation of energy flexibility potential of a thermal zone with radiant floor heating system.

4.1.5 Utilizing the slab thermal mass to shift energy and power consumption

A slab design with pipes in the middle of the slab is considered. As the reference case and business as usual operating condition, the heat load that provides a slab temperature of +2°C is considered. Then, another case is introduced as the active demand response (ADR) scenario in which the slab is preheated by increasing the surface temperature setpoint from +2°C to +4°C. The ambient temperature is assumed to be constant at -15°C. Figure 0-17 shows the heating load for the reference case and the active demand response (ADR) case. It can be observed that with constant setpoint of +2°C for surface temperature, the reference heating load is around 250 W/m^2. However, when the surface temperature is increased to +4°C and maintained at +4°C for 8 hours, a change in the ADR heating load profile is observed.
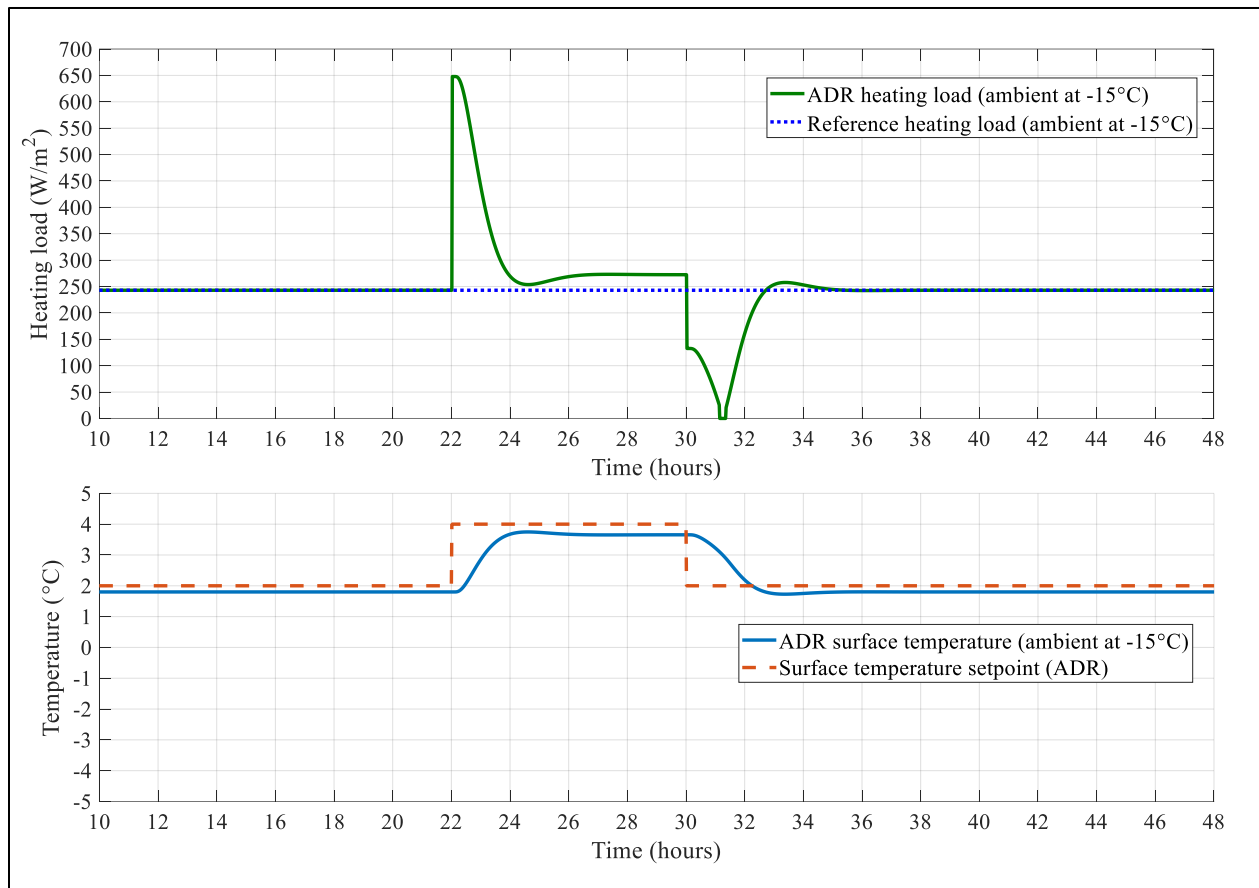
Figure 0-17. Heating load & surface temperatures for ADR and reference case

This strategy is applicable for the peak power and energy demand reduction during peak hours. As it can be observed by preheating the slab starting at 10pm (hour 22) the night before until 6am (hour 30) of the following day, a significant reduction in the slab heating load during the peak demand hours which here in Quebec is usually between 6am to 9am (hours 30 to 33 in the graph) is expected. Therefore, this strategy can be categorized as a predictive reaction to the grid penalty/price signal as shown in Figure 0-18.
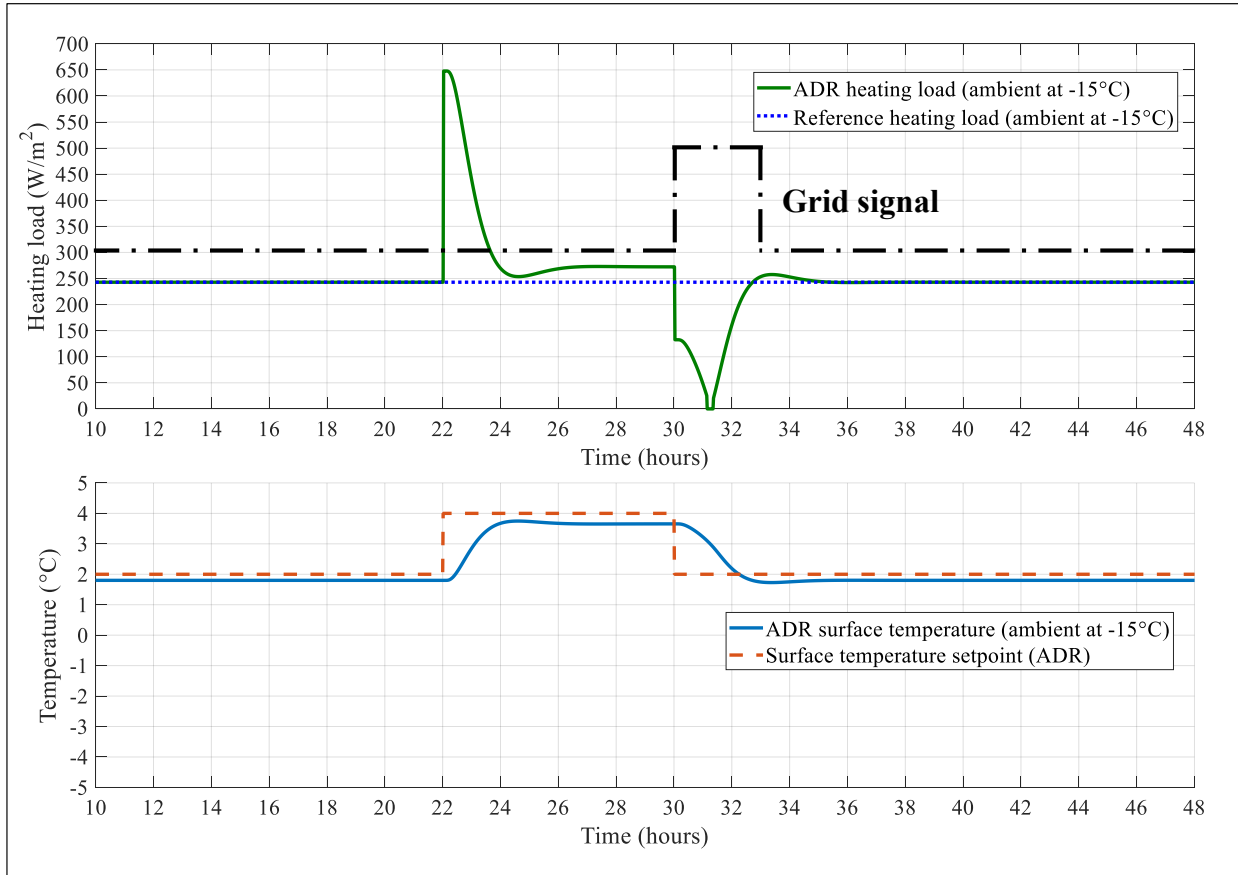
Figure 0-18. Grid penalty signal

The total change in the energy consumption between the reference and ADR cases during the 8 hours period is calculated and equal to 568 Wh/m^2 or in total 5.05 MWh. This parameter can be reported as the energy flexibility offered by the slab thermal mass. Also, there is a significant reduction in the peak power demand during the high penalty signal period of up to 250 W/m^2 (around hour 31) and on average a reduction of about 100 W/m^2 between hours 30 to 33.

As can be observed from Figure 0-17, when the surface temperature setpoint is increased suddenly form +2°C to +4°C, there is a jump in heating load from 250 W/m^2 to 650 W/m^2 which is higher than our maximum capacity of 615 W/m^2. This peak can be reduced by using a ramp setpoint instead of a sudden sharp increase.

80
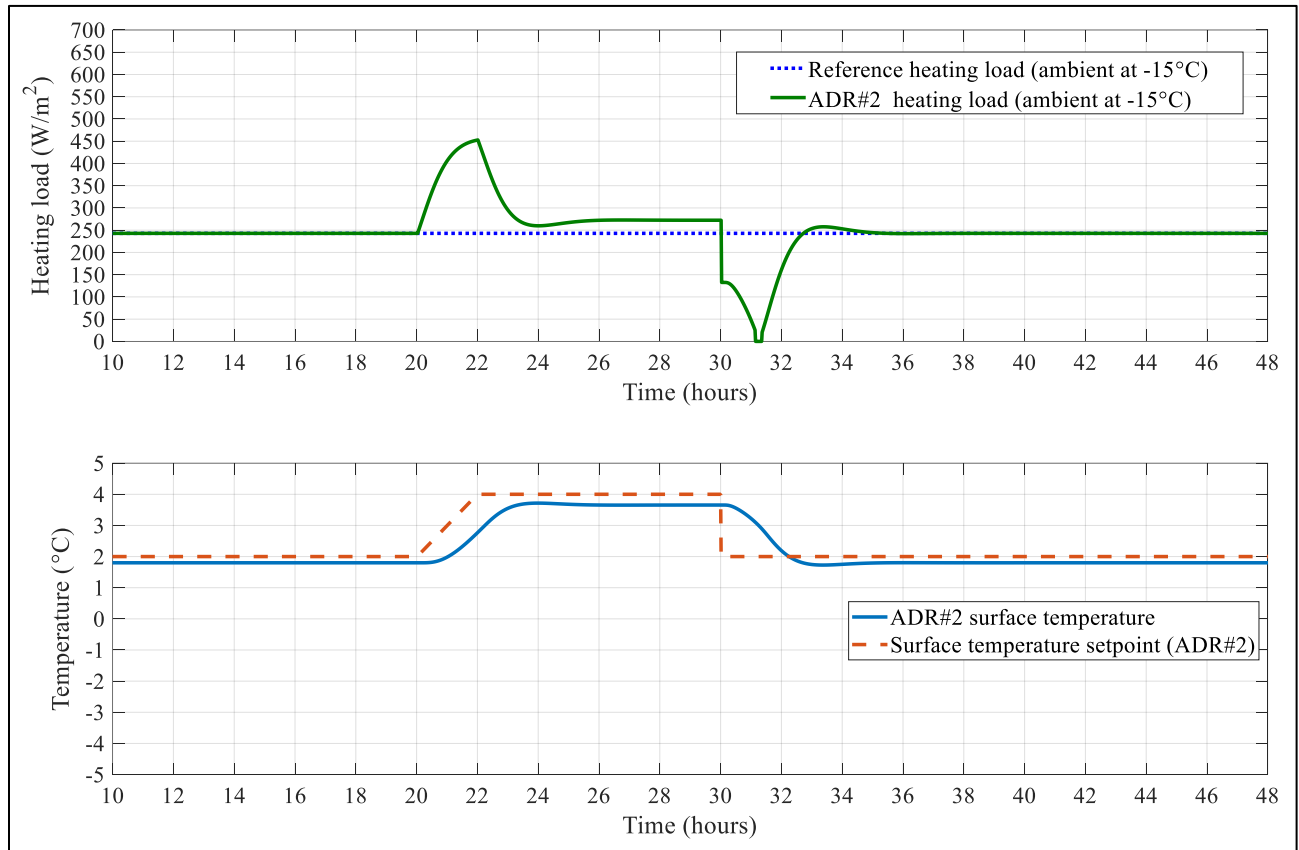
Figure 0-19. Heating load & surface temperatures for ADR#2 and reference case

As shown in Figure 0-19, by applying a 2-hour linear ramp for transition from +2°C to +4°C, the maximum peak load is now 450 W/m^2 instead of 650 W/m^2 which is a considerable reduction of 30% in the peak load. The difference in energy consumption between the reference and ADR#2 cases for these 10 hours (hours 20 to 30) is 597 Wh/m^2 or 5.312 MWh in total.

4.2 Experimental results on energy flexibility analysis of a radiant floor heating system[11]

The case study presented here is the perimeter zone test cell (PZTC) located at Concordia University's solar simulator/environmental chamber (SSEC) laboratory. As introduced previously, the temperature of the EC can be controlled within a wide range (between -40 °C and +50 °C) through the air handling unit (AHU), thus allowing a great deal of flexibility in terms of testing conditions. Figure 0-20 shows the schematic of the SSEC laboratory, the perimeter zone test cell (PZTC), radiant floor system and the mechanical room for the PZTC.
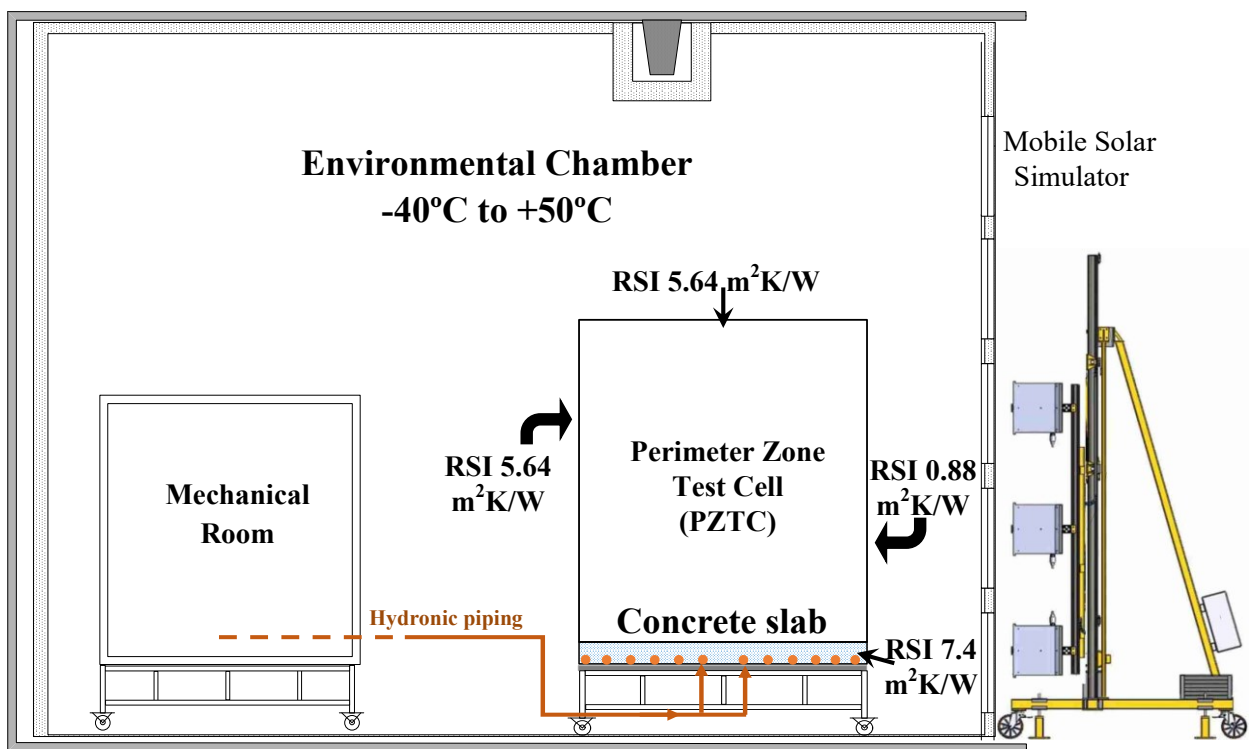
Figure 0-20. Schematic of SSEC with PZTC and radiant floor

---

[11] based on journal paper #1: Saberi Derakhtenjani, Ali, Athienitis, Andreas K. (2020)." A Frequency Domain Transfer Function Methodology for Thermal Characterization and Design for Energy Flexibility of Zones with Radiant Systems". Journal of Renewable Energy, 163:1033-1045

The PZTC is a 3m×3m×3m office placed inside the environmental chamber and it has a radiant floor heating system. The side and back walls and ceiling consists of 4 inches of insulation having the R-value of R32. The front wall is a BIPV/T façade with an approximately R5 thermal resistance. The floor is made of an 8cm thick concrete with insulation at the bottom. The pipes of the radiant floor system are made of conventional cross-linked polyethylene (PEX), and a have an external diameter of 1.75cm. The pipes are installed in a "foam matrix" of insulating material that also facilitates keeping them in place. The pipes have an approximate separation of 15cm between them. A mechanical room provides controlled flow rate of fluid (propylene-glycol and water mixture) for the radiant floor.

This experimental study is an energy flexibility case study using the zone thermostat. The Thermostat controls the room air and floor temperature for a hydronic heating zone using Pulse Width Modulation (PWM) technology. A slab sensor is included with the thermostat to measure floor temperature to protect the floor from overheating and enhance comfort. In the experiment the maximum allowable floor temperature was set to be 29ºC based on the ASHRAE standard.

The control of the system was based on an assumed price signal. Therefore, it was observed how much flexibility can be achieved by modulating the air temperature setpoint from the baseline room temperature (22ºC) to the comfort limits of the zone (20ºC and 24ºC). The increasing/decreasing of the setpoint was done manually by entering the room and increasing the temperature on the thermostat, waiting for the desired period (about 6 hours) and then put the temperature back to the baseline again manually. Also, both setpoint increase and decrease from the baseline was considered to examine the upward and downward flexibility of the system.
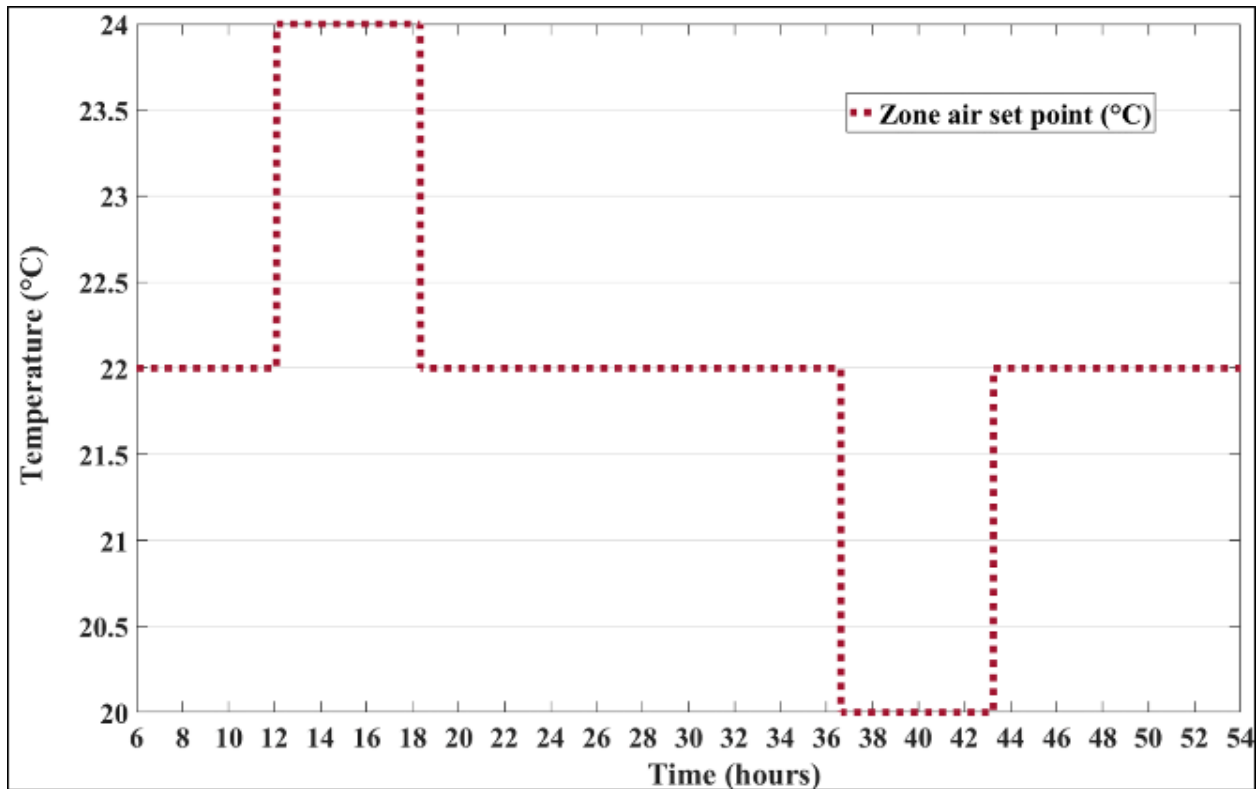
Figure 0-21. Implemented control strategy (zone air setpoint)

Figure 0-22 shows the system flowrate before and during the ADR event (12-18 hours & 37-43 hours), when the zone air temperature is modulated accordingly. As it can be observed from Figure 0-22, before hour 12 there is a more steady on/off to the system flowrate though pulse-width modulation in order to keep the zone temperature at 22°C. Then, between hours of 12 and 18 when the temperature was set to be increased to 24°C the controller keeps the flowrate near maximum and keeps the flow running for a much longer period until it gets really hot around the hour of 14.5 and then the flow is stopped for about 1.5 hours and then the flow is started again for another 1.5 hours (16-17.5 hours) and then at hour 18 when the setpoint is reduced to 22°C from 24°C, no heating power is observed in the system for more than 4 hours. Therefore, it is observed that this strategy gives us a 4 hours power shifting capacity compared to the baseline heating power profile (22°C zone temperature).
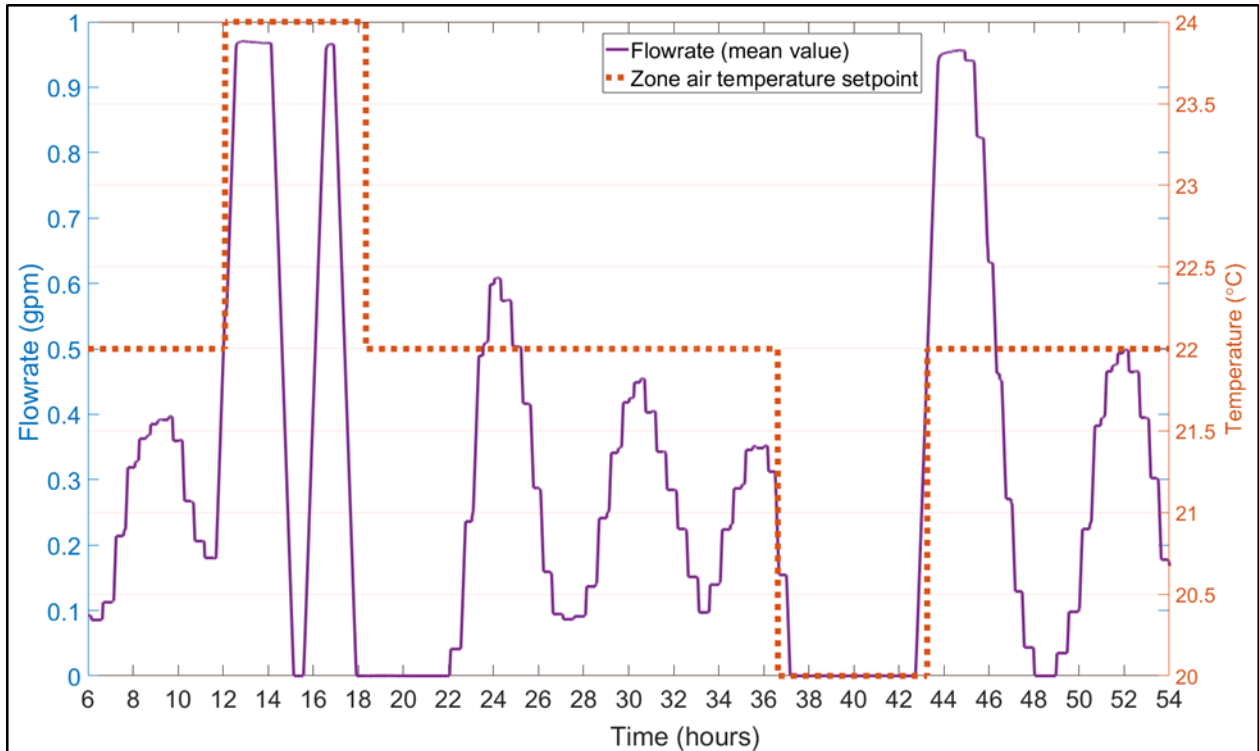
Figure 0-22. Radiant floor System flowrate vs room setpoint modulations

Then, the heating power of the radiant floor was calculated by using the flowrate, supply and return temperatures as: $Q = m \times C_p \times \Delta T$. Then for the ADR events, hours 12 to 18 and 37 to 43, the flexibility of the system was calculated. As shown in Figure 9, the upward flexibility is equal to 195 Wh/m² and the downward flexibility is 237 Wh/m². Also, an increase of 125W in heating power can be observed in the rebound effect of downward flexibility (hour 43) compared to the one for the upward flexibility (hour 12). This increase in heating power is due to the fact that at hour 43 there was no heating in the system for 6 hours before that time and therefore we observe a higher spike in the heating power compared to hour 12.
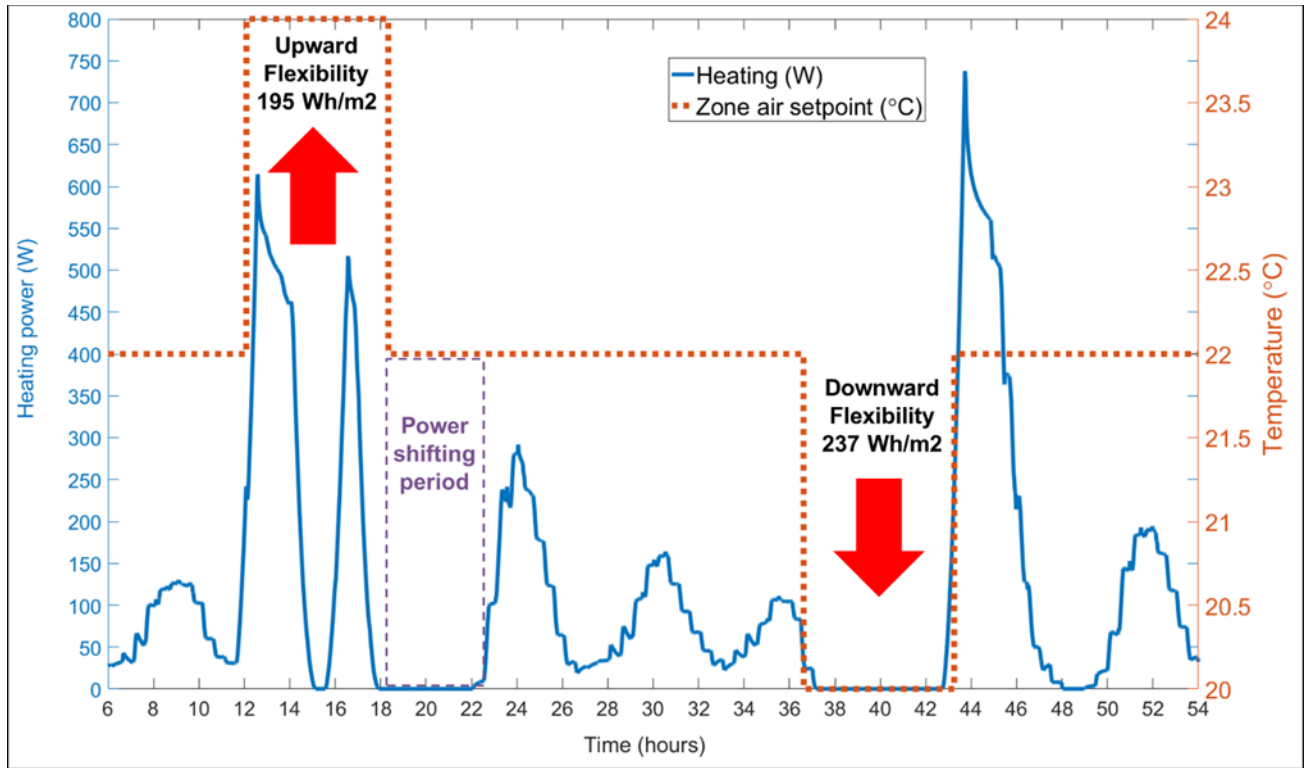
Figure 0-23. Heating power of the radiant floor system and the upward/downward flexibility calculation

This setpoint modulation strategy described above can be defined and applied to a price signal as shown in Figure 0-24. Therefore, when there is a high price signal for a certain period of time in the forecast, the zone setpoint can be increased by 2ºC for a certain period and then get back to the normal operating condition. It is observed that with this strategy our system offers about 4 hours of power shifting potential. Also, with the downward flexibility it will be possible to decrease the rebound effect by using a ramp profile or other transition paths for which it is required to install a programmable thermostat.
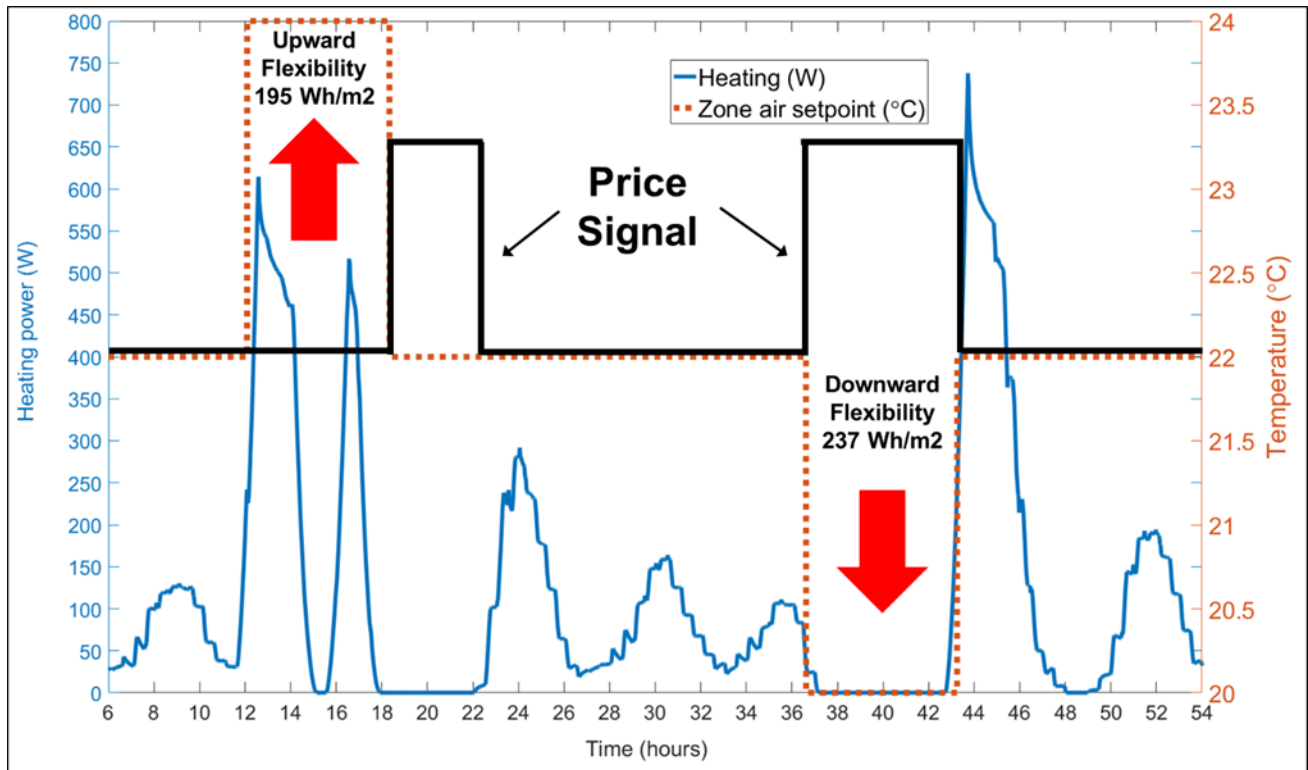
Figure 0-24. Price signal

Figure 0-25 shows the radiant floor surface temperature as well as the zone operative temperature and the exterior temperature conditioned by the environmental chamber. It is observed that the operative temperature is within the comfort limits almost all the time. Also, can see that when the floor temperature reaches the 29ºC limit (around hours of 15), that's when the controller shuts down the heat input by turning off the flowrate of the radiant floor.
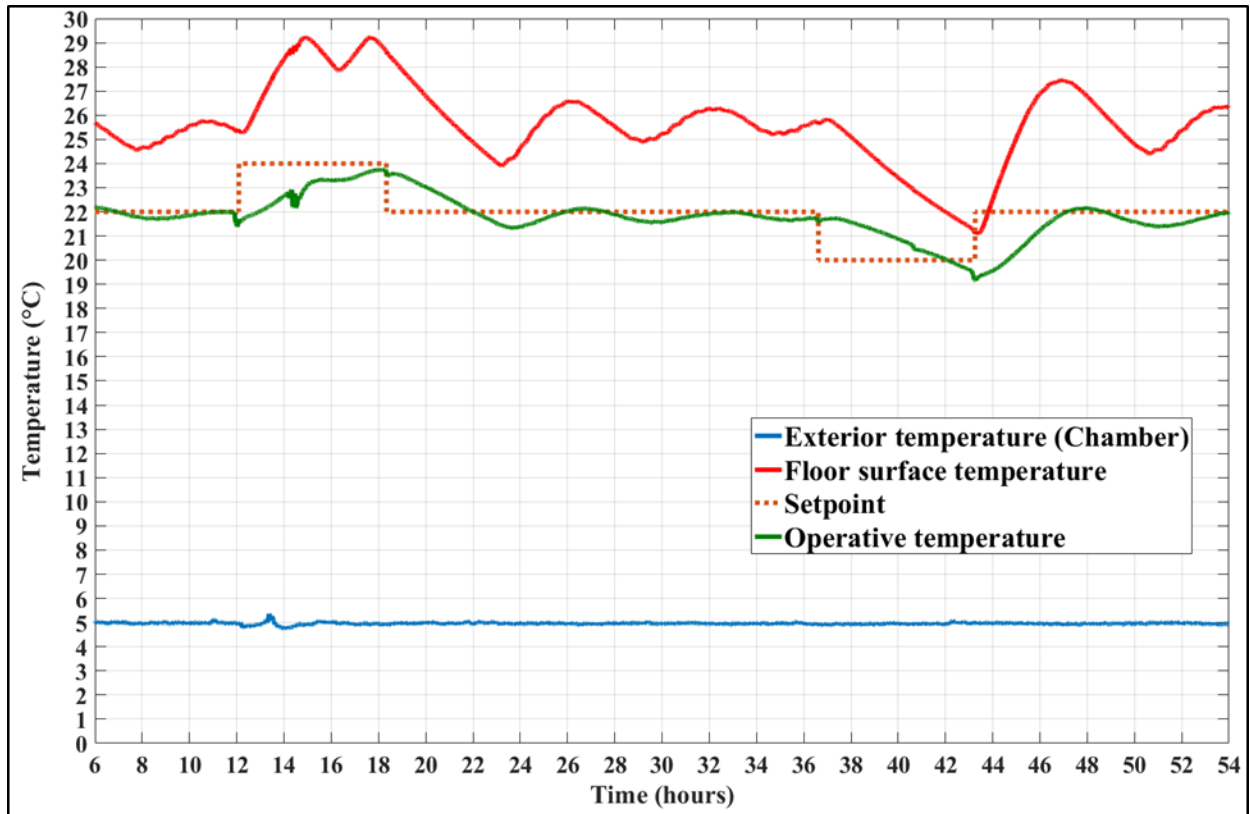
Figure 0-25. Floor surface and operative temperatures

4.2.1 Results from frequency domain modeling and transfer function $Z_{1,aux}$

Considering the physical properties of the PZTC, a detailed frequency domain model was developed for the zone and the magnitude and phase angle of the transfer function $Z_{1,aux}$ was calculated at discrete frequencies using equation (3.24). Figure 0-26 shows the phase angles of $Z_{1,aux}$ at different harmonics (cycles per day).
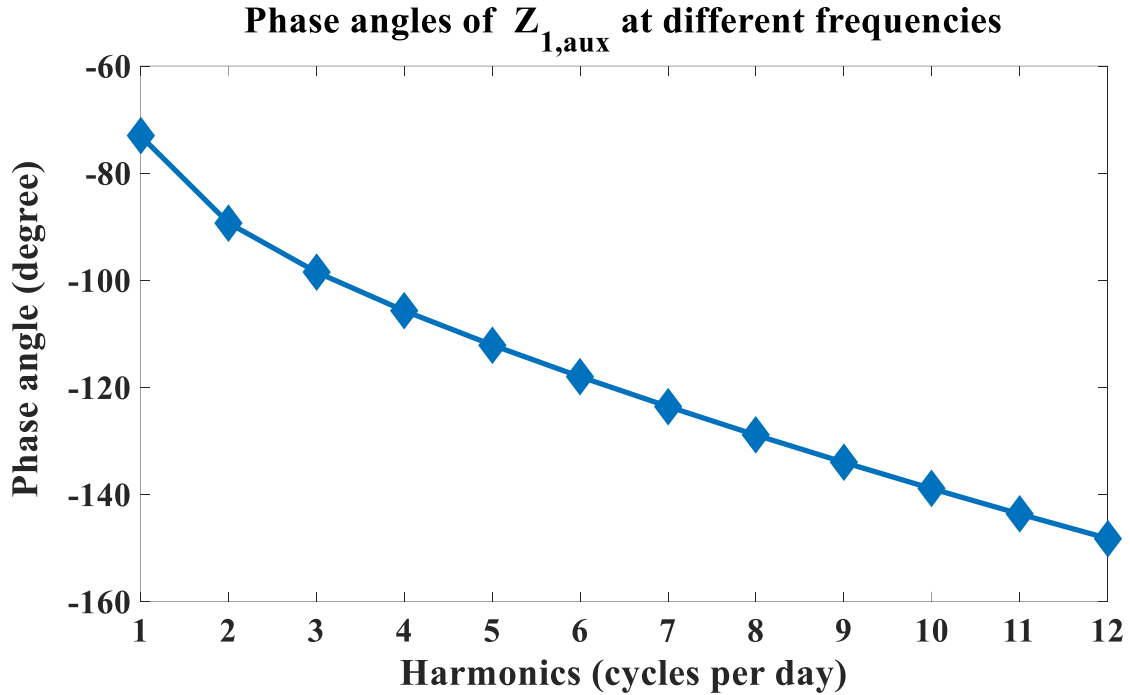
Figure 0-26.Phase angles of transfer function $Z_{1,aux}$

As observed from Figure 0-26, the phase angle of the fundamental harmonics is -73.02° with negative sign indicating the delay. Therefore, considering the period of one day for the first harmonic, the magnitude of the delay in units of time was calculated as:

$$73.02 \times 24h / 360° \cong 4.9 \text{ h} \qquad (4.2)$$

This means that there will be about 4.9 hours of delay between the heat input from the hydronic system of the concrete slab and the peak effect on PZTC air temperature. This calculated delay between the hydronic floor heat input and the zone air temperature can be observed from the experimental measurements. As shown in Figure 0-27, when the PZTC air temperature setpoint was suddenly raised at t=42.3 hour, the thermostat commanded the controller to immediately increase the radiant heat input. However, as calculated from the transfer function $Z_{1,aux}$ (between room air and heat input) there was a delay of around 4.9 hours between the peak heating power and its full effect on the room air temperature peak. The result shows that in a zone that is mainly

89

heated by a radiant floor system, when it is desired to reach a specific zone air temperature at a specific time, the controller of the heating system needs to be designed in such a way that considers this delay.
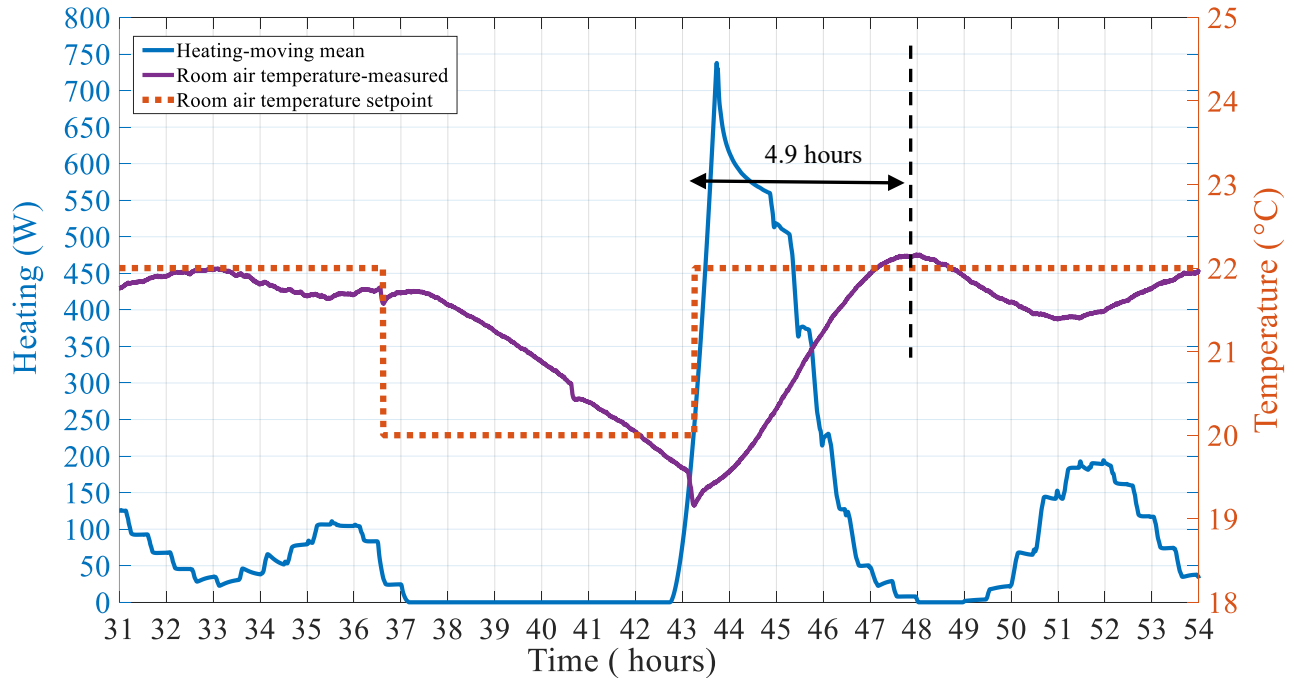
Figure 0-27. Delay between the radiant floor heat input and PZTC air temperature

4.3 Low-order thermal modelling of PZTC for predictive control [12]

This section presents the results of low-order thermal modelling for PZTC for which the methodology was presented in pervious chapter. A model with fewer parameters facilities setting up the initial conditions which is a key parameter for control studies. The models must be accurate enough to provide reliable information but also flexible enough for quick and computationally efficient decision-making, especially in reaction to electric grid's short notices on the change of

---

[12] based on journal paper #3: Saberi Derakhtenjani, Ali, Athienitis, Andreas K. (2020)." Predictive Control Strategies for Energy Flexibility in Response to Dynamic Electricity Prices for Zones with Radiant Systems". Submitted to journal of Applied Energy, under review

the price signals. The radiative and convective heat transfer are inherently nonlinear processes however, the respective heat transfer coefficients are usually linearized so that the system energy balance equations can be solved with linear algebra techniques and represented with a linear thermal network. In the case of radiant floor heating, this linearization generally introduces less error for the for long-wave radiation heat transfer than the convection heat exchange between the radiant floor surface and room air. Therefore, usually certain amount of calibration for the convection heat exchange between the radiant floor and room air is required for a model and especially when considering the low-order models.
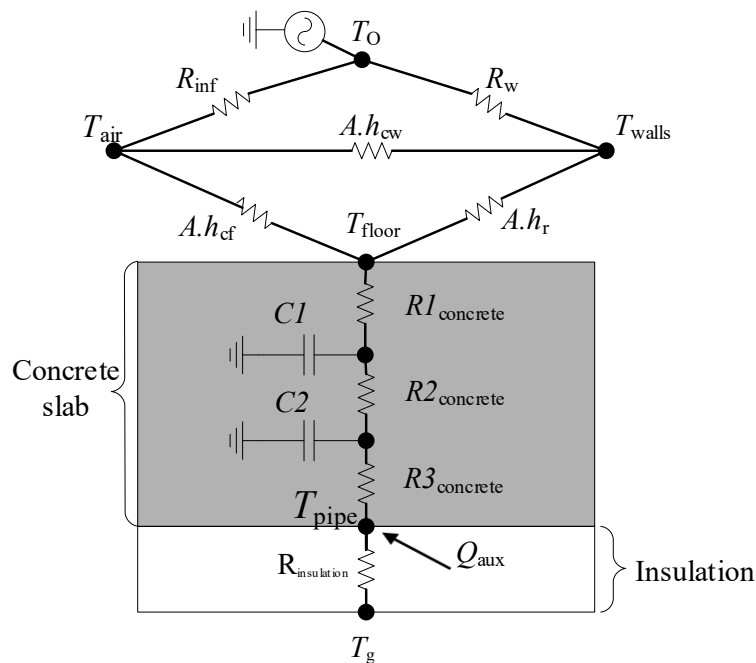
Figure 0-28. Second-order model thermal network

The floor convective heat can vary significantly depending on the temperature difference between the floor surface temperature and the air in the zone. Therefore, an objective function is defined to find the effective values of h_{cf} so that the floor surface temperature calculated from the simulations matches with experiment as accurate as possible. Therefore, the objective function is defined as:

$$Min \quad J = \left\| T_{floor,simulated} - T_{floor,measured} \right\| \qquad (4.3)$$

The optimization result is shown in Figure 0-29. As observed, a well calibrated second-order model, for which the thermal network shown in Figure 0-28, can capture thermal dynamics of a zone that contains radiant floor heating system with a good accuracy.
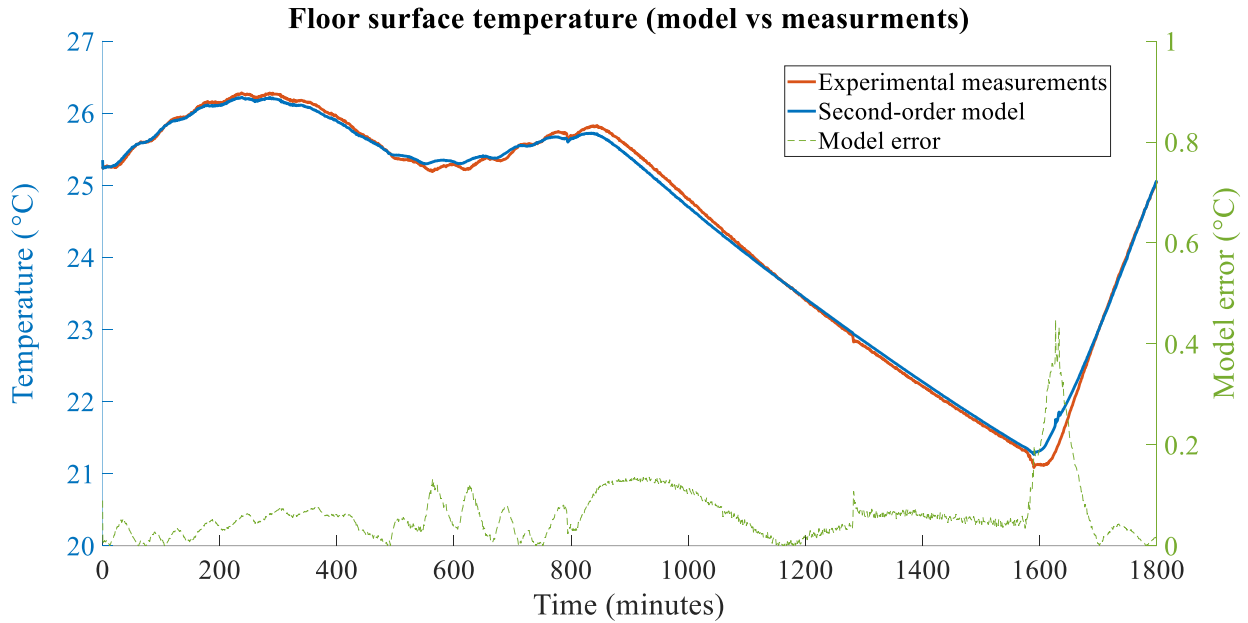
Figure 0-29. Second-order model versus experimental measurements (top) and model error (bottom)

As observed from Figure 0-29, the maximum error between the model and the measurements is about 0.45°C. However, majority of time the model error is less than 0.1°C and considering the prediction horizon of 1800 minutes (30 hours), the model is performing very well.

This validated model is used in the following sections to study the reactive and predictive strategies while dealing with different price signals from the grid.

The flexibility indicators presented in chapter 2 are mostly focused to quantify the energy that is reduced/increased over certain period of time. However, for certain applications the focus can be

explicitly on power (Watts) consumption reduction and how that can be reported to the electricity grid. In the next section the indicator utilized here is introduced.

4.3.1 Predictive Control and Building Energy Flexibility Index (BEFI)

Predictive control strategy is one of the key approaches in activating energy flexibility in buildings to meet smart grid needs. Model predictive control is one way to activate the energy flexibility that can be offered by the building especially when considering the storage in building elements and thermal lag. An appropriate index that is customized to the requirement of the local utility and building occupants is needed to quantify a building's energy flexibility.

The BEFI can be considered like a state variable, which quantifies available power (reduction or increase) from a building (Athienitis et al. 2020). It should be usable in real time in a building and its grid-interaction. It could be used in simulation and model predictive control (MPC) to maximize its value at a specific time in the future. It could be applied to a system (thermal zone) or a subsystem (thermal storage), and then aggregated to building level. It could also be aggregated at grid level by the utility to quantify flexibility potential. It should be defined according to the needed duration.

A building energy flexibility index (BEFI) is defined by Athienitis et al. (2020) (Athienitis et al. 2020) as the amount of power (kW) that can be increased or decreased relative to a reference profile (the "as-usual operation") by the building during a certain period of time (Dt):

$$\overline{BEFI}(t, Dt) = \frac{\int_{t}^{t+Dt} Q_{\text{ref}} dt - \int_{t}^{t+Dt} Q_{\text{flex}} dt}{\text{Duration time of flexibility}} \qquad (4.4)$$

The BEFI could be predicted continuously with a certain accuracy/uncertainty depending on the configuration and duration length. Generally, the shorter the duration, the less the uncertainty is

expected. Another factor to consider is the time of activation. For some grid needs, activation time must be within seconds and must be totally autonomous. For others, it can be different and may rely on communication protocols, but once the signal is received by the building, BAS response must be automated. Then, for some others, the need may be planned half a day in advance and the building can be designed and operated to maximize its flexibility during the period of need with potential significant financial benefits in terms of reduced operational costs. In this paper, the BEFI is calculated with dynamic tariffs and a floor heating system.

4.3.2   Peak demand periods in Quebec

In Quebec two peak demand periods are observed in a day during the heating season which are typically in the morning from 6 to 9 am and in the evening from 4 to 8 pm. Therefore, the price of the electricity can be different and higher during these periods compared to other times of the day. The price signals that are introduced and utilized in the following sections are created based on those typical peak demand periods in Quebec.

4.3.3 Predictive Strategies with a Short Notice

In this section thermal response of the radiant floor in reaction to a sudden change in the grid price signal is presented. The control of the radiant floor heating is based on the floor surface temperature. The heating is controlled through proportional control as:

$$Q_{aux} = K_p(T_{sp} - T_{floor})$$ (4.5)

Where T_{sp}=floor surface temperature setpoint, T_{floor}=floor surface temperature and K_p is the proportional constant. The maximum heating output is limited to the size of the system which is 2.7kW.

94

The ambient temperature profile considered is shown Figure 0-30. The ambient temperature varies between -7°C and -18°C with a mean of about -12°C, a relatively cold day in Quebec when high demand for electric space heating is expected.
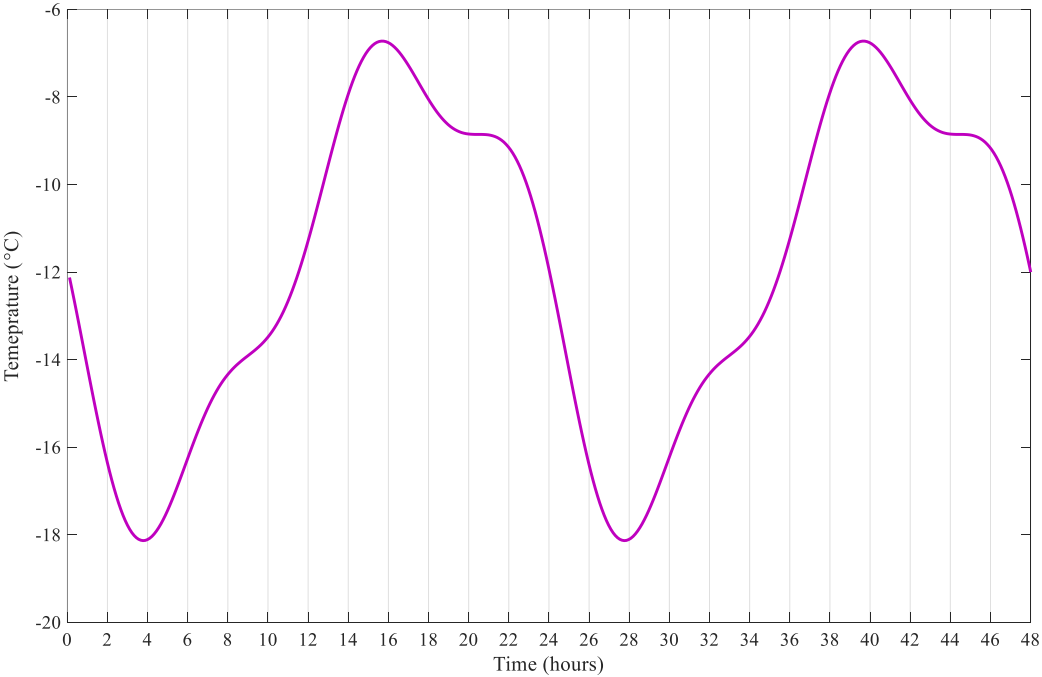
Figure 0-30. Ambient temperature profile

Figure 0-31 shows the heating load, floor surface temperature and zone air temperature for maintaining a constant floor surface temperature setpoint of 24°C which is considered the reference surface temperature. The results shown in Figure 0-31 are for a day when the electricity price remains constant for the whole day at the reference value which is assumed to be 10$ per kW for power.
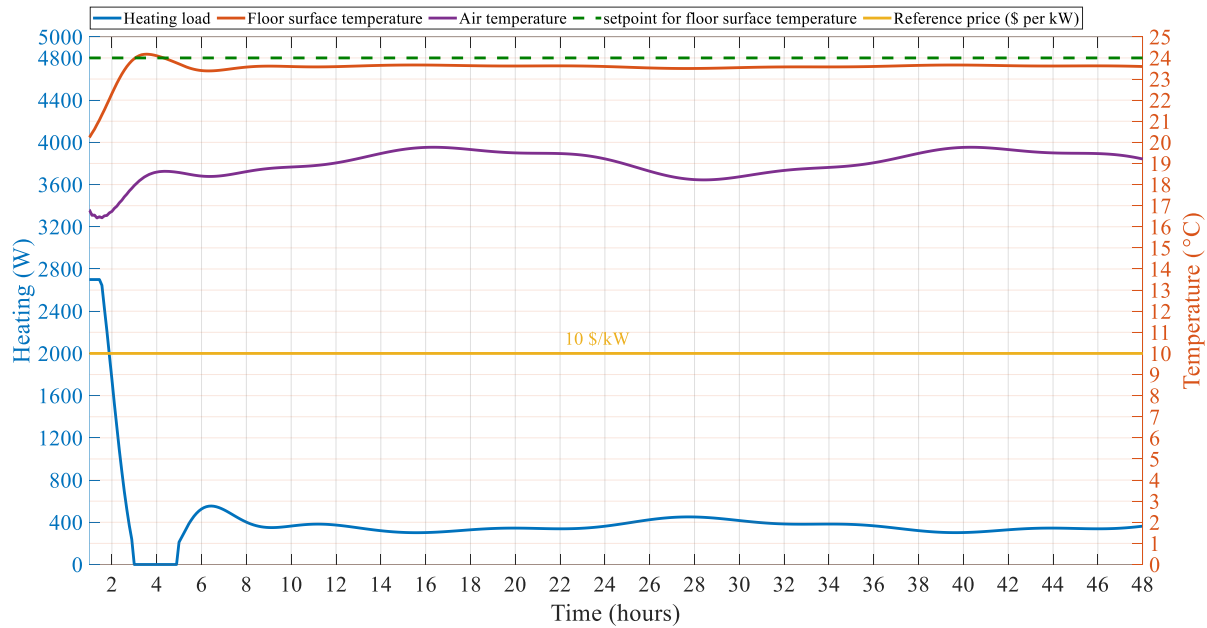
Figure 0-31. Reference profile for surface temperature setpoint of 24°C

As it can be observed from Figure 0-31, when keeping the floor surface temperature around 24°C, the zone air temperature stays between 18°C to 20°C which is within the comfort range (18-24°C) for occupants (ASHRAE 2010) and the operative temperature also stays within the comfort range.

Figure 0-32 shows the short-notice predictive (almost reactive) behavior to sudden increase, from 10$/kW to 20$/kW, in the price signal for a period of 3.5 hours (hours between 30 and 33.5) which is the typical morning peak demand period in Quebec (6-9:30am). It is assumed that the price of energy (kWh) is constant and only the power (kW) price is changing. The simplest strategy to deal with this sudden increase in the price signal is to turn off the heating system. It can be observed that due to shutdown of the heating system during that the period, the floor surface temperature (red line) falls to 22.2°C and air temperature (purple line) to 18°C. Considering the typical comfort boundaries of 18-24°C for the zone air temperature, the air temperature is at the lower threshold of the comfort boundary. It can be calculated that the BEFI would be about 400W for 3.5 hours. For the sake of comparison and accuracy, the floor surface temperature is also shown for the case

when using the non-linear equation for the convective heat transfer coefficient between floor surface and air temperature (h_{cf}). As observed, there is no significant difference between the two curves.
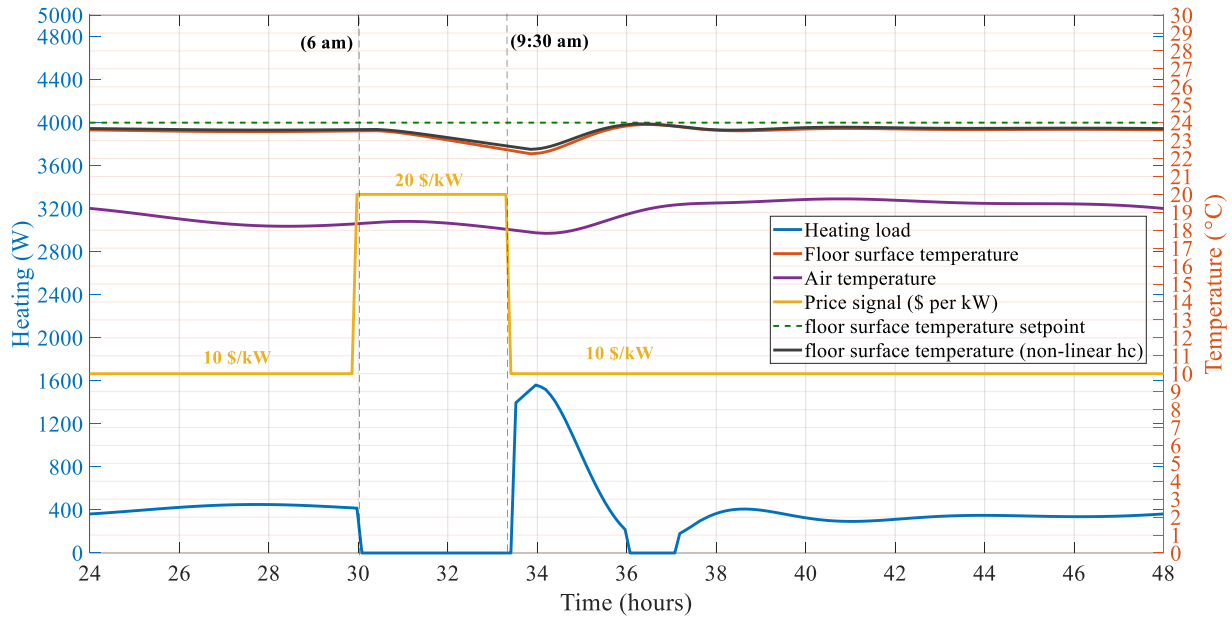
Figure 0-32. Reactive response to sudden increase in the price signal

Figure 0-33 shows another increase in the price signal during the evening on the same day. This second increase is during the evening peak demand hours (4-8pm) in Quebec during winter. As observed, since the second increase event happens when the zone air temperature was higher compared to the first event and generally the system was at a higher state of charge, the air temperature drops to 18.5°C at the lowest and the building can provide the average BEFI of 400W for 4 hours during this period.
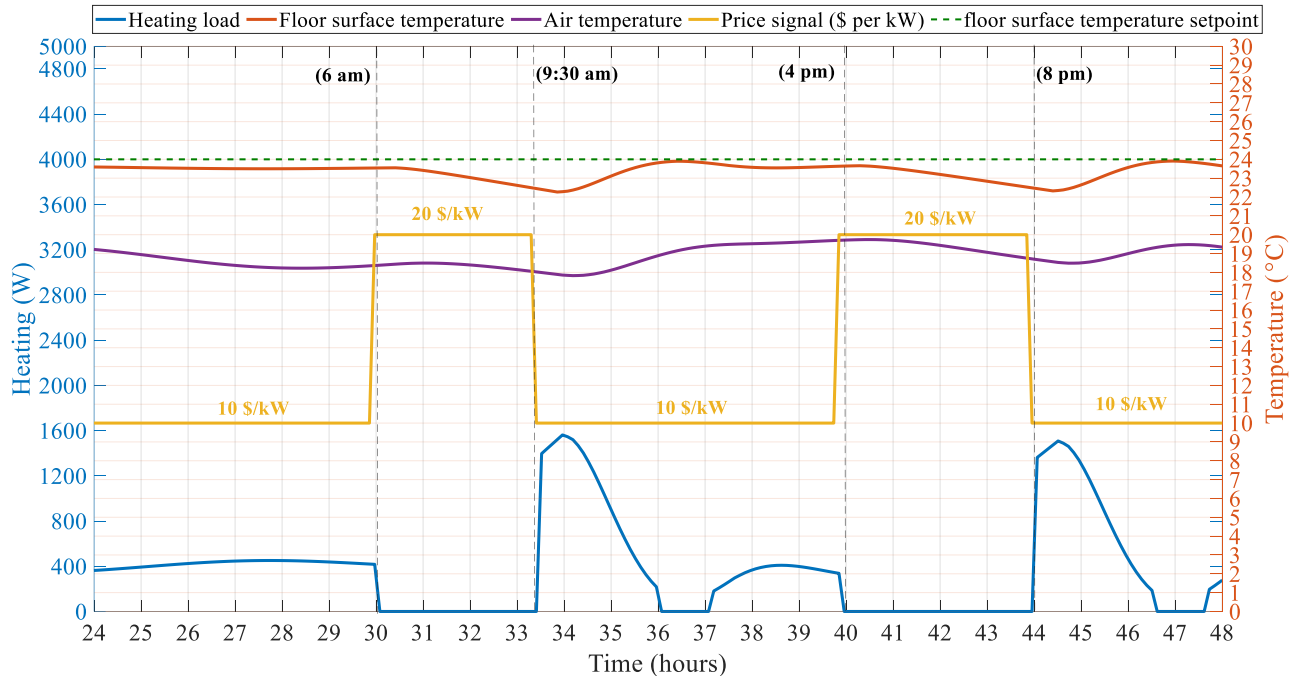
Figure 0-33.Reactive responses to sudden increase in the price signal

The intermittent nature of renewable energy sources increases the need for backup power to deal with the unpredicted fluctuations of power production. This results in an increasing need for liquidity in markets whose price closure approaches real-time (Morales et al. 2013b). Therefore, change in the price signal can be more frequent and the price signal from the grid can vary every hour during the day depending on the availability of electricity from renewable energy sources, weather conditions, emergency events, etc. For example, the dynamic price signal for the following 48 hours can look like the profile shown in Figure 0-34. As it can be observed from Figure 0-34, the price signal is changing almost every hour during the day and if the 10$ per kW is considered as the normal, reference operating price signal, there are some periods with price signals higher and as well as lower than the reference.

98
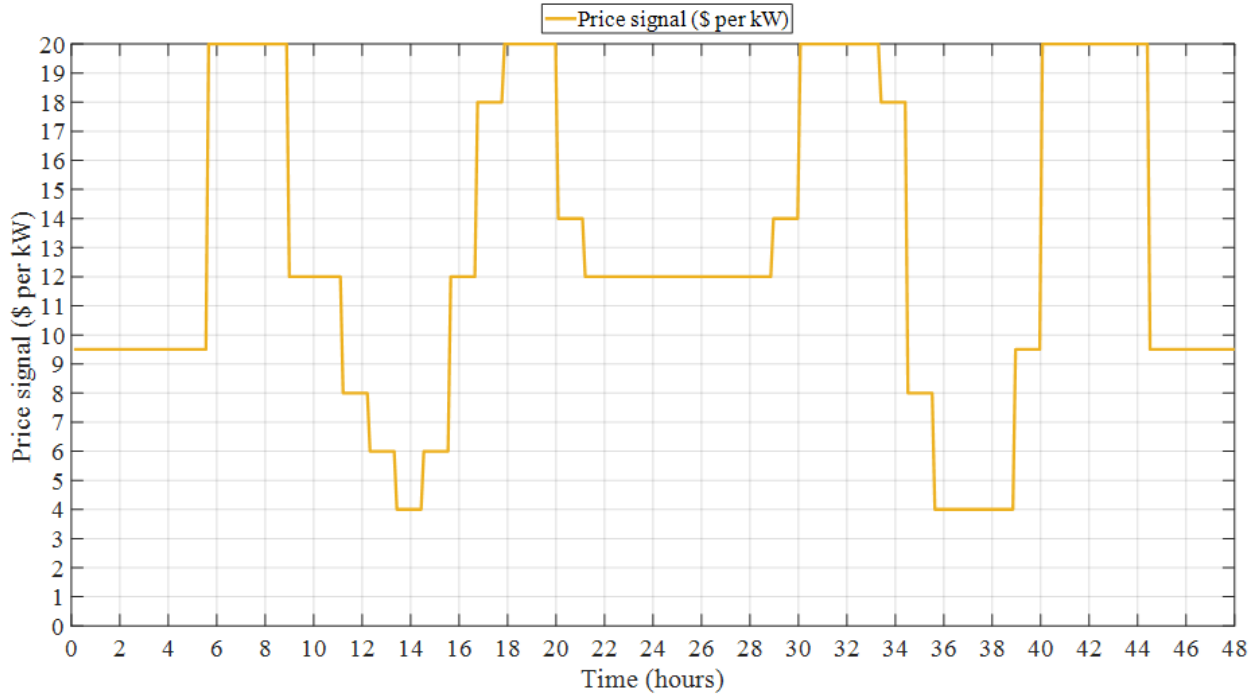
Figure 0-34. Dynamic price signal considered

It should be noted that a short notice (10-15 mins or shorter) of a price change from the grid may be given. The following control strategy is presented for these situations. First let us categorize the upcoming hour price signal into two categories:

1. Price signal lower than the normal reference operating price signal that is:

$$P(t) < P_{reference}$$

In this case since the price signal is lower than reference then the heating control can be just kept as usual and operating in the reference case ($Q_{aux}(ref)$). Therefore:

$$Q_{aux}(ref) = K_p(T_{sp} - T_{floor})$$

99

2. Price signals higher than the normal reference operating price signal:

$$P(t) > P_{reference}$$

In this case the strategy will be to keep the floor surface temperature at 24°C, however, the heating load will be a fraction of the reference heating and this fraction gets smaller as the price increases. Therefore, the strategy is defined as:

$$Q_{aux}(high\text{-}price)=(P_{reference}/P(t)) \times K_p(T_{sp}\text{-}T_{floor})$$

and the heating load can be named as the flexible heating load.

Figure 0-35 shows the application of this strategy to the thermal zone:
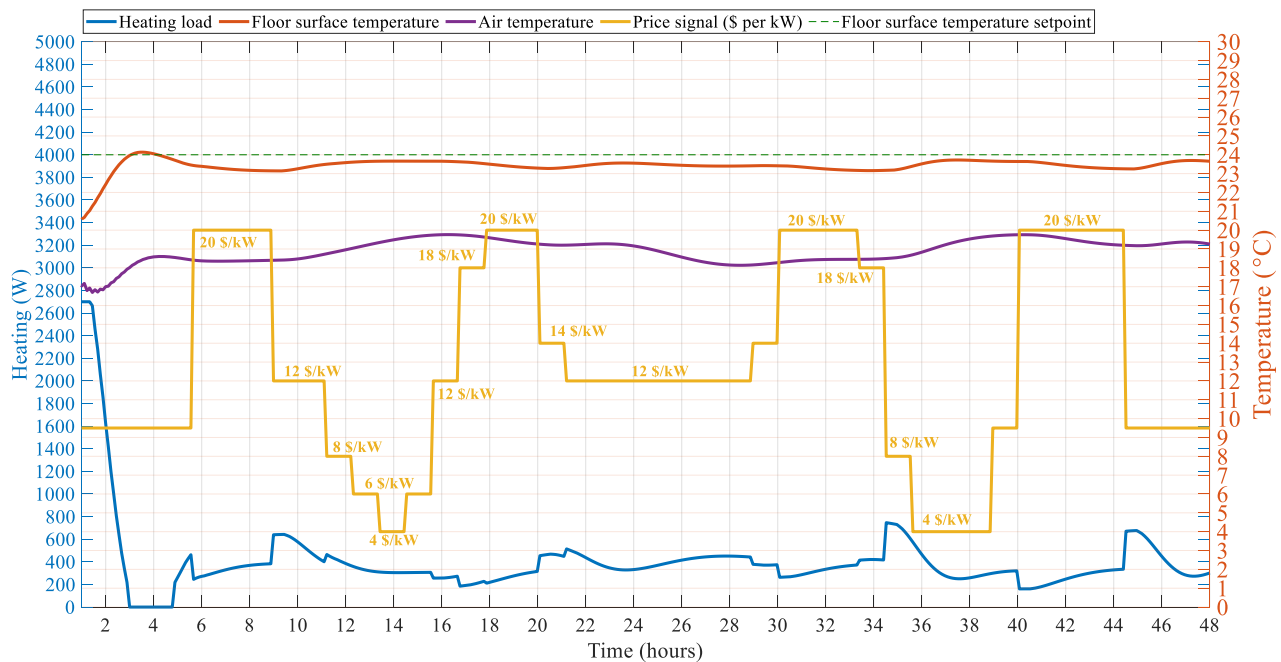
Figure 0-35. Application of the nearly reactive strategy to deal with the changing price signal

As can be observed from Figure 0-35, during the high price signal periods, whenever necessary, the heating load was turned on as a fraction of the reference heating load to keep the floor surface temperature near the setpoint hence reducing the amount of heating power and reducing the cost.

Figure 0-36 shows the comparison between the reference heating load and the flexible heating load from the strategy above. It can be observed how the above strategy decreases the heating load during the high price periods. As mentioned earlier, BEFI is the amount of power (W) that the building can reduce during certain periods of time. Therefore, BEFI during high price signal is the difference between the two curves which is shown by the area covered by the grey arrows.
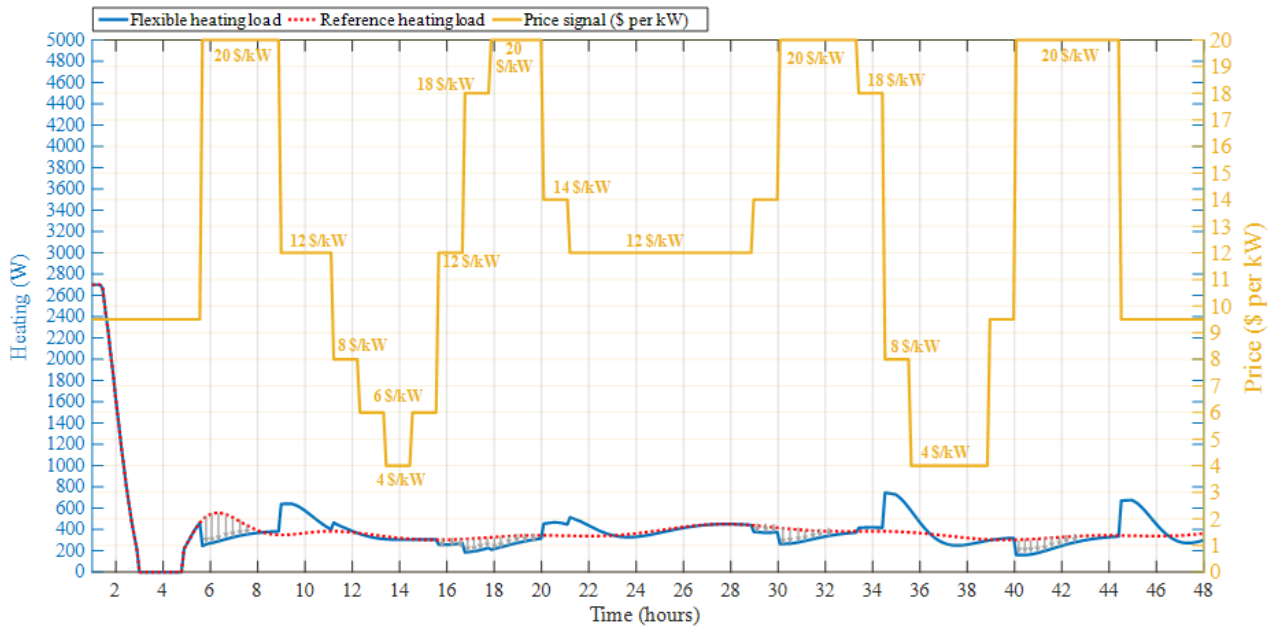
Figure 0-36.BEFI during high price signal periods

4.3.4 Predictive strategies

When the prediction of the following days for weather as well the grid price signals are available, the system can be designed to take predictive measures in order to minimize the power and/or

energy consumption during the high price signal period. In this section the predictive strategies for the price signals that are already presented in the previous sections are presented.

Here, the aim is to find a setpoint profile for the floor surface temperature proportional controller so that the surface temperature stays within the comfort range. Therefore, the objective function is defined as:

$$\text{minimize } J = \sum Psig \times Q_{aux} \rightarrow \text{ so that : } 23°C \leq T_{floor} \leq 29°C$$

where $Psig$ is the value of the price signal at every time step. Considering the above range for the floor surface temperature with the maximum of 29°C [5], the operative temperature (T_{op}) stays between 20°C and 24°C which is the recommend range by ASHRAE [5].

Figure 0-37 shows the results for the first price signal. As observed, the optimized floor surface temperature setpoint modulates the heating load of the floor in a way to keep the floor surface temperature very close to the minimum of 23°C during the periods with reference price signal but as it get closer to the high price signal period, it starts preheating the floor slab by increasing the

setpoint as high as 26°C. Therefore, we can see that the heating load is zero during the high price period.
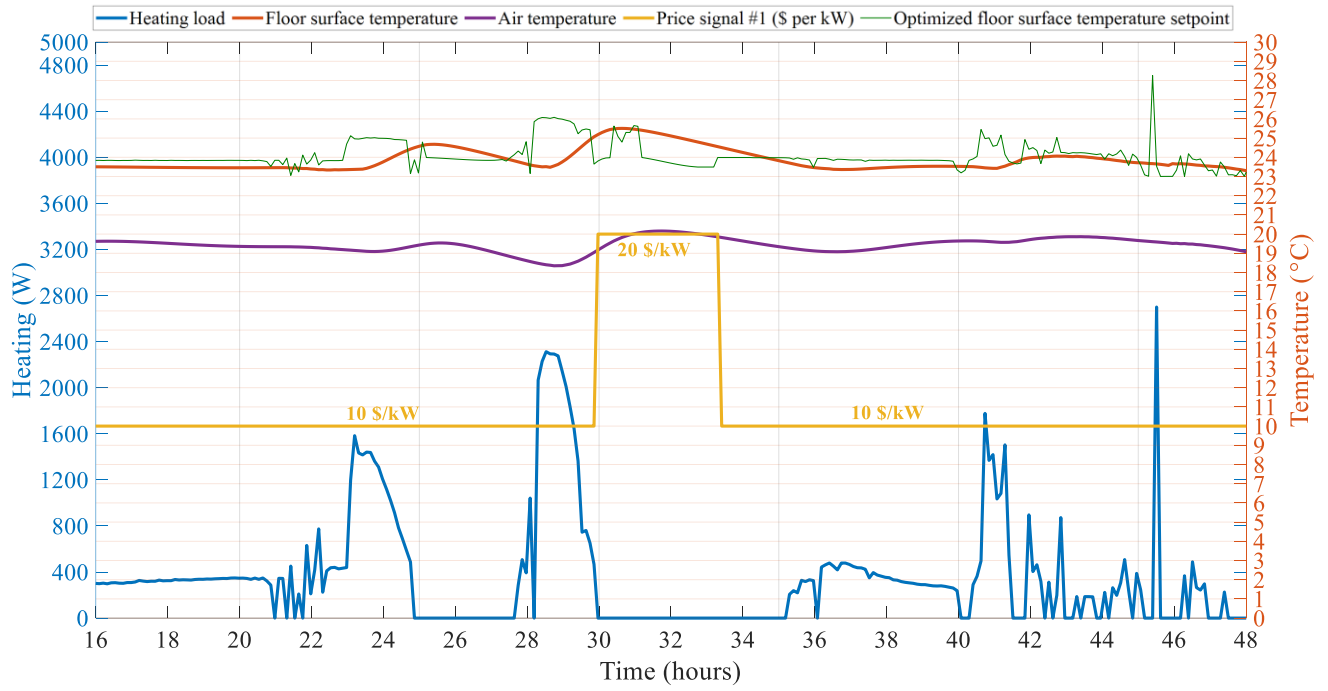
Figure 0-37. Predictive strategy for price signal #1

Now if another price signal was in the forecast in which two periods of high price is observed during the 48 hours, then a new setpoint found from the optimization is applied as shown in Figure 0-38.
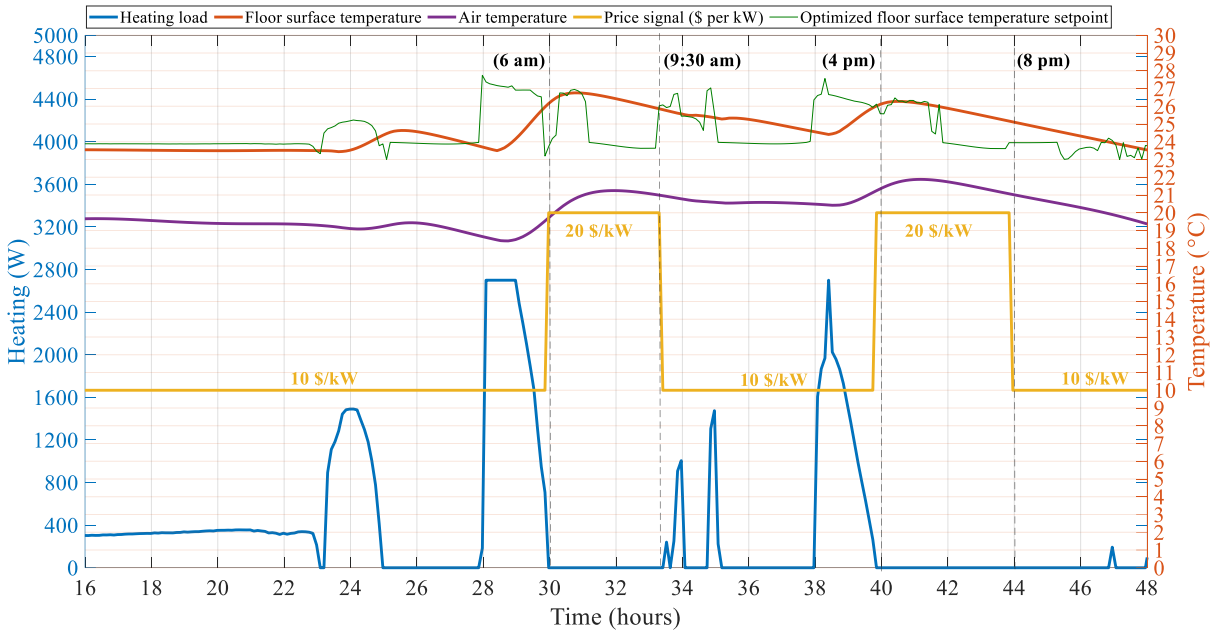
Figure 0-38. Predictive strategy for price signal #2

As it can be observed from both Figure 0-37 and Figure 0-38, the setpoint is designed in way that our zone is heated up until just before the periods of high price signal and then the setpoint is relatively low during that period so that due the thermal mass of the radiant floor concrete slab, the surface temperature does not drop below that setpoint and therefore, no heating is needed.

There can be more complicated price signals in the forecast as well. Figure 0-39 shows the predictive strategy for the price signal that was introduced in the reactive section which changes almost every hour. This price signal is already known from the forecast of the day before.
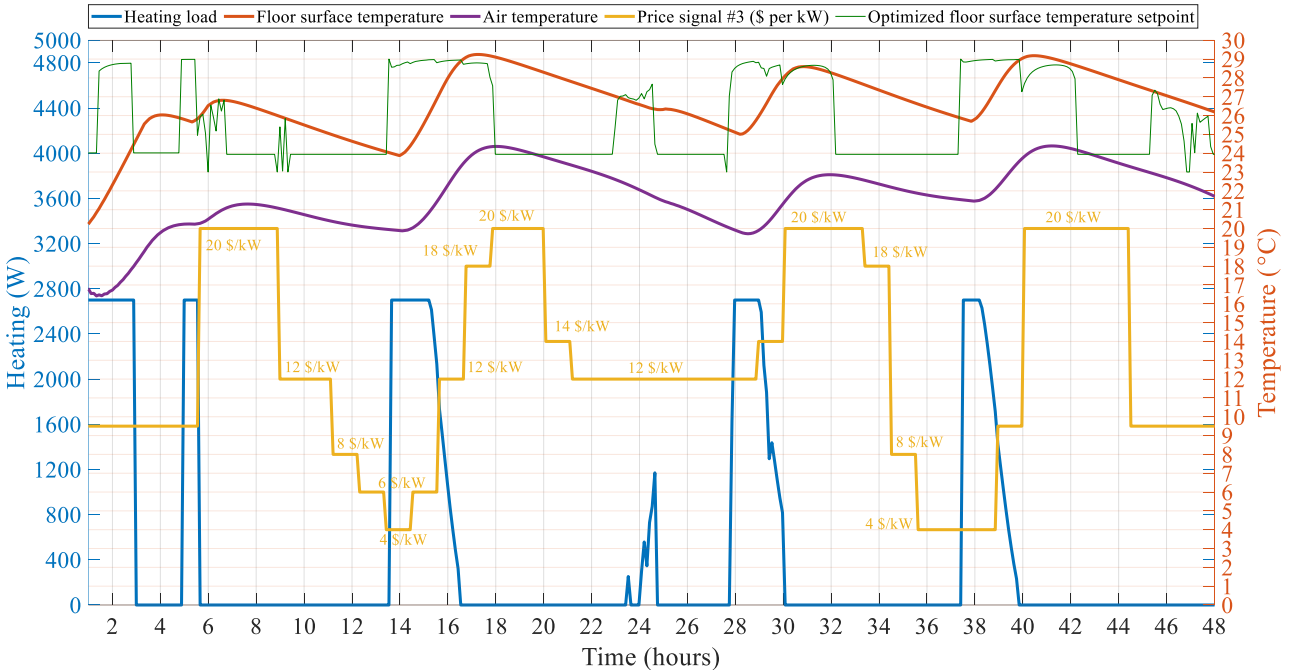
Figure 0-39. Predictive strategy for price signal #3

As can be observed from Figure 0-39, the building is heated up during the low-price period (until around 6am) and the setpoint is increased to the maximum upper threshold for floor surface temperature which is 29°C. Then after hour 6, there is no heating during the peak demand period (6-9:30am) and the slab thermal mass let the heating be turned off until the hour 13. Then, the setpoint is again increased to 29°C to preheat the building and in order to minimize the heating during the afternoon peak demand hours (4-8pm). A similar trend is observed during the next day as well.

4.3.5 Emergency and non-predicted change in the price signal

Contingency reserve is the amount of power that utility may call when needed to face the loss of a generation unit or other unexpected load balance(Wang et al. 2005). This reserve needs to be available within a ten-minute notification time, for a duration of one hour. Therefore, the building

should be able to quantify the amount of power that it can decrease from its current consumption profile for the following hour.

Figure 0-37 to 38 showed the strategy for when prediction of the weather as well as the price signal is available. Now, when there can be an unexpected situation that due to an emergency, there is a sudden increase in the price signal which was not predicted and expected. Therefore, a short notice (about 10 minutes before) is sent from the grid asking about the possibility of reduction in the current power consumption of the building and therefore, a BEFI can be requested. Figure 0-40 shows such an event when the original predictive strategy was based on the price signal #2 (Figure 0-38).
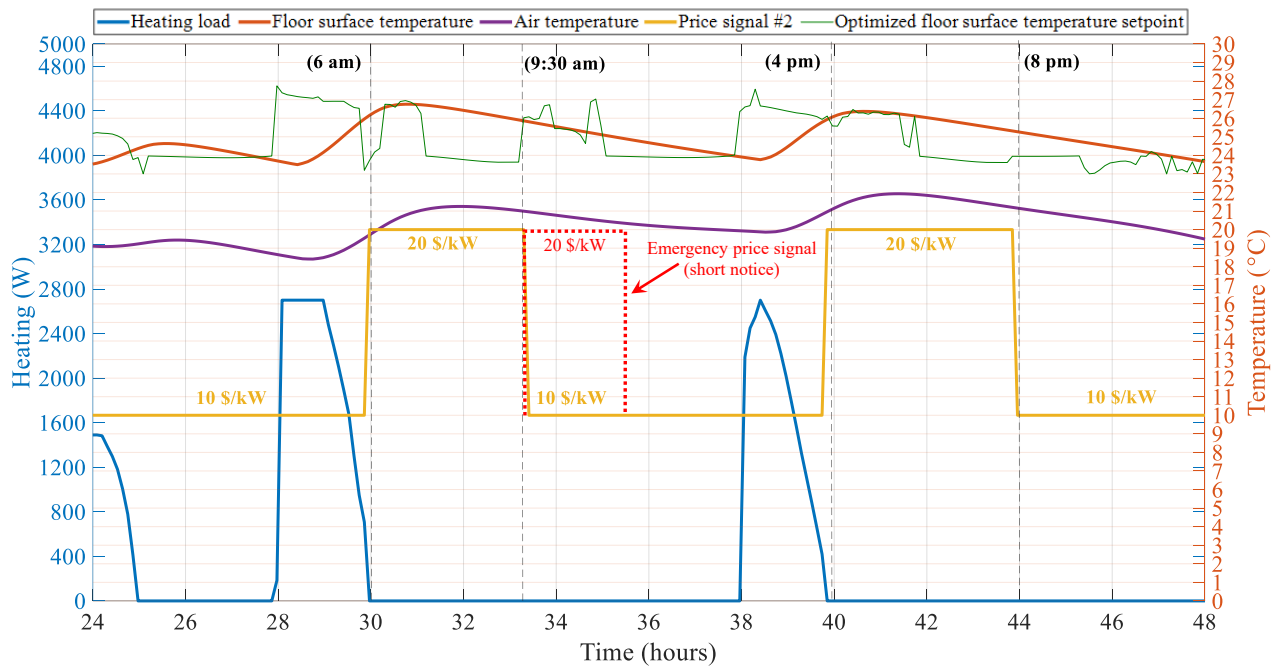
Figure 0-40. Unexpected increase in the price signal #2

As observed, there is a sudden unexpected increase in the price signal between hours 33.5 and 35.5 (9:30-11:30am) and therefore, heating load was turned off immediately. As shown in Figure 0-40,

turning off the heating between during that period has a little impact on the floor surface and air temperatures. The BEFI which is the amount of power that is reduced compared to the reference case (Figure 0-38) and is calculated on average as, BEFI= 270 W.

Therefore, the grid can be informed that the zone can possibly reduce the power consumption for an average of 84W during the following hour.

The timing of the unexpected change in the price signal is also particularly important. For example, if the unexpected change happens in a different hour that is closer to the period with a high price, then it could be more challenging to deal with this sudden change. As shown in Figure 0-41, if the sudden increase in price signal happens between hours 38.5 and 39.5, then the controller which is acting based on the predictions would not have enough time to follow back the optimized setpoint profile and as the result, some heating is observed during the predicted high price signal period as shown in Figure 0-41 with black dashed circle. However, as observed from Figure 0-41, there is no need for the heating since our floor surface temperature is already above the lower threshold of 23°C. Therefore, here in this case the setpoint temperature needs to be modified for the period between 40 and 44 hours and put at the lower threshold of 23°C. This modification let us have zero power consumption during that period as show in Figure 0-42.
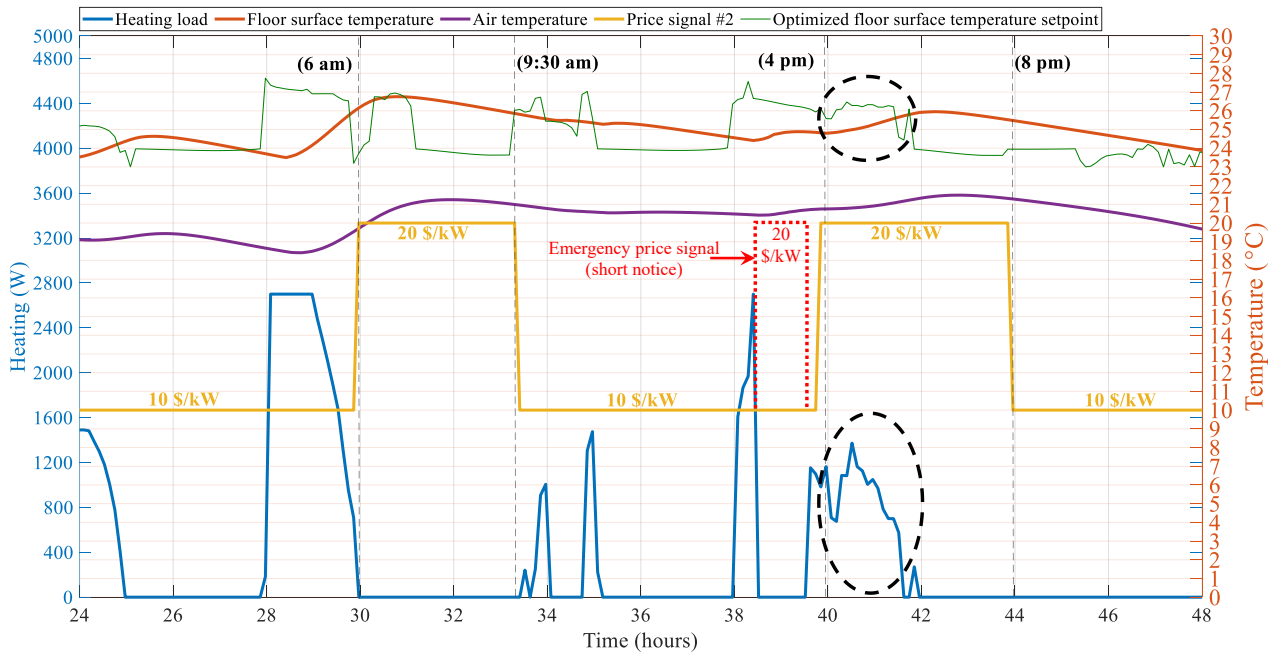
Figure 0-41. Unexpected change in the heating load
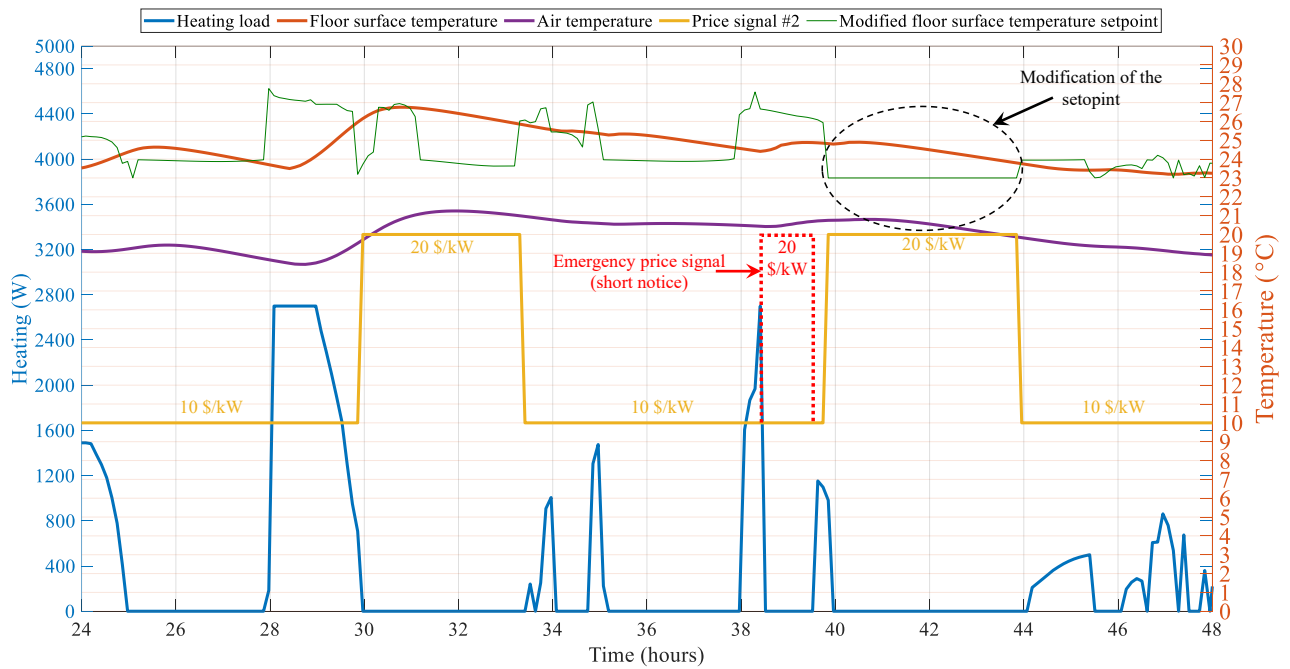
Figure 0-42. Modified setpoint to correct the heating load

4.3.6 Dynamic pricing of energy

There are certain situations in which the dynamic pricing is explicitly mentioned for energy consumption (kWh) instead of power (kW). In this case the optimization must be done for energy and the cost for energy (kWh) is minimized instead of power (kW). The unit of the price signal will be cents per kWh (c/kWh). Figure 0-43 shows the results.
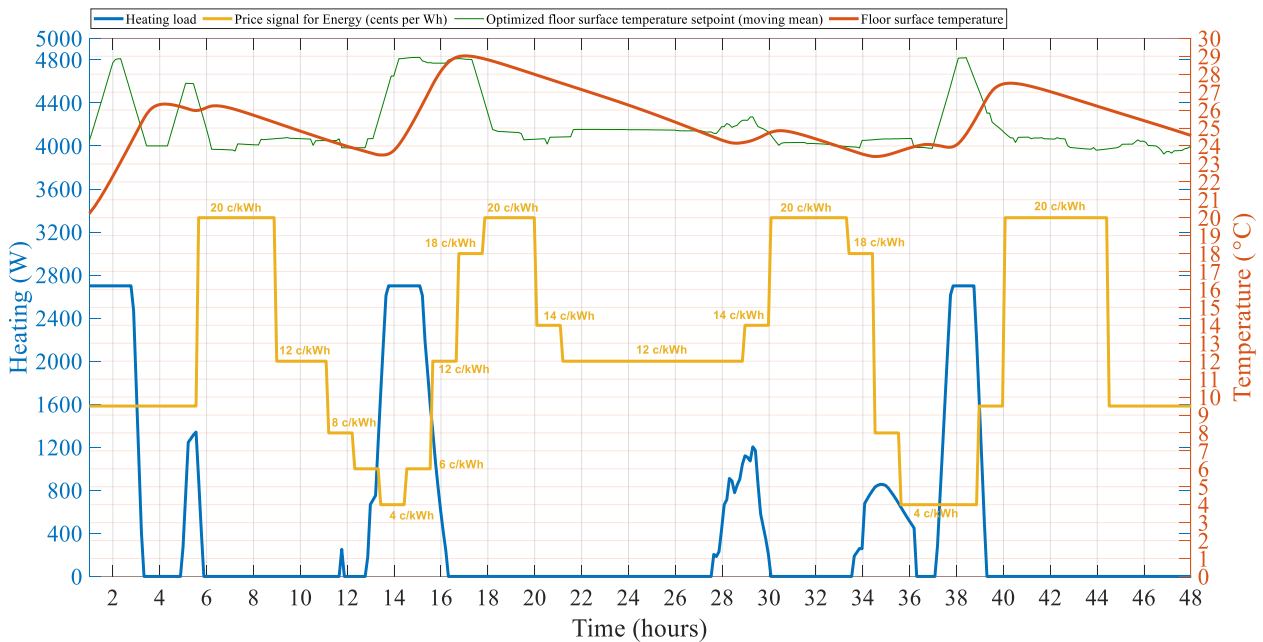
Figure 0-43. Predictive strategy for dynamic energy price signal

As observed from Figure 0-43, the heating works in a similar way to when it was used to minimize the power consumption. As you may notice the moving mean value of the setpoint profile obtained from the optimization is used since the optimized setpoint contained lots of spikes in the temperature which consequently causes spikes in the heating loads and lots of on/off which is not practical. Therefore, it is observed when minimizing the cost of power, we are actually minimizing the cost of energy at the same time.

4.4   Summary

This chapter presented major applications of the methodology to radiant slab heating systems used in de-icing and predictive control to optimize interaction with a smart grid.

In the first section, several analyses were presented for different design options of de-icing slab of a major transportation infrastructure and the thermal dynamics of the slab was studied under different ambient conditions assuming cloudy day with sky temperature close to the ambient temperature. The time required to reach +2°C surface temperature was evaluated for two different piping depths, ambient temperature and system capacity. Also, a number of important scenarios were studied and an idling strategy was presented for each scenario. Then, utilization of slab thermal mass for energy flexibility and power shifting was presented.

In the next section, application of radiant slab heating for providing building heat demand was presented. A perimeter zone test cell located inside the environmental chamber was used as the case study. 1D low-order modelling was presented for the zone and the model calibration was explained. It was observed that the low-order model is very sensitive to the convective heat transfer coefficient between the floor surface and the air temperature of the zone and a well-calibrated model can perform quite accurately in capturing thermal dynamics of the zone. The model was used in the following section to study different predictive control strategies in response to different price signals including short notice as well as the day-ahead predictions to minimize the cost of electricity.

CHAPTER 5: CONCLUSION

This thesis presented a methodology for modeling of hydronic radiant slab heating system of buildings and slab de-icing of infrastructure as well as studies of predictive control and energy flexibility strategies by means of the developed models.

A frequency domain transfer function methodology to characterize building thermal dynamics and design for energy flexibility was presented for a zone with a hydronic floor heating/cooling system that has significant thermal mass. It was observed that since the pipes are buried deep in concrete, the one-dimensional heat transfer models can be used with an acceptable accuracy. It was discussed that managing the quantified energy flexibility in heating demand by means of the models is especially beneficial in interaction with smart grids and facilitating the integration of intermittent renewable energy sources to the grid and reducing the peak power demand significantly.

It was shown how the analysis of building transfer functions, obtained from a frequency domain model of the zone, can be practical in evaluating different parameters in the zone that affect the zone thermal dynamics and energy flexibility. It was shown how increasing thermal mass in the zone affects the dominant harmonics of the zone important transfer functions when considering different types of heating systems. By studying the transfer function $Z_{1,2}$, between the zone air temperature (node 1) and the source at node 2 (floor surface), the optimum floor thickness for the minimum air temperature fluctuation (and maximum flexibility) was found for different types of concrete. This optimum is an important consideration for the zone occupant comfort and energy flexibility.

The transfer function $Z_{1,aux}$ which represents the effect of the floor auxiliary heating source on the zone air temperature, was derived and the effect of different floor concrete thicknesses on the magnitude of the transfer function's dominant harmonic was analyzed. By means of transfer function $Z_{1,aux}$ the delay between the heat input of radiant floor at pipes level and the air temperature was calculated which is a crucial piece of information for designing control strategies for radiant floor systems and utilizing the energy flexibility of the thermal mass. Experimental measurements in an environmental chamber were used to validate the results. A control strategy based on the calculated time delay from the transfer function was applied to the case study. It was observed that this control strategy reduces the peak power and energy consumption by 100% during the peak demand hours by means of the quantified energy flexibility using the floor thermal mass, while maintaining satisfactory comfort conditions.

Predictive control strategies in response to different price signals from the electricity grid with short and long-term predictions were presented to enhance the energy flexibility for a thermal zone equipped with a hydronic floor heating system and significant amount of thermal mass. The flexibility is especially beneficial in interaction with the smart grid to reduce the peak power demand significantly during the critical periods. A methodology to create low-order thermal network models was presented and utilized to develop the thermal model of the zone. The model was validated with experimental measurements and subsequently used to study the control strategies. Then, a methodology was presented to deal with a short notice price signal that changes every hour during the day and for which the prices can be either higher or lower than the reference operating condition. It was observed that this methodology can significantly reduce the cost of electricity consumption while ensuring the occupant comfort is not violated. Then, an optimization methodology was introduced to minimize the cost function defined based on the predicted price

signal for the following days. The optimized floor surface temperature setpoint was found for different price signals to minimize the cost of the heating power (kW) as well as the energy (kWh). It was shown that the strategy can be modified if the price signal prediction would not go as expected and sudden increase in the price happens especially during the critical periods.

Finally, a methodology to develop thermal models for predictive control of hydronic de-icing systems for urban infrastructure as well as a number of control strategies by means of the developed models were presented. It was demonstrated that low-order RC models can represent thermal dynamics of a hydronic de-icing system accurately and the model can be efficiently utilized to analyze slab thermal dynamics and perform control studies.

The developed models were used to study the performance of a hydronic system of an urban transportation infrastructure with different piping designs and system capacities under different ambient conditions. For structural reasons it was desired to put the hydronic pipes as low as possible in the concrete slab to minimize the risk of damage to the pipes due to structural stresses from passing cars and trucks. The thermal mass of the concert slab causes significant delay in the system thermal response to heat input. However, it provides an excellent opportunity to apply predictive control strategies and utilize the energy flexibility offered by the slab thermal mass.

Two different piping designs were considered for a case study, with the pipes placed in the middle of the slab and at the bottom with total slab thickness of 35cm. It was observed that if the hydronic system is turned on only certain hours before the precipitation event starts (no consideration of previous heat idling) it can take more than a day for the system to reach to the above freezing surface temperature (+2°C) at cold ambient temperature of -20°C. Then, it was observed that by idling certain amount of heating and maintaining the slab surface at -4°C, it will take a much less amount of time for the slab to reach the desired +2°C surface temperature. Also, during a period

of extremely cold ambient temperature with precipitation in the forecast it was observed that with the design that considers pipes in the middle it will be possible to keep the surface temperature much lower than -4ºC (in order to save more energy) and still reach the desired +2ºC in a reasonable amount of time (less than a day). It was observed that insulation under the slab plays a significant role in terms of heating power and energy required to reach the desired surface temperature specifically during the period of cold ambient conditions and it is highly recommended to consider an insulation layer under the concrete slab.

A predictive control strategy was presented based on a specific piping depth and slab design. It was observed that the predictive control strategy can significantly reduce the peak power demand and energy consumption of the system during the peak demand period while still ensuring the safety of the surface by keeping it within the required temperature range.

5.1 Contributions of this research work

The major contributions resulting from this thesis are the following:

- Development of a comprehensive methodology to design hydronic slab de-icing systems while taking into account their predictive control and potential flexibility in interaction with smart grids; this methodology is based on development of low-order models for thermal zones with hydronic radiant floor heating system that can be used for design and model-based predictive control

- A method based on frequency domain techniques for designing control strategies to enhance the energy flexibility of zones with hydronic floor heating systems;

- A method for short notice predictive control in response to the change in the grid price signal for the zones with hydronic floor heating systems;

- A method for day-ahead predictive control in response to the change in the grid price signal for the zones with hydronic floor heating systems;

- A method for analysis of thermal dynamics of hydronic pavement heating systems under cold weather to be used for de-icing and predictive control.

5.2 Publications

The published papers from this thesis, as well as the submitted papers that are under review are listed below:

Journal articles:

1. **Saberi Derakhtenjani, Ali**, Athienitis, Andreas K. (2020).” A Frequency Domain Transfer Function Methodology for Thermal Characterization and Design for Energy Flexibility of Zones with Radiant Systems”. Journal of Renewable Energy, 163:1033-1045.
2. **Saberi Derakhtenjani, Ali**, Athienitis, Andreas K. (2020).” A numerical and experimental study of hydronic de-icing and its predictive control”. Submitted to ASHRAE journal of Science and Technology for the Built Environment, under review.
3. **Saberi Derakhtenjani, Ali**, Athienitis, Andreas K. (2020).” Predictive Control Strategies for Energy Flexibility in Response to Dynamic Electricity Prices for Zones with Radiant Systems”. Submitted to journal of Energies, under review.

Refereed conference papers:

1. **Saberi Derakhtenjani, Ali,** Athienitis, Andreas K. (2020). “Energy Flexibility Assessment of a Zone with Radiant Floor Heating System by Means of Experimental Measurements”. Proceedings of 12th Nordic symposium on building physics, September 2020, Tallinn, Estonia, online conference.
2. **Saberi Derakhtenjani, Ali**, Athienitis, Andreas K., D’Avignon, Katherine (2019). “Analysis of thermal dynamics of hydronic de-icing system designs by means of control-oriented thermal models”. Proceeding of Intelligent Transport Systems (ITS) 2019 World Congress, October 2019, Singapore.
3. **Saberi Derakhtenjani, Ali**, Athienitis, Andreas K., Candanedo, José A., D’Avignon, Katherine (2019). “A frequency domain methodology for design and control of radiant floor heating systems”. Proceeding of Building Simulation 2019 conference, September 2019, Rome, Italy.

4. **Saberi Derakhtenjani, Ali,** D'Avignon, Katherine, Athienitis, Andreas K. (2018)." Development of a Predictive Control Methodology for a Hydronic De-icing System for Urban Infrastructure". Proceedings of Intelligent Transport Systems (ITS) World Congress 2018, September 2018. Copenhagen, Denmark.

5. Candanedo, José A., **Saberi Derakhtenjani, Ali,** D'Avignon, Katherine, Athienitis, Andreas K. (2018). "A Pathway for the Derivation of Control-oriented Models for Radiant Floor Heating Applications." Proceedings of esim 2018 conference, May 2018, Montreal, Quebec.

6. **Saberi Derakhtenjani, Ali,** Athienitis, Andreas K. (2017). "A Study of the Effect of Model Resolution in Analysis of Building Thermal Dynamics". Proceedings of Building Simulation 2017 conference, August 2017, San Francisco, CA, U.S.A.

7. **Saberi Derakhtenjani, Ali,** Athienitis, Andreas K. (2016). "A Study of the Effect of Zone Design Parameters on Frequency Domain Transfer Functions for Radiant and Convective Systems". Proceedings of 4th international high-performance buildings conference, July 2016, Purdue University, West Lafayette, IN, U.S.A.

Reports:
- **Saberi Derakhtenjani, Ali,** Candanedo, Jose, Athienits, Andreas K. (2019). "Experimental assessment of energy flexibility potential of a zone with radiant floor heating system". IEA EBC Annex 67, Energy Flexible Buildings, deliverable report.

5.3 Future research opportunities and needs

This thesis presented a methodology to quantify and utilize the energy flexibility offered by a building or/and a transportation infrastructure. The future research can be on how to expand and apply this methodology to clusters of buildings and communities. It is necessary to investigate how to aggregate the energy flexibility from different clusters of buildings which can be in various multi-carrier energy systems. Therefore, the future research objectives can be categorized as:

- Generating knowledge from simulations as well as case studies aiming at optimally controlling different clusters of buildings equipped with various levels of thermal mass, and other energy storage systems to exploit the flexibility

- Studying frequency characteristics of building clusters through the admittance model of the clusters

- Quantifying and establishing contingency reserves for clusters for different periods of time and active demand response (ADR) events

- Developing MPC strategies at cluster level considering cluster dynamics and those of any centralized energy storage

REFERENCES

"The Danish Government. The Danish climate policy plan: towards a low carbon society, 2013.".

"Directive 2009 of the European Parliament and of the Council of 23 April 2009 on the promotion of the use of energy from renewable sources and amending and subsequently repealing Directives 2001/77/EC and 2003/30/EC. OJ L 140, 5.6.2009, p. 16–62. Available at: http://data.europa.eu/eli/dir/2009/28/oj. ."

"The Federal Ministry for Economic Affairs and Energy (BMWi). The energy of the future: Fourth "energy transition" monitoring report – summary. Berlin, 2016. Available at: https://www.bmwi.de/BMWi/Redaktion/PDF/V/vierter-monitoring-bericht-energie-der-zukunft-englische-kurzfassung,property=pdf,bereich=bmwi2012,sprache=de,rwb=true.pdf."

"IEA. Technology roadmap – smart grid, 2011. Available at: https://www.iea.org/publications/freepublications/publication/smartgrids_roadmap.pdf.".

AdlZarrabi, B., R. Mirzanamadi and J. Johnsson (2016). "Hydronic pavement heating for sustainable ice-free roads." *Transportation Research Procedia* 14: 704-713.

Aduda, K. O., T. Labeodan, W. Zeiler, G. Boxem and Y. Zhao (2016). "Demand side flexibility: Potentials and building performance implications." *Sustainable Cities and Society* 22: 146-163.

Arteconi, A., A. Mugnini and F. Polonara (2019). "Energy flexible buildings: A methodology for rating the flexibility performance of buildings with electric heating and cooling systems." *Applied Energy* 251.

ASHRAE (2010). Standard 55: Thermal Environmental Conditions for Human Occupancy.

ASHRAE (2011). HVAC Applications chapter 51: snow melting and freeze protection. Atlanta, GA.

ASHRAE (2017). ASHRAE HVAC Applications. Atlanta, GA.

Athienitis, A. K. (1994). Building thermal analysis. Boston,MA, USA, MathSoft Inc.

Athienitis , A. K., E. Dumont, N. Morovat, K. Lavigne and J. Date (2020). Development of a dynamic energy flexibility index for buildings and their interaction with smart grids. ACEEE 2020 Summer Study on Energy Efficiency in Buildings, California, USA.

Athienitis, A. K. and W. O'Brien, Eds. (2015). <u>Modelling, design and optimization of net-zero energy buildings</u>. Berlin, Wiley Ernst & Sohn.

Athienitis, A. K. and M. Santamouris (2002). <u>Thermal analysis and design of passive solar buildings</u>. London, UK, James & James.

Athienitis, A. K., M. Stylianou and J. Shou (1990). "A methodology for building thermal dynamics studies and control applications." *ASHRAE Transactions* 96(2).

Babiak, J., B. W. Olesen and D. Petras (2007). <u>REHVA Guidebook No 7: Low temperature heating and high temperature cooling</u>

Balbay, A. and M. Esen (2010). "Experimental investigation of using ground source heat pump system for snow melting on pavements and bridge decks." *Scientific Research and Essays* 5: 3955-3966.

Balbay, A. and M. Esen (2013). "Temperature distributions in pavement and bridge slabs heated by using vertical ground-source heat pump systems." *Acta Sci.* 35: 677-685.

Bauer, P., A. Thorpe and G. Brunet (2015). "The quiet revolution of numerical weather prediction." *Nature* 525: 47–55.

Bean, R., B. W. Olesen and K. W. Kim (2010a). "History of Radiant Heating and Cooing Systems, Part 1

" *AsHRAE Journal*(1): 40-46.

Bean, R., B. W. olesen and K. W. Kim (2010b). "History of Radiant Heating and Cooling Systems, Part 2." *AsHRAE Journal*(2): 50-55.

Boßmann, T. and I. Staffell (2015). "The shape of future electricity demand: Exploring load curves in 2050s Germany and Britain." *Energy* 90: 1317-1333.

Braun, J. E. (1990). "Reducing energy costs and peak electrical demand through optimal control of building thermal storage." *ASHRAE Transactions* 96(2): 876-887.

Brunner, C., G. Deac, S. Braun and C. Zöphel (2020). "The future need for flexibility and the impact of fluctuating renewable power generation." *Renewable Energy* 149: 1314-1324.

Candanedo, J., A. Allard and A. K. Athienitis (2011). "Predictive control of radiant floor heating and transmitted irradiance in a room with high solar gains." *ASHRAE Transactions* 117(2): 652-665.

Candanedo, J. and A. K. Athienitis (2011). "Predictive control of radiant floor heating and solar-source heat pump operation in a solar house." *HVAC & R Research* 17(3).

Candanedo, J., V. Dehkordi and P. Lopez (2013). A control-oriented simplified building modeling strategy. IBPSA Chambery , France.

Candanedo, J., A. Saberi Derakhtenjani, K. D'Avignon and A. K. Athienitis (2018a). A pathway for the derivation of control-oriented models for radiant floor heating applications. esim 2018, Montreal, Canada.

Candanedo, J., E. Saloux, J. M. Hardy, R. Platon, V. Dehkordi and A. CÔTÉ (2018b). Preliminary Assessment of a Weather Forecast Tool for Building Operation. Proceedings of 5th international High Performance Building conference, Purdue University, West Lafayette, IN.

CanMETEO (2017). *Natural Resources Canada*.

Cao, Y. G., S. Guo and J. Chen (2014). "The research on preventing tunnel freezing damages using heat pipe and ground source heat pump system." *Railway Standard Design* 58(10): 97-101.

Cardinaels, W. and I. Borremans, Eds. (2014). Demand response for families – linear final report. Genk, EnergyVille.

Champagne, F. and R. Drouin (2017). Bridge slippery Conditions Advisory and De-icing Systems – an Extensive Pilot and Comparative Study. Proceedings of ITS World Congress 2017, Montreal, Quebec, Canada.

Chen, M., S. Wu, H. Wang and J. Zhang (2011). "Study of ice and snow melting process on conductive asphalt solar collector." *Solar Energy Materials and Solar Cells* 95: 3241-3250.

Chen, Y., A. K. Athienitis and K. Galal (2013a). "Frequency domain and finite difference modeling of ventilated concrete slabs and comparison with field measurements: Part 1, modeling methodology." *International Journal of Heat and Mass Transfer* 66: 948-956.

Chen, Y., A. K. Athienitis and K. Galal (2013b). "Frequency domain and finite difference modeling of ventilated concrete slabs and comparison with field measurements: Part 2. Application." *International Journal of Heat and Mass Transfer* 66: 957-966.

Cochran, J., M. Miller, O. Zinaman, M. Milligan, D. Arent and B. Plmintier "NREL report: Flexibility in 21 st century power system. Available at: https://www.nrel.gov/docs/fy14osti/61721.pdf."

Cole, W. J., K. M. Powell, E. T. Hale and T. F. Edgar (2014). "Reduced-order residential home modeling for model predictivecontrol." *Energy and Buildings* 74: 69-77.

Converse, A. O. (2012). "Seasonal energy storage in a renewable energy system." *IEEE* 100: 401-409.

Cristóvão, R. O., V. M. S. Pinto, R. J. E. Matins, J. M. Loureiro and R. A. R. Boaventura (2016). "Assessing the influence of oil and grease and salt content on fish canning wastewater biodegradation through respirometric tests." *Journal of Cleaner Production* 127: 343-351.

Cui, B., S. Wang, C. Yan and X. Xue (2015). "Evaluation of a fast power demand response strategy using active andpassive building cold storages for smart grid applications." *Energy Conversion and Management* 102: 227-238.

Davis, R. E., M. B. Lowit and P. C. Knappenberger (1999). "A climatology of snowfall-temperature relationships in Canada." *Journal OF Geophysical Research* 10: 11985-11994.

De Coninck, R. and L. Helsen (2016). "Quantification of flexibility in buildings by cost curve – methodology and application." *Applied Energy* 162: 653-665.

Duffie, J. A. and W. A. Beckman (2013). Solar engineering of thermal processes. U.S.A, John Wiley & Sons, inc.

Eugster, W. J. (2007). Proceedings European Geothermal Congress, Unterhaching, Germany.

Fang, X., S. Misra, G. Xue and D. Yang (2012). "Smart grid – the new and improved power grid: a survey." *IEEE Community Survey Tutorials* 3: 944-980.

Foteinaki, K., L. Rongling, A. Heller and C. Rode (2018). "Heating system energy flexibility of low-energy residential buildings." *Energy and Buildings* 180: 95-108.

Gellings, C. (1985). "The concept of demand-side management for electric utilities." *IEEE* 73: 1486-1470.

Georges, E., G. Masy, C. Verhelst, V. Lemort and P. Andre (2014). <u>Smart Grid Energy Flexible Buildings Through The Use Of Heat Pumps In The Belgian Context</u>. International High Performance Buildings Conference, Purdue university, Westlaffayette, IN.

GWEC (2019). "Global wind statistics 2019."

Hong, S. H., M. M. Yu and X. F. Huang (2015). "A real-time demand response algorithm for heterogeneous devices in buildings and homes." *Energy* 80: 123-132.

Hu, L. N. (2013). "Application of electric heating system in the tunnel." *Shanxi Electronic Technology no. 3*: 11–12.

Hu, M. and F. Xiao (2020). "Quantifying uncertainty in the aggregate energy flexibility of high-rise residential building clusters considering stochastic occupancy and occupant behavior." *Energy* 194.

Huang, P., T. Xu and Y. Sun (2019). " A genetic algorithm based dynamic pricing for improving bi-directional interactions with re duce d power imbalance " *Energy and Buildings* 199: 275-286.

Ialam, M. S., T. Fukuhara and H. Watanabe (2006). "Horizontal U-tube road heating system using tunnel ground heat." *Journal of Snow Engineering of Japan* 22: 23-28.

IEAPVPS (2020). "Snapshot of global PV markets 2020."

Incropera, F. P., D. P. DeWitt, T. L. Bergman and A. S. Lavine (2006). <u>Fundamentals of heat and mass transfer</u>, John Wiley & Sons Canada, Ltd.

Jenks, S. C. (2001). A Model Predictive Control Strategy for a Bridge Deck Heated by a Geothermal Heat Pump System. Stillwater, OK, Oklahoma State University. **M.S. Thesis**.

Jensen, S., A. J. Marszal, R. Lollini, W. Paust, K. Armin, P. Engelmann, A. Stafford and G. Reynders (2017). "IEA EBC Annex 67 Energy Flexible Buildings." *Energy and Buildings*.

Jin, X. and X. Zhang (2011). "Thermal analysis of a double layer phase change material floor." *Applied Thermal Engineering* 31(10): 1576-1581.

Junker, R. G., A. GhasemAzar, R. A. Lopes, K. B. Lindberg, G. Reynders, R. Relan and H. Madsen (2018). "Characterizing the energy flexibility of buildings and districts." *Applied Energy* 225: 175-182.

Kim, D. and J. E. Braun (2012). Reduced-order building modeling for application to madel-based predictive control. Fifth National Conference of IBPSA-USA, Madison, Winsconsin.

Kim, K. W. and B. W. Olesen (2015a). "Radiant Heating and Cooling Systems, Part 1." *AsHRAE Journal*(2): 28-37.

Kim, K. W. and B. W. Olesen (2015b). "Radiant Heating and Cooling Systems, Part 2." *AsHRAE Journal*(3).

Kimura, K. (1977). Scientific basis for air-conditioning. London, UK, Applied Science Publishers Ltd.

Lai, J. X., J. L. Qiu, J. X. Chen, H. B. Fan and K. Wang (2015). "New technology and experimental study on snow-melting heated pavement system in tunnel portal." *Advances in Materials Science and Engineering*.

Le Dreau, J. and P. Heiselberg (2016). "Energy flexibility of residential buildings using short term heat storage in the thermal mass." *Energy* 111: 991-1002.

Li, C., H. Liangliang, Z. Mingdong, X. Jing, M. Hongwei, Z. Shuliang and W. Li (2013). "Synthesis, structure and characterization of two new open-framework gallium phosphite-oxalates of varying dimensionality." *Journal of Solid State Chemistry* 208: 86-92.

Lienhard, J. H. (2003). A Heat Trasnfer Textbook.

Lim, J. H., J. Jo, Y. Kim, M. S. Yeo and K. W. Kim (2006). "Application of the control methods for radiant floor cooling system in residential buildings." *Building and Environment* 41: 60-73.

Liu, H., P. Maghoul, A. Bahari and M. Kavgic (2019). "Feasibility study of snow melting system for bridge decks using geothermal energy piles integrated with heat pump in Canada." *Renewable Energy* 136: 1266-1280.

Liu, X., S. J. Rees and J. D. Spitler (2003). Simulation of a geothermal bridge deck anti-icing system and experimental validation. Proceedings of the Transportation Research Board 82nd Annual Meeting, Washington DC.

Liu, X., S. J. Rees and J. D. Spitler (2007a). "Modeling snow melting on heated pavement surfaces. Part I: Model development." *Applied Thermal Engineering* 27: 1115-1124.

Liu, X., S. J. Rees and J. D. Spitler (2007b). "Modeling snow melting on heated pavement surfaces. part II: experimental validation." *Applied Thermal Engineering* 5: 1125-1131.

Liu, X. and J. Spitler (2004). A Simulation Tool for the Hydronic Bridge Snow Melting System. 12th International Road Weather Conference, Bingen, Germany

Lund, P., J. Lindgren, J. Mikkola and J. Salpakari (2015). "Review of energy system flexibility measures to enable high levels of variable renewable electricity." *Renewable and Sustainable Energy Reviews* 45: 785-807.

Mirzanamadi, R., C. E. Hagentoft, P. Johansson and J. Johansson (2018). "Anti-icing of road surfaces using Hydronic Heating Pavement with low temperature." *Cold Regions Science and Technology* 14: 106-118.

Morales, M., J. M. Conejo, A. J. Madesn, H. Pinson and P. Zungo (2013a). "Managing uncertainties with flexibility." *Dordrecht: Springer Science & Business Media* 205.

Morales, M. J., A. J. Conejo, H. Madsen, P. Pinson and M. Zungo (2013b). Integrating Renewables in Electricity Markets, Springer.

Niu, J., Z. Tian, Y. Lu and H. Zhao (2019). "Flexible dispatch of a building energy system using building thermal storage and battery energy storage." *Applied Energy* 243: 274-287.

Oldewurtel, F., D. Sturzenegger, G. Andersson, M. Morari and R. S. Smith (2013). Towards a standardized building assessment for demand response. 51nd IEEE conference on Decision and Control Maui, Hawaii.

Olesen, B. W. (2001). Control of Floor Heating and Cooling Systems. Clima 2000/Napoli 2001 World Congress, Napoli.

Palensky, P. and D. Dietrich (2011). "Demand side management: demand response, intelligent energy systems and smart loads." *IEEE Transformation and Industry Information* 7(3): 1150-1156.

Peterson, M., K. Edlund, L. Hnasen, J. Bendtsen and J. Stoustrup (2013). A taxonomy for modelling flexibility and a computationally efficient algorithm for dispatch in smart grid. American control conference (ACC), Golden, CO.

Ren, W. Y. (2013). "On application of electric heat tracing insulation in water fire-fighting system of road tunnels." *Shanxi Architecture* 39: 177-178.

Rey, A., R. Dumoulin and A. K. Athienitis (2018). Comparison Of Three Transient Models For Slab Heating/Cooling Systems. International High Performance Buildings Conference, Purdue University.

Reynders, G. (2015). "Quantifying the impact of building design on the potential of structural storage for active demand response in residential buildings." *PhD thesis*.

Reynders, G., J. Diriken and D. Saelens (2015). A generic quantification method for the active demand response potential of structural storage in buildings. 14th International Conference of the International Building Performance Simulation Association, Hyderabad, India.

Reynders, G., J. Diriken and D. Saelens (2016). Quantifying the active demand response potential: impact of dynamic boundary conditions. CLIMA 2016 – proceedings of the 12th REHVA World Congress.

Reynders, G., R. A. Lopes, A. Marszal-Pomianowska, D. Aelenei, J. Martins and D. Saelens (2018). "Energy flexible buildings: An evaluation of definitions and quantification methodologies applied to thermal storage." *Energy and Buildings* 166: 372-390.

Rhee, K. N., M. S. Yeo and K. W. Kim (2011). "Evaluation of the control performance of hydronic radiant heating systems based on the emulation using hardware-in-the-loop simulation." *Building and Environment* 46: 2012-2022.

Saberi Derakhtenjani, A. and A. K. Athienitis (2020). "A frequency domain transfer function methodology for thermal characterization and design for energy flexibility of zones with radiant systems." *Renewable Energy* 163: 1033-1045.

Saberi Derakhtenjani, A., J. Candanedo, Y. Chen, V. Dehkordi and A. K. Athienitis (2015). "Modeling approaches for the characterization of building thermal dynamics and model-based control: A case study." *Science and Technology for the Built Environment* 21(6): 824-836.

Salpakari, J. and P. Lund (2016). "Optimal and rule-based control strategies for energy flexibility in buildings with PV." *Applied Energy* 161: 653-665.

Six, D., J. Desmedt, D. Vanhout and J. Vanbael (2011). Exploring the flexibility potential of residential heat pumps combined with thermal energy storage for smart grids. 21st International conference on electricity distribution, Frankfurt.

Stauch, V., C. Hug, F. Schubiger and P. Steiner (2010). "Weather forecasts, observations and algorithms for building simulation and predictive control." *Zürich: MeteoSwiss*.

Sun, D., A. K. Athienitis and K. D'Avignon (2018a). <u>Application of smie-transparent photovoltaics in transportation infrustructure for energy savings and solar electricity production: towards novel net-zero energy tunnel design</u>. Proceedings of EU PVSEC conference, Brussels,Belgium.

Sun, Y., K. Panchabikesan, M. MastaniJoybari, D. Olsthoorn, A. Moreau, M. Robichaud and F. Haghighat (2018b). "Enhancement in peak shifting and shaving potential of electrically heated floor residential buildings using heat extraction system." *Journal of Energy Storage* 18.

Thieblemont, H., F. Haghighat and A. Moreau (2016). "Thermal Energy Storage for Building Load Management: Application to Electrically Heated Floor." *Applied Science* 6.

Thieblemont, H., F. Haghighat, A. Moreau, A. Bastani and F. Kuznik (2013). <u>Alternative Method to Integrate Electrically Heated Floor in TRNSYS: Load Management</u> CLIMA 2013.

Thieblemont, H., F. Haghighat, A. Moreau and G. Lacroix (2018). "Control of electrically heated floor for building load management: A simplified self-learning predictive control approach." *Energy and Buildings* 172: 442-458.

Wang, J., X. Wang and Y. Wu (2005). "Operating Reserve Model in the Power Market." *IEEE Transactions on Power Systems* 20.

Weiß, T., A. M. Fulterer and A. Knotzer (2019). "Energy flexibility of domestic thermal loads – a building typology approach of the residential building stock in Austria." *Advances in Building Energy Research* 13(1): 122-137.

Werner Juszczuk, A. J. (2018). "Experimental and numerical investigation of lightweight floor heating with metallised polyethylene radiant sheet." *Energy & Buildings* 177: 23-32.

Xie, F. and J. R. Whiteley (2007). <u>Model Predictive Control of a Geothermally Heated Bridge Deck</u>. American Control Conference, New York City, USA.

Xu, H., D. Wang, Y. Tan, J. Zhou and M. Oeser (2017). "Investigation of design alternatives for hydronic snow meltingpavement systems in China." *Journal of Cleaner Production* 170: 1413-1422.

Xue, X., S. Wang, C. Yan and B. Cui (2015). "A fast chiller power demand response control strategy for buildingsconnected to smart grid." *Applied Energy* 137: 77-87.

Zhou, Y. and S. Cao (2019). "Energy flexibility investigation of advanced grid-responsive energy control strategies with the static battery and electric vehicles: A case study of a high-rise office building in Hong Kong." *Energy Conversion & Management* 199.

Zhou, Y. and S. Zheng (2020). "Machine-learning based hybrid demand-side controller for high-rise office buildings with high energy flexibilities." *Applied Energy* 262.

APPENDIX1: CALIBRATION OF RC MODELS IN FREQUENCY DOMAIN

The radiant slab can be modeled using a number of lumped thermal capacitances. Here an approach is presented to obtain the transmission matrix for different lumped parameter models with different resolutions. Initially, a first order model is considered for the slab as shown in Figure 0-1:
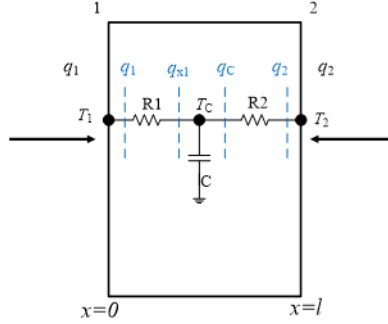

Figure 0-1. 1C2R model for the slab

The transmission matrix for this model can be obtained by writing the energy balance equation for the nodes T_1 and T_2 in Laplace domain considering all the heat fluxes and the intermediate node:

$$\begin{cases} q_1(t) = q_{x1}(t) \\ q_{x1}(t) = \dfrac{T_C(t) - T_1(t)}{R_1} \\ q_C(t) - q_{x1}(t) = C(dT_C(t)/dt) \end{cases}$$

By applying the Laplace transform to equation above:

$$\begin{cases} q_1(s) = q_{x1}(s) \\ q_{x1}(s) = \dfrac{T_C(s) - T_1(s)}{R_1} \\ q_C(s) = q_{x1}(s) + sCT_C(s) \quad (T_C(0) = 0) \end{cases}$$

then:

$$
\begin{cases} T_C(s) = T_1(s) + R_1 q_1(s) \\ q_C(s) = sCT_1(s) + q_1(1 + sCR_1) \end{cases} \Rightarrow \begin{bmatrix} T_C \\ q_C \end{bmatrix} = \underbrace{\begin{bmatrix} 1 & R_1 \\ sC & 1 + sCR_1 \end{bmatrix}}_{TR1} \begin{bmatrix} T_1 \\ q_1 \end{bmatrix}
$$

TR1 is the transmission matrix between nodes T_C and T_1 and can be written as:

$$
\begin{bmatrix} 1 & R_1 \\ sC & 1 + sCR_1 \end{bmatrix} = \begin{bmatrix} 1 & 0 \\ sC & 1 \end{bmatrix} \begin{bmatrix} 1 & R_1 \\ 0 & 1 \end{bmatrix}
$$

Then, writing the energy balance equations for the nodes T_C and T_2 (interior wall surface) gives:

$$
\begin{cases} q_C(t) = q_2(t) \\ q_2(t) = \dfrac{T_2(t) - T_C(t)}{R_2} \end{cases} \xrightarrow{\text{Laplace transfrom}} \begin{cases} q_C(s) = q_2(s) \\ q_2(s) = \dfrac{T_2(s) - T_C(s)}{R_2} \end{cases}
$$

by rearranging the equations we will have:

$$
\begin{cases} T_2(s) = T_C(s) + R_2 q_C(s) \\ q_2(s) = q_C(s) \end{cases} \Rightarrow \begin{bmatrix} T_2 \\ q_2 \end{bmatrix} = \underbrace{\begin{bmatrix} 1 & R_2 \\ 0 & 1 \end{bmatrix}}_{TR2} \begin{bmatrix} T_C \\ q_C \end{bmatrix}
$$

where TR2 is the transmission matrix between T_C and T_2. Using equations above it can be observed that:

$$
\begin{bmatrix} T_2 \\ q_2 \end{bmatrix} = \overbrace{\underbrace{\begin{bmatrix} 1 & R_2 \\ 0 & 1 \end{bmatrix}}_{TR2} \underbrace{\begin{bmatrix} 1 & 0 \\ sC & 1 \end{bmatrix} \begin{bmatrix} 1 & R_1 \\ 0 & 1 \end{bmatrix}}_{TR1}}^{TRtot} \begin{bmatrix} T_1 \\ q_1 \end{bmatrix}
$$

The matrix TRtot is the total transmission matrix between nodes T_1 and T_2. It can be observed from equation that generally, the transmission matrix for every layer that contains only a thermal resistance, R, is written as:

$$\begin{bmatrix} 1 & R \\ 0 & 1 \end{bmatrix}$$

and for a layer that contains only thermal capacitance, C, is written as:

$$\begin{bmatrix} 1 & 0 \\ sC & 1 \end{bmatrix}$$

Using this rule, the transmission matrix for higher order RC circuits can be obtained. Now, considering a second-order circuit (2C3R) for the slab as shown in Figure 0-2, the transmission matrix is formed as:

$$\begin{bmatrix} T_2 \\ q_2 \end{bmatrix} = \begin{bmatrix} 1 & R_3 \\ 0 & 1 \end{bmatrix}\begin{bmatrix} 1 & 0 \\ C_2 s & 1 \end{bmatrix}\begin{bmatrix} 1 & R_2 \\ 0 & 1 \end{bmatrix}\begin{bmatrix} 1 & 0 \\ C_1 s & 1 \end{bmatrix}\begin{bmatrix} 1 & R_1 \\ 0 & 1 \end{bmatrix}\begin{bmatrix} T_1 \\ q_1 \end{bmatrix}$$
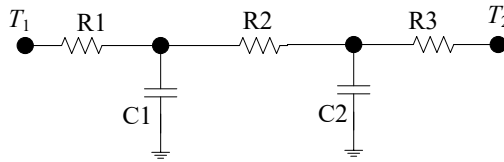

Figure 0-2. 2C3R model

In Figure 0-2 all the resistances are assumed each to be equal to the one-third of the total resistance (R_{tot}) and the capacitances are assumed each equal to the half of the total slab thermal capacitance. These assumptions are discussed in the next section. Also, the procedure to find the equivalent circuit parameters (resistances and capacitances) by means of optimization techniques is presented.

Results

Figure 0-3 compares the magnitude and phase angle of the transfer function $Y_{1,1}$ from the exact theoretical solution (no discretization) and different RC circuits approximation.
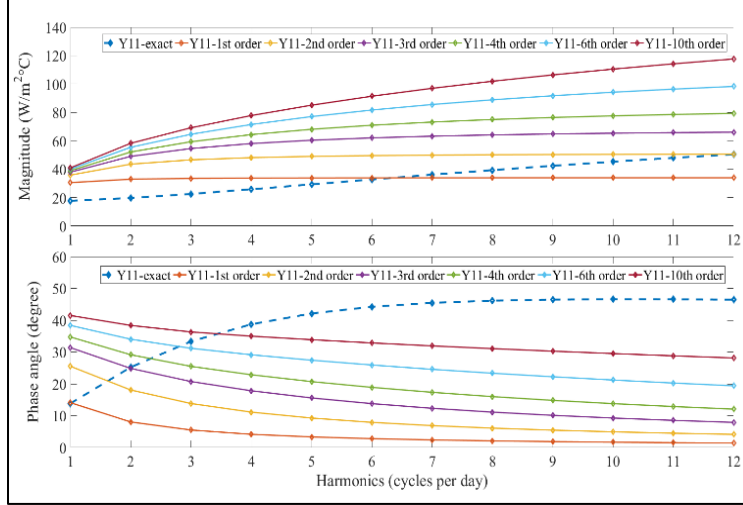
Figure 0-3. Magnitude and phase angle plot for transfer functions $Y_{1,1}$

It is observed that the RC circuit models act like a low-pass filters and pass signals up to a certain frequency (cut-off frequency) and attenuates higher frequency signals. This cut-off frequency increases as the model order is increased and after that the magnitude of the transfer function remains constant. Therefore, significant differences between the magnitude and phase angles of the exact model response and RC models response were observed. Hence, an optimization routine is considered to find the effective RC circuit parameters (resistances and capacitances) that improve the match between the two models.

An objective function is defined as the second norm of the summation of the differences between the magnitude (*M*) and the phase angles (*Ph*) of the transfer functions with each having their respective weighting factor. $(Y_E)_n$ is the value of the theoretical self-admittance transfer function at frequency n and *Ye* is the self-admittance transfer function of the low-order RC circuit estimation.

$$ J = W_M \sqrt{\sum_n \left[M(YE)_n - M(Ye)_n \right]^2} + W_{PH} \sqrt{\sum_n \left[Ph(YE)_n - Ph(Ye)_n \right]^2} $$

The frequency range considered (1-12 cycles per day) is rational for majority of heat transfer phenomena that happen inside a building. The MATLAB optimization toolbox (fmincon function which uses the simplex algorithm) is used. Initially, it is decided to consider an equal weight for the magnitudes and the phase angles differences ($W_M=W_{PH}=1$). Therefore, the objective function J_1 will be:

$$J_1 = \sqrt{\sum_n \left[M(YE)_n - M(Ye)_n \right]^2} + \sqrt{\sum_n \left[Ph(YE)_n - Ph(Ye)_n \right]^2}$$

Now considering the first-order (1C2R) model, Figure 0-4 shows the optimization results:
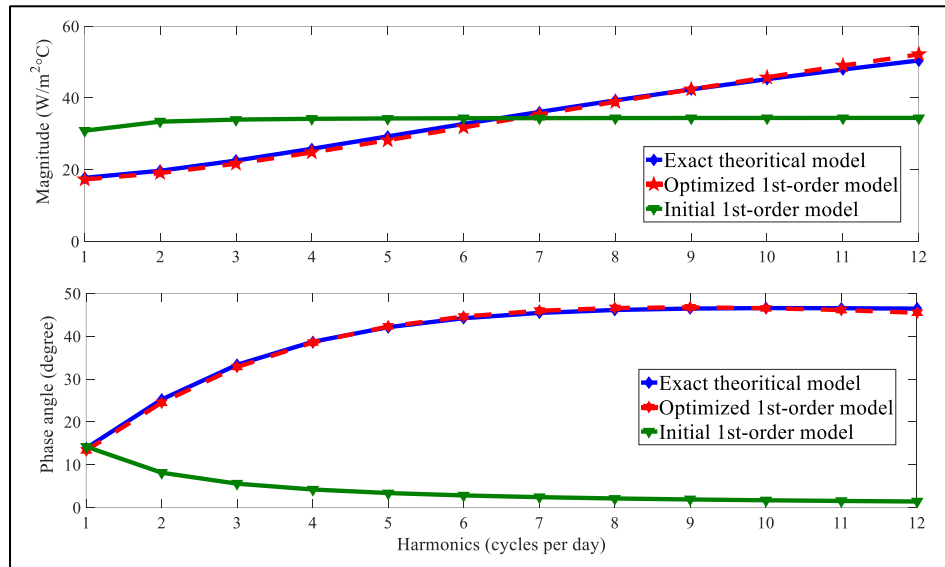

Figure 0-4 Comparison of the optimized first-order model with the theoretical model

It is observed from Figure 0-4 that the match has improved considerably both in terms of magnitudes and phase angles. However, let us verify the new circuit parameters obtained through optimization with the initially proposed values (based on physical properties of the slab materials). The parameters are shown in Table 1:

Table 1. First-order RC circuit parameters

Parameters	Initial values	Optimized values
C (J/K)	1.58E+06	7.71E+04
R1 (m^{2}K/W)	3.00E-02	5.07E-02
R2 (m^{2}K/W)	3.00E-02	9.43E-03
R1+R2	6.00E-02	6.01E-02

It can be seen that the thermal capacitance has been reduced significantly and in terms of the resistance distribution between R1 and R2, more than eighty percent of the total R-value has been given to R1. However, the total R-value which is the summation of the R1 and R2 is very close to the initial total R-value of the slab from the physical model. Nevertheless, the new thermal capacitance value does not make sense physically since it is less than five percent of the physical model. Thus, it is clear that higher order models should be considered.

Now, let us consider a second-order circuit (2C3R model). Figure 0-5 shows the optimization results for the second-order circuit. From Figure 0-5 we can see a very good match between the optimized second-order circuit and the theoretical model. Table 2 shows the RC circuit parameters. From Table 2, we can see that the optimized circuit total capacitance value has become closer to its initial total physical value (8.66E05/1.58E06 ≈55%) compared to the first-order model (7.71E04/1.58E06≈4%). For the resistances, the total resistance is almost the same for both the initial and optimized circuits. In the optimized circuit, the largest resistance is considered to be the middle resistance R2 (more than 75% of the total R) and R3 considered to be the smallest. Therefore, it can be observed that the initial assumption to consider all the thermal resistances to be the same is not the best approximation. It can also be seen that increasing the order of the model from first-order (1C2R) to second-order (2C3R) has improved the optimization results in a sense that the equivalent circuit parameters are closer to the physical values.
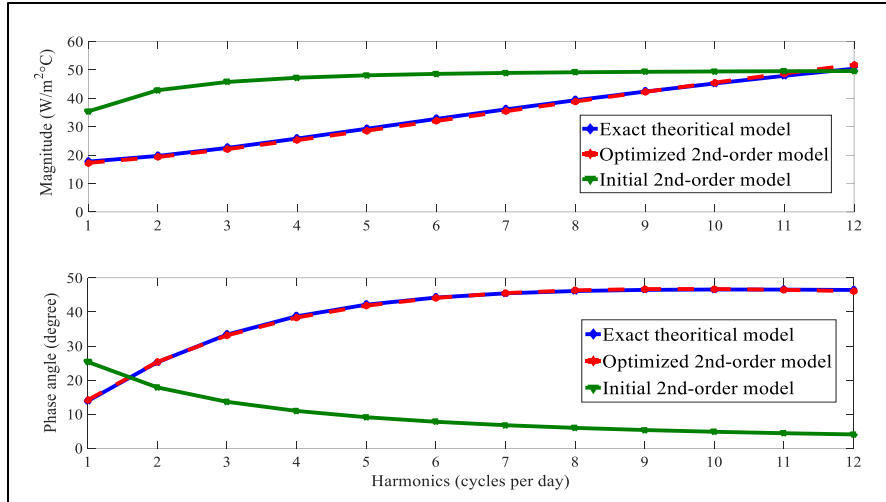
Figure 0-5 Comparison of the optimized second-order model with the theoretical model

Table 2. Second-order RC circuit parameters

Parameters	Initial values	Optimized
C1 (J/K)	7.92E+05	7.92E+05
C2 (J/K)	7.92E+05	7.40E+04
C1+C2 (J/K)	1.58E+06	8.66E+05
R1 (m^2K/W)	2.00E-02	4.67E-03
R2 (m^2K/W)	2.00E-02	4.71E-02
R3 (m^2K/W)	2.00E-02	8.89E-03
R1+R2+R3	6.00E-02	6.06E-02

Considering the same procedure for a third-order model (3C4R), the results are shown in Figure 0-6 and Table 3.
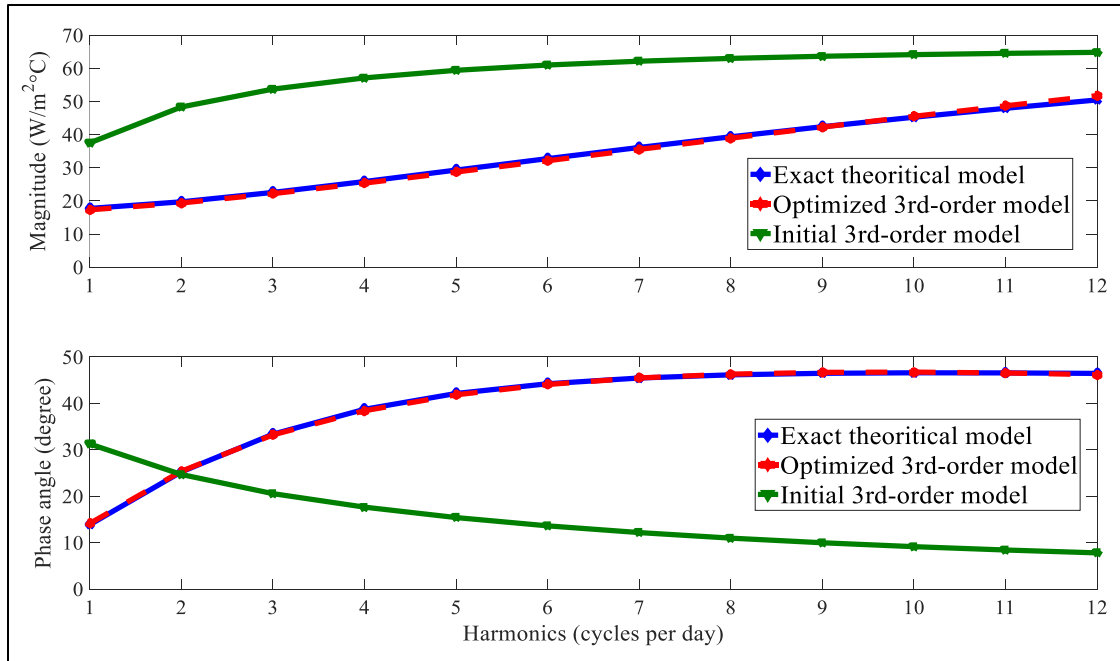
Figure 0-6 Comparison of the optimized Third-order model with the theoretical model

Table 3. Third-order RC circuit parameters

Parameters	Initial values	Optimized
C1 (J/K)	5.28E+05	5.28E+05
C2 (J/K)	5.28E+05	5.28E+05
C3 (J/K)	5.28E+05	7.30E+04
C1+C2+C3	1.58E+06	1.13E+06
R1 (m^{2}K/W)	1.50E-02	1.35E-05
R2 (m^{2}K/W)	1.50E-02	5.92E-03
R3 (m^{2}K/W)	1.50E-02	4.58E-02
R4 (m^{2}K/W)	1.50E-02	8.75E-03
R1+R2+R3+R4	6.00E-02	6.05E-02

It is observed that for the third-order model the values of the capacitances C1 and C2 are identical before and after the optimization and the total value of the capacitances are closer to each other compared to the second-order model.

For the third-order model, the value of model's total capacitance after optimization is almost seventy-two percent of the total value considered in the initial physical model. Thus, it can be observed that by increasing the model order the results are getting closer to the initial model created based on the physical properties.

Objective function based on the magnitude difference only

The objective function J_1 considered in the previous simulations considered same weight for both magnitudes and phase angles. Now, here it is studied how the results will change if we consider a different objective function in which the weighting factor of the phase angles difference is put equal to zero as:

$$J_2 = \sqrt{\sum_n \left[M(YE)_n - M(Ye)_n \right]^2}$$

Now considering this objective function J_2, Table 4 and Figure 0-7 show the results for the third-order model of the concrete slab:

Table 4. Third-order circuit parameters using different objective functions

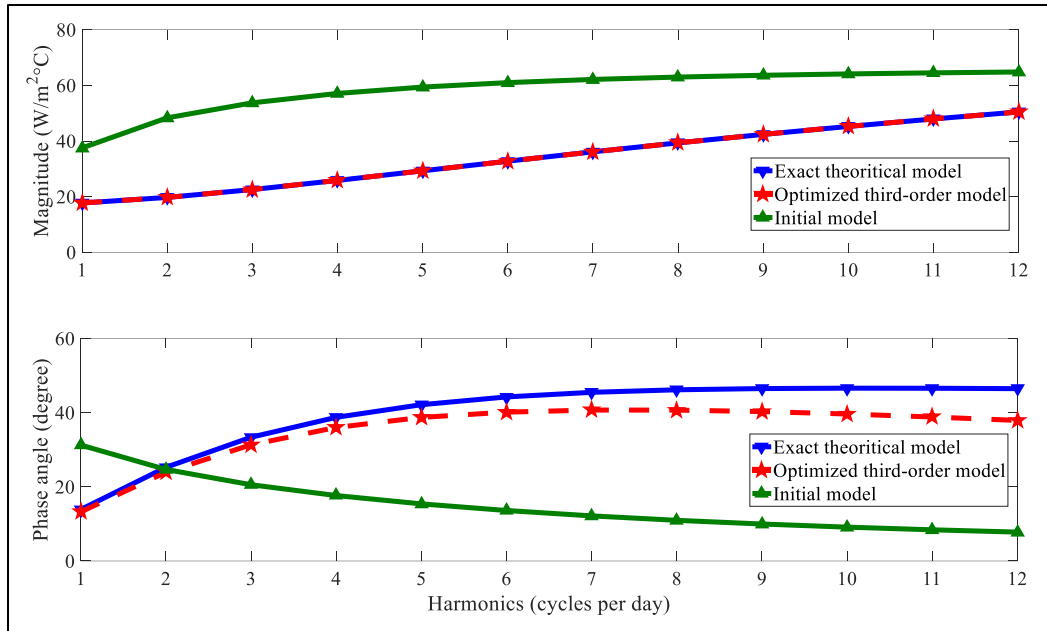| Parameters	Initial values	J_1	J_2
C1 (J/K)	5.28E+05	5.28E+05	5.28E+05
C2 (J/K)	5.28E+05	5.28E+05	5.28E+05
C3 (J/K)	5.28E+05	7.30E+04	8.54E+04
ΣC	1.58E+06	1.13E+06	1.14E+06
R1 (m²K/W)	1.50E-02	1.35E-05	2.26E-05
R2 (m²K/W)	1.50E-02	5.92E-03	3.55E-03
R3 (m²K/W)	1.50E-02	4.58E-02	4.33E-02
R4 (m²K/W)	1.50E-02	8.75E-03	1.20E-02
ΣR	6.00E-02	6.05E-02	5.89E-02

Figure 0-7. Comparison of the new third-order model for the concrete slab

It is observed from Table 4 that the change in the total value of the thermal capacitances and resistances is not significant compared to the previous optimization results. Also, from Figure 0-7 it is observed that although the phase angles difference was removed from the objective function, the phase angle plot has improved noticeably compared to the initial model. Therefore, the important observation here is that the most important parameter is the magnitude of the transfer function over this frequency range.

Summary and conclusion

The procedure to obtain the exact theoretical solution for a slab transfer functions (self-admittance and transfer admittance) is described. Then, a methodology is presented to find the cascade matrix for the low-order resistance capacitance (RC) models of a slab and the self-admittance transfer functions of the low-order RC models were compared with the ones from the exact theoretical solution.

Then, an optimization algorithm (simplex method) is used to find the equivalent RC circuit parameters to improve the match with the theoretical model. The first objective function considered to be the second norm of the difference between the magnitudes and the phase angles of the transfer functions with an equal weighting factor. It is discussed that for different low-order RC models if the optimized model parameters physically make sense compared to the initial physical model or not. It is observed that depending on the level of thermal mass, higher order models are needed to have a good match with the exact solution while having a physically meaningful model at the same time. Then, by removing the phase angles from the objective function, it is also observed that the most important parameter is the magnitude of a transfer function and considering only magnitudes differences in the optimization objective function improves the phase angles match to a certain degree too.

APPENDIX 2: COMSOL MODEL

This appendix provides more details on the 3D COMSOL model for the radiant slab of the perimeter zone test cell. This was a collaborative study with Dr. Jose Candanedo at Natural resources Canada who created the COMSOL model and did the relevant analysis presented below.

A detailed model of the two slabs was built in COMSOL^{TM}, an environment for multi-physics simulations, i.e. simulations treating multiple physical phenomena that occur simultaneously. This study attempted to approximate the geometry of the foam matrix underneath the concrete slabs and the piping installed within its grooves (Figure 0-1). The COMSOL model was used to determine the evolution of the temperature field over time within the concrete slab over time using a finite element scheme. The heat transfer conduction analysis focused only on the concrete section of each slab. The solution was found for time steps of 300 seconds (5 min) for the time period from t = -4 h to t = 44 h, using a MUMPS solver, a solver for finite element applications.
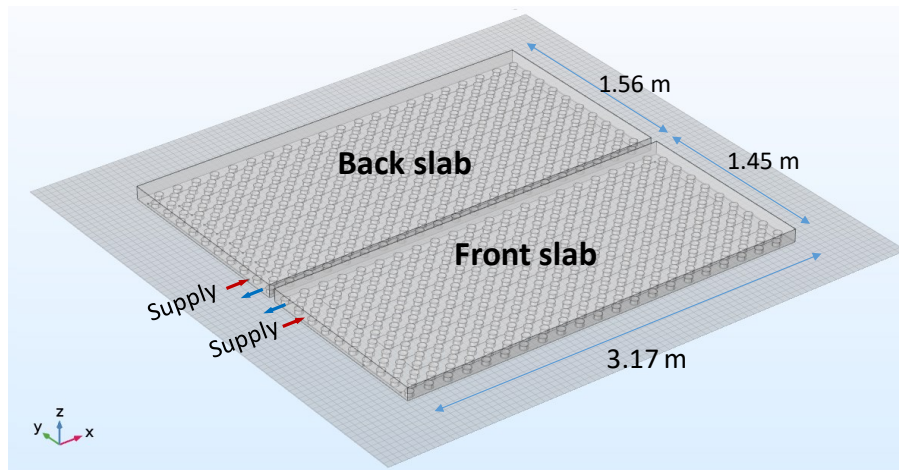

Figure 0-1. Perspective of the COMSOL model

The foam base and its "bumps" were modelled with a rectangular block with an array of cylindrical objects on top of it (Figure 0-2). The cylinders had a diameter of 6.25 cm and were about 3 cm high. As mentioned before, the thickness of the concrete slab poured on top was 8 cm. A geometric

"subtraction" operation was then performed in COMSOL, so that each of the slabs had a set of cylindrical holes underneath it.
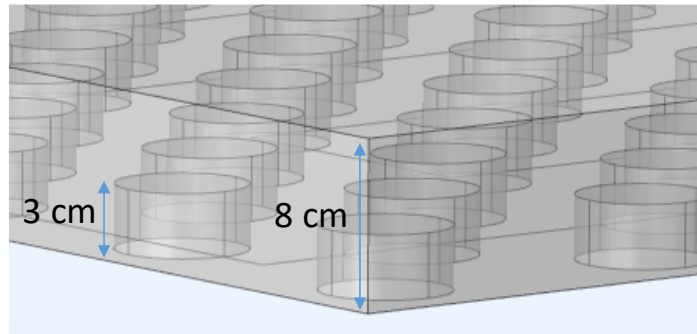

Figure 0-2. Cylindrical "bumps" in the model

A relatively "coarse" mesh was used, with nearly 72,000 elements in it, with an average volume 9.8 cm^3.
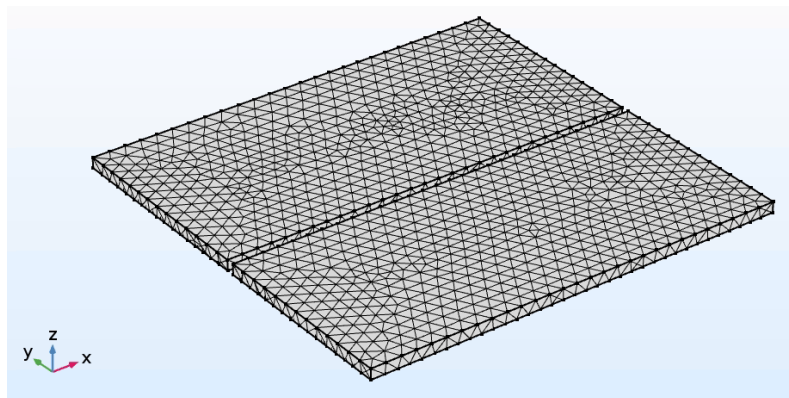

Figure 0-3. Meshing of the domain

Assumptions used in the detailed model include:

• The properties of a 50/50 water-glycol were used.

• The bottom surfaces of both slabs are assumed to be perfectly connected to the insulation.

- The bottom of the insulation is assumed to be exposed to the temperature of the room. This assumption is made because there is an air space underneath the insulation (the test hut is a mobile room on wheels).

- It is assumed that these bottom surfaces lose heat to the air with an "effective" heat transfer coefficient of 0.5 Wm^{-2}K^{-1}.

$$q_{ins} = (0.50 \text{ Wm}^{-2}\text{K}^{-1})(T_{bottom} - T_{room}) \tag{4.6}$$

This value was chosen considering an R-10 insulation, and neglecting the heat transfer coefficient between the insulation and the air.

• The lateral surfaces facing outwards are assumed to be connected to the wooden frame, with no insulation. Again, it is assumed that this wooden frame is exposed to the room air temperature. The boundary condition is:

$$q_{wood,sides} = (8 \text{ Wm}^{-2}\text{K}^{-1})(T_{lateral surfaces} - T_{room}) \tag{4.7}$$

This heat transfer coefficient is calculated based on a typical thermal conductivity of wood.

- The lateral surfaces facing inwards (i.e., the small gap between the slabs connected to the wooden frame) is assumed to be adiabatic.

- A uniform initial temperature of -5 °C was assumed for the entire domain of both concrete slabs.

- COMSOL employs by default the correlation by Lloyd and Moran (1974), as cited by Incropera and DeWitt (2002), to evaluate natural convection between the floor surface and the air.

$$Nu = \begin{cases} 0.54 Ra^{1/4} & \text{if } 10^4 \le Ra \le 10^7 \\ 0.15 Ra^{1/3} & \text{if } 10^7 \le Ra \le 10^{11} \end{cases} \tag{4.8}$$

The Rayleigh number was calculated using the length scale proposed by Goldstein et al. (1973), where L = A/P.

•   Radiative heat transfer is assumed for the top surface of the concrete slabs, assuming grey-body radiation from a diffuse surface with an emissivity of 0.95, and an ambient temperature ("sky temperature") equal to the room air temperature shown in Figure 7.

•   For the purpose of conduction heat transfer in the slabs, the PEX pipes are treated as linear heat sources.

•   The simulation flow rates in each slab are based on the measured flow rates.

•   The temperature at the inlets used in the simulation are the measured inlet temperatures.

The properties used for the concrete are as follows:

• $\rho = 2010$ kg/m^3,

• $c_\mathrm{p} = 800$ J/(kg·K);

•   and $k = 1.7$ W/(m·K).

RESULTS OF THE DETAILED MODEL

Figure 0-4 and 0-5 show the average temperature at the surfaces of the back and front slabs respectively. The temperatures predicted by the model for the back slab are higher (by about 1 °C) than the ones measured in the experiment. Given that the flow rate is higher in the back slab, it would be reasonable to expect higher temperatures there. The discrepancy might be due to the

location of the sensors near the slab surface, which may not be representative of the average temperature. The temperatures predicted for the front slab match quite well the experimental results. The simulation predicts similar temperatures for both slabs.
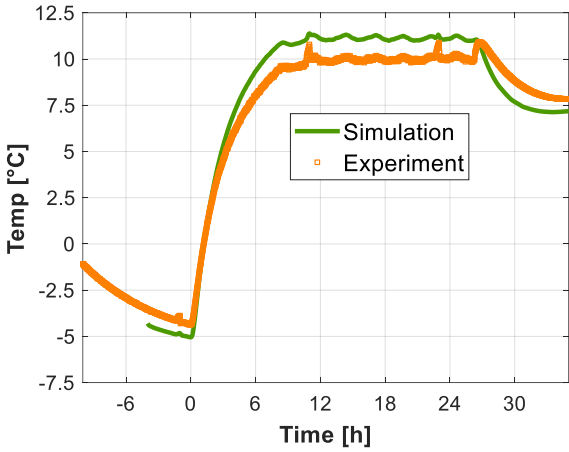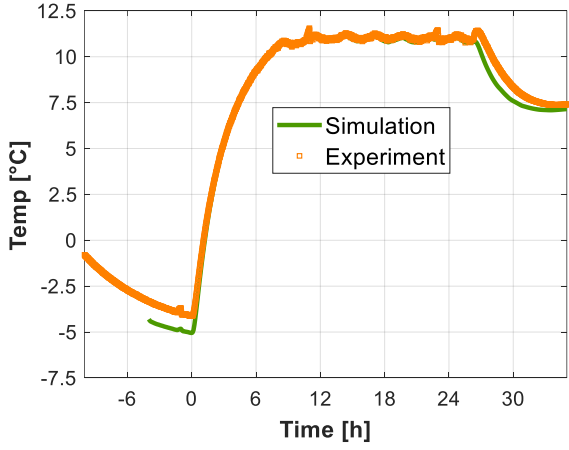

Figure 0-4. Average surface temps (back slab)

Figure 0-5. Average surface temperature (front slab)

The results of the temperature distribution at the surface of the slab (Figure 0-6) are quite informative. In both slabs, the temperatures at t = 23.75 h are between 10 and 14 °C in the central

area of the concrete slabs. The path of the fluid can nevertheless be clearly seen, and it is clear that the concrete temperature is lower near the edges of the slabs and near the points where the fluid exits the slab.
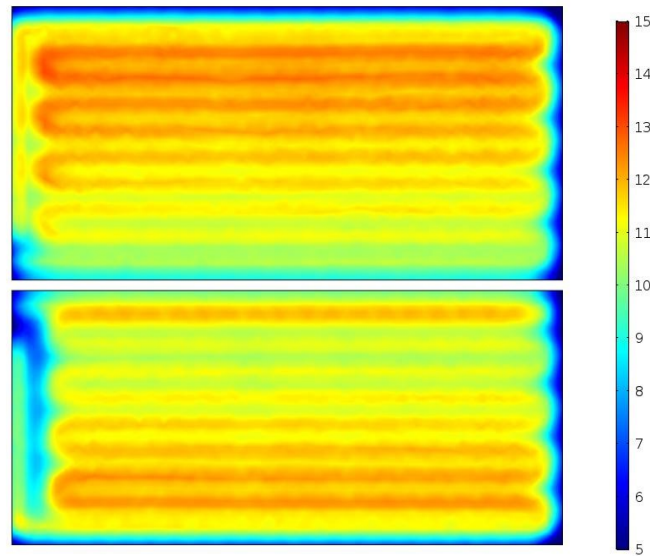

Figure 0-6. Surface temperature distribution (°C), t = 23.75 h

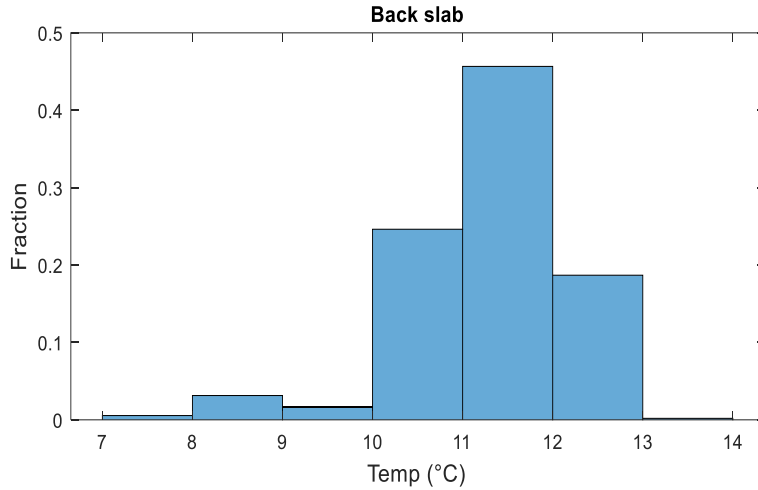Histograms from simulation results show that about 90% of the back slab surface is between 10 and 13 °C.

Figure 0-7. Surface temperatures (back slab), t=23.75 h.

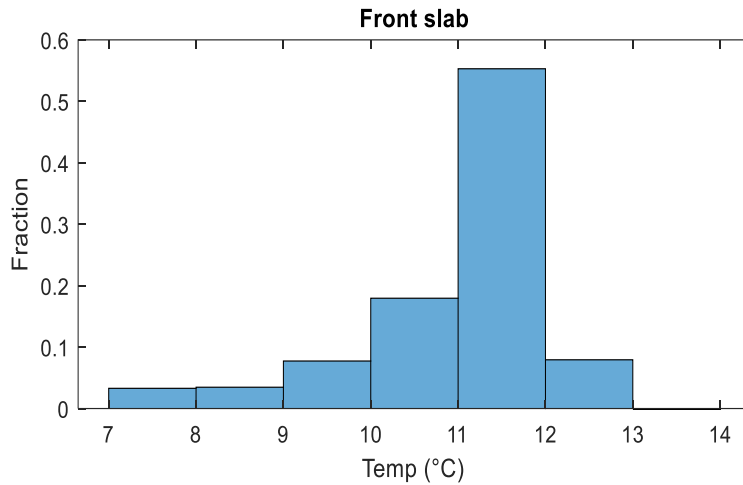Regarding the front slab, about 75% of temperatures are between 10 and 12 °C.

Figure 0-8. Surface temperatures (front slab), t = 23.75 h.

Further insight can be obtained by analyzing the heat transfer rate from the pipes to the slab and then comparing it with the heat transfer from the floor surface to the room.

Figure 0-9 shows the heat transfer rate from the pipes to the concrete. Its peak value occurs at t = 0 (i.e., the moment when the temperature differences between the water and the concrete are the

largest). The heat transfer rate declines steadily until about t = 8 h. At this point, the fluctuations

in the supply water temperatures cause similar oscillations in the heat transfer rates.
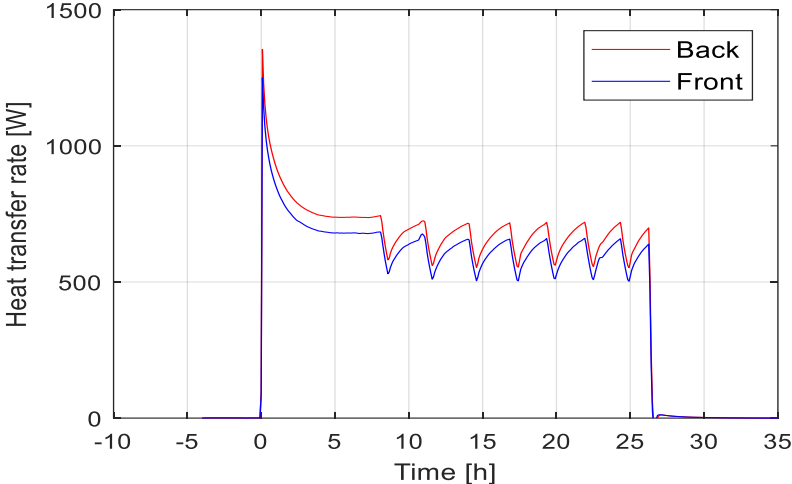

Figure 0-9. Heat transfer rates from pipes to slabs

Figure 0-10 shows the heat flux from the surface of both slabs to the room. As expected, there is a

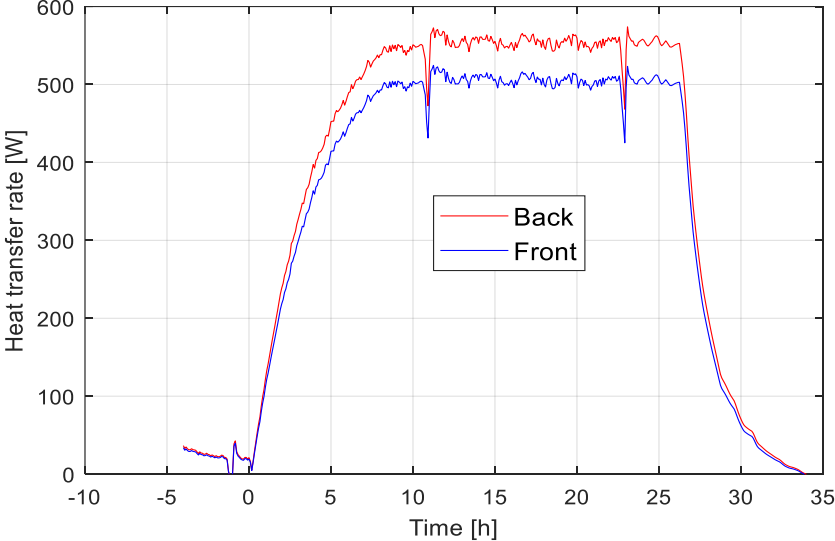delay of several hours when compared to the heat transfer rate from the pipes to the concrete.

Figure 0-10. Heat flux from the floor to the room

146